CRANFIELD UNIVERSITY

YIN-LIEN LO

DESIGN AND ANALYSIS OF NUMERICAL TRAJECTORY OPTIMISATION ALGORITHMS FOR MARS ENTRY PROBLEM

SCHOOL OF AEROSPACE, TRANSPORT AND MANUFACTURING
MSc in Astronautics and Space Engineering

MSc
Academic Year: 2019 - 2020

Supervisor: Runqi Chai
August 2020

CRANFIELD UNIVERSITY

SCHOOL OF AEROSPACE, TRANSPORT AND MANUFACTURING
MSc in Astronautics and Space Engineering

MSc

Academic Year 2019 - 2020

YIN-LIEN LO

DESIGN AND ANALYSIS OF NUMERICAL TRAJECTORY OPTIMISATION ALGORITHMS FOR MARS ENTRY PROBLEM

Supervisor: Runqi Chai

August 2020

This thesis is submitted in partial fulfilment of the requirements for the degree of MSc

ABSTRACT

The problem of numerical trajectory optimisation of Mars atmospheric entry problem is considered in this thesis. The optimisation is done by a Matlab package GPOPS-II with two nonlinear programming (NLP) solvers IPOPT and SNOPT, corresponding to interior point (IP) method and sequential quadratic programming (SQP) method respectively. For the considered scenario, two mission objectives are considered respectively. One is minimising terminal velocity, and another one is minimising terminal time. The aim is to search the optimal bank angle profile as well as the corresponding translational state trajectories. In the beginning, the orthogonal collocation method called *Radau pseudospectral method* is utilised with LGR discretised points to convert optimal control problem (OCP) into NLP problems. Next, two optimisation methods are constructed and applied to search the optimal solutions. The obtained solutions are then compared in order to analyse key features of different methods. Also, further attention is given to the path-constrained cases as well as the path-unconstrained cases. The results show the differences in IP and SQP methods, and reveal the advantages and disadvantages of applying different methods.

Keywords:

Mars atmospheric entry

Trajectory optimisation

Optimal control problem

Bank angle control

Sequential quadratic programming

Interior point method

ACKNOWLEDGEMENTS

I truly appreciate Dr. Runqi Chai for his supervision during the entire project. Firstly, the help I received from him is way beyond what I expected. Secondly, he always thoroughly explained each question that I asked. Last but not the least, his is not only an excellent mentor but also a friend to me. Thank you, Runqi. It was a fantastic experience to work with you.

Next, I would like to thank my parents. Thank you for your unlimited supports so I can focus on this project without anything to worry about.

To my sister, Yin-Chih Lo. Thank you for encouraging me when I was lost and tired. I know you will always by my side.

To my mentor at Fu-Jen University, Nai-Sher Yeh. Thank you for inspiring me during my study at the University and helping me on academic problems, even if I was graduated.

To my friend Li-Hsiang Chu. Thank you for discussing many science questions with me. Although they might be irrelative to this project, the way you look at the questions provided a new way to think.

To my friend Ming-Yuan Chuang. Thank you for lending me your laptop when mine was malfunctioning.

To my friends at Cranfield. Thank you for giving me help on my study. I have learnt a lot of things from you guys. Thank you for being my friends.

Last, I would like to thank Cranfield University and the staffs in ASE course. Thank you for giving me excellent education and this opportunity. Thank you.

TABLE OF CONTENTS

LIST OF FIGURES

LIST OF TABLES

LIST OF EQUATIONS

LIST OF ABBREVIATIONS

COV	Calculus of Covariant
EDL	Entry, Descent, Landing
GPM	Gauss pseudospectral method
IMMACS	Internal Moving Mass Actuator Control System
IP	Interior Point
MSL	Mars Science Laboratory
NLP	Nonlinear programming
OCP	Optimal Control Problem
PMP	Pontryagin’s Maximum Principle
PSO	Particle Swarm Optimisation
RCS	Reaction Control System
SQP	sequential quadratic programming
TPBVP	Two-Point Boundary Value Problem

LIST OF SYMBOLS

t	Time if flight
h	Altitude
r	Distance from centre of Mars to vehicle's centre of mass
v	Vehicle's velocity with respect to Mars
θ	Longitude
λ	Latitude
γ	Flight path angle
ψ	Azimuth angle
σ	Bank angle
σ_c	Bank angle control
g_M	Gravitational acceleration
ω_M	Rotation rate of Mars
L	Lift acceleration
C_L	Lift coefficient
D	Drag acceleration
C_D	Drag coefficient
ρ	Atmospheric density of Mars
ρ_0	Sea level atmospheric density of Mars
h_s	Density scale height
S	Reference area of vehicle
m	Mass of vehicle
r_M	Radius of Mars
q	Dynamic pressure
a	Aerodynamic load
$\dot{Q}$	Heating rate

1 Introduction

In the last few decades, several innovative technologies in science and engineering fields have been developed. However, many technologies and engineering work have negative impacts on Earth. In the end, Earth may become uninhabitable planet for human beings. This attracts the scientists' attention to find the solutions. One of the solutions is moving human to Mars and establishing a settlement on Mars. To achieve this goal, Martian exploration missions and Mars sample-return missions are firstly required. It is necessary to know the environment on Mars, so that risks of human staying on Mars will be reduced. Next, human Mars missions and Mars settlements missions can be generated. On the other hand, Mars missions are also in an essential place of Solar system exploration. To understand our solar system deeper, it is necessary to explore Mars. Mars missions are a necessary preparation for the upcoming space age.

1.1 Mission background

These Mars missions have a lot in common. One of them is delivering payloads to Martian surface which involves entry, descent and landing (EDL) process in each mission. On top of that, the entry process dominates the accuracy of landing site which is important for missions. Mars atmospheric entry typically starts from vehicle entry Martian atmosphere (~125 km altitude) and ends at the point of parachute deployment, which largely determines the final landing accuracy. Apart from the accuracy, delivering payload or human to the surface safely is also a top priority. The velocity, heating rate and dynamic pressure of vehicle are crucial factors in the protection of the payload and human. It is necessary to design a trajectory that satisfied all requirements.

1.2 Mission objective

To achieve mission requirements, an optimised reference trajectory is often used. Moreover, trajectory optimisation is considered a significant part of guidance

system design. In this thesis, mission objective is to find optimised Mars entry trajectories while all requirements, such as boundary conditions and path constraints, are satisfied.

1.3 Current development

The past development and current state-of-art of Mars atmospheric entry guidance and control technology was summarised in [1]. A comprehensive study of MSL EDL system design and performance requirement was addressed by [2], which provided areas of improvements for future Mars EDL missions. [3] studied the effect of lift on the entry corridor. NASA's Mars Science Laboratory (MSL) implemented a guided entry mode in 2012 [1] [4], and achieved to a high landing accuracy.

1.4 Structure of work

This thesis is organised as the following

- **Chapter 2 Literature review**: This chapter provides basic background knowledge for the latter sections, including different methods for solving trajectory optimisation problems, and the decision the methods used in the following research.
- **Chapter 3 Problem formulation**: This chapter explains the mathematic models for Mars atmospheric problems and addresses the problems studied in this thesis, as well as the structure of optimisation.
- **Chapter 4 Orthogonal collocation method**: This chapter describes the method that transforms the OCP into NLP problem.
- **Chapter 5 Results and conclusion**: The first part of this chapter includes the initial setting of parameters and conditions. The second part explains the simulation results of the problems. The last part is conclusion.

2 Literature review

2.1 Optimal control problem

As previous section mentioned, optimised trajectory is a crucial part of the guidance system, which performs controls of vehicle during entry process and modifies trajectory to achieve mission requirements. For example, the minimum parachute deployment speed can be achieved by using bank angle control. This is an optimal control problem (OCP) with objective of minimum terminal speed. In [5] [6], the influence of bank angle control and angle of attack control were analysed. The results showed that wider range of bank angle control increases the maximum parachute deployment altitude. On the other hand, the results of the control of angle of attack showed that the increase of altitude was more than the altitude increase gain from bank angle control.

Mars entry trajectory optimisation can be illustrated as a nonlinear OCP with the path constraints and terminal constraints. Due to the complexity of nonlinear characteristics in the Mars entry dynamic model, it is difficult to obtain precise analytic solutions. There are several methods to solve the nonlinear OCP, which can be divided into two categories: indirect method [7] and direct method [8] [9] [10].

2.1.1 Indirect methods

Indirect methods, based on Pontryagin's maximum principle (PMP), transform the OCP into a two-point boundary value problem (TPBVP). However, the process of solving a TPBVP is extremely hard because of the high sensitivity of the initial guesses of the variables.

The following shows the advantages and disadvantages of indirect methods provided from [11]:

Advantage:

- Local optimality can be reasonably assumed

- The optimal control is determined analytically
- The costates represent sensitivity of cost to changes in their corresponding state variables

Disadvantages:

- The dimension of the system largely increases
- Tabular data cannot be accommodated easily
- A TPBVP is made and it is difficult to solve without proper initial guess
- The system equations change if the terminal conditions or constraints are changed

2.1.2 Direct methods

On the other hand, direct methods convert continuous OCP into a discrete nonlinear programming problem (NLP). The result of solving NLP is the solution of OCP. There are various numerical methods to solve the NLP, such as particle swarm optimisation (PSO) algorithm, sequential quadratic programming (SQP) method [12], Gauss pseudo-spectral method (GPM) and interior point (IP) method [13]. In this thesis, only SQP method and IP method will be discussed and be used to analysis the Mars atmospheric entry trajectory.

The following shows the advantages and disadvantages of direct methods provided from [11]

Advantages:

- Easy to code
- Tolerant of poor initial guess
- Constraints, which are problematic for COV methods, are simply included.
- Changes in constraints and terminal conditions are easy to make

Disadvantages:

- An initial guess of solution for NLP solver is required to improve

- Controls and states are known at discrete points
- Likely to converge to a minimum in the neighbourhood of the initial guess
- No information about improvement is provided from the solution

2.2 Methods of discretisation

In [14], the authors aimed at developing a hybrid trajectory optimisation strategy for Mars entry to improve efficiency under the uncertainty of initial state. The strategy was using the combination of global optimisation and local optimisation with PSO and GPM to generate the optimal entry trajectory for Mars pin-point landing mission. [15] and [16] proposed different PSO algorithm, the former provided two types of PSO algorithms for single and multiple objectives, and the latter provided a new PSO method for solving an OCP.

According to [12], the benefits of PSO were low sensitivity of initial guess and high performance for some large-scale complicated nonlinear problems. On the other hand, the work of [17] showed that the GPM is sensitive to the initial value at the collocation points. In the work of [18], Gauss orthogonal polynomial was used to approximate control and state variables, which are often used in spectral methods for transforming OCP into NLP. Hence, the authors of [14] concluded that combining GPM with SQP solved optimisation problem efficiently and precisely when proper initial guess was given.

In the work of [5], a local direct collocation method was used to convert OCP into NLP problem, and an adaptive mesh refinement method was implemented to refine discretisation points. [5] showed that the accuracy of direct method depends on the number of discrete points. Although a fine discretisation made solution more accurate, NLP problem became very large scale, which increases the computational cost. Therefore, choosing the optimal discretisation points which balance the solution accuracy and computational cost is important. From

the work of [19], a data compression algorithm provided by in [20] was improved by the authors of [5].

2.3 Methods of optimisation

In this section, two NLP solvers are discussed: Interior point optimiser (IPOPT) and Sparse nonlinear optimiser (SNOPT). IPOPT corresponds to IP method [13] and SNOPT corresponds to SQP method [12].

[13] studied at IPOPT method, including the feasibility restoration phase for filter method [21], second-order corrections and inertia correction of the KKT matrix. Primal-dual interior-point algorithm with a filter line-search method proposed in [22] was implemented in IPOPT code for NLP problem and tested in 954 problems of CUTEr test set. The Convergence properties of interior-point methods was provided in [23]. The authors of [24] proposed several heuristics based on the idea of filter methods that improved efficiency.

In terms of SNOPT method, [25] firstly proposed a SQP method for special case of convex optimisation. In [12], sequential quadratic programming (SQP) methods is thoroughly discussed. The work in this thesis showed the high efficiency of solving NLP problem with large numbers of constraints and variables. A few assumptions were made: first derivatives are available, constraints gradients are sparse and second derivatives are unavailable or computational expensive.

An SQP algorithm proposed in [12] involves a smooth augmented Lagrangian merit function and makes explicit provision for infeasibility in the original problem and QP subproblems. A limited-memory quasit-Newton method was utilised to approximate the Hessian of the Lagrangian in [26]. A reduced-Hessian semidefinite QP solver for the QP subproblems [27] was used in SNOPT and maintained a dense approximation to reduce Hessian. [28] [29] also provided reduced-Hessian methods. The purpose of this method was to cope with the

problems with large numbers of constraints and variables. However, a proper number of degrees of freedom was important in the method.

The structure of an SQP method contained major and minor iterations [30]. The former generated a sequence of iterates (x_k, π_k) that converged to (x^*, π^*). A search direction toward the next iterate (x_{k+1}, π_{k+1}) was generated by QP subproblem at each iterate. Solving a subproblem was an iterative process, with the minor iterations of an SQP method being the iterations of the QP method.

The CUTEr and COPS3.0 test sets [31] [32] were used to test SNOPT, and the numerical results showed the high efficiency in most of problems, including examples with up to 40,000 constraints and variables, and some with 20,000 degrees of freedom.

It is noted that [33] [34] provided alternative implementation of SNOPT. [33] provided a combination of SNOPT and PSO and the authors of [34] considered the uncertainties in trajectory optimisation models

2.4 Method decision

In this thesis, the OCP are solved by direct method due to the simplicity and efficiency. The simulations are performed by a software GPOPS-II [35] with two NLP solvers: IPOPT and SNOPT.

2.5 Assumptions

A few basic background assumptions are made in this section for the latter research. Firstly, the Mars Science Laboratory (MSL) vehicle have been used in Mars entry missions [4] [36] [37]. The guidance is performed by adjusting bank angle with reaction control system (RCS) or internal moving mass actuator control system (IMMACS) and the vehicle is assumed to fly at a trim angle of attack. Next, a uniform gravitational field is used, because the altitude changed during the entry

process is much less than the radius of Mars. Lastly, the rotation of Mars is ignored.

- MSL-type entry vehicle is utilised to performed simulation
- Entry vehicle flies at a trim angle of attack
- The guidance is performed by adjusting bank angle of the vehicle only
- Uniform gravitational field
- The rotation of Mars is ignored

3 Optimal problem description

3.1 Mars atmospheric entry dynamics

Mars atmospheric entry phase begins from the atmosphere entry point to the parachute deployment point. The Mars atmospheric entry dynamic equations with respect to Mars inertial coordinate system are shown below [38]:

$$\begin{cases} \dot{r} = v\sin\gamma \\ \dot{v} = -D - g_M\sin\gamma \\ \quad +r\omega_M^2\cos\lambda\,(\sin\lambda\cos\gamma\cos\psi - \cos\lambda\sin\gamma) \\ \dot{\theta} = \dfrac{v\cos\gamma\sin\psi}{r\cos\lambda} \\ \dot{\lambda} = \dfrac{v}{r}\cos\gamma\cos\psi \\ \dot{\gamma} = \dfrac{L\cos\sigma}{v} + \left(\dfrac{v}{r} - \dfrac{g_M}{v}\right)\cos\gamma + 2\omega_M\sin\psi\cos\lambda \\ \quad + \dfrac{r\omega_M^2}{v}\cos\lambda\,(\cos\lambda\cos\gamma + \sin\lambda\sin\gamma\cos\psi) \\ \dot{\psi} = \dfrac{L\sin\sigma}{v\cos\gamma} + \dfrac{v}{r}\sin\psi\cos\gamma\tan\lambda \\ \quad +2\omega_M(\sin\lambda - \tan\gamma\cos\psi\cos\lambda) \\ \quad + \dfrac{r\omega_M^2}{v\cos\gamma}\cos\lambda\sin\lambda\sin\psi \end{cases} \qquad \textbf{Equation 3-1}$$

where r is the distance from the centre of Mars to the centre of mass of the vehicle, v is the velocity of the vehicle with respect to the Mars, θ is the longitude and λ is the latitude; γ is the flight path angle, ψ is the azimuth angle and σ is the bank angle; ω_M is the rotation rate of Mars and g_M is gravitational acceleration of Mars

g_M is calculated by

$$g_M = \frac{\mu_M}{r^2} \qquad \textbf{Equation 3-2}$$

L and *D* are the lift and drag accelerations respectively.

$$\begin{cases} L = \frac{1}{2}\rho v^2 \frac{C_L S}{m} \\ D = \frac{1}{2}\rho v^2 \frac{C_D S}{m} \end{cases}$$ **Equation 3-3**

where ρ is the atmospheric density of Mars, C_L and C_D are the lift and drag coefficients respectively; S is the reference area of vehicle and m is the mass of vehicle. The aerodynamic coefficients C_L and C_D are the functions of angle of attack.

Atmospheric density model ρ [39]

$$\rho = \rho_0 \cdot exp\left[-\left(\frac{r - r_M}{h_s}\right)\right]$$ **Equation 3-4**

where ρ_0 is the sea level atmospheric density of Mars, r_M is Mars' radius and h_s is the density scale height.

To improve the efficiency of calculation of numerical optimisation calculation, reducing the difficulty of iterative convergence and avoiding singularity are extremely helpful. A set of dimensionless equations are introduced here to achieve higher performance. To convert the original **Equation 3-1** into a dimensionless form, six dimensionless substitute variables are defined as:

$$\begin{cases} R = \frac{r}{r_M} \\ V = \frac{v}{\sqrt{g_0 r_M}} \\ T = \frac{t}{\sqrt{g_0 / r_M}} \\ \bar{L} = \frac{L}{g_0} \\ \bar{D} = \frac{D}{g_0} \end{cases}$$ **Equation 3-5**

where R is distance from the centre of Mars to the centre of mass of the vehicle

V is the velocity of vehicle

T is time of flight

$\bar{L}$ is lift acceleration

$\bar{D}$ is drag acceleration

g_0 is gravitational acceleration on the surface of Mars

The effects of rotation of Mars, such as Coriolis and Centrifugal acceleration, are ignored in order to simplify the optimal problem, because these accelerations are relatively small compared with aerodynamic accelerations, which are **Equation 3-3**. Hence, **Equation 3-1** are transformed to the dimensionless form.

$$\begin{cases} \dot{R} = V\,sin\,\gamma \\ \dot{V} = -\bar{D} - \dfrac{sin\,\gamma}{R^2} \\ \dot{\theta} = \dfrac{V}{R}\dfrac{cos\,\gamma\,sin\,\psi}{cos\,\lambda} \\ \dot{\lambda} = \dfrac{V}{R}cos\,\gamma\,cos\,\psi \\ \dot{\gamma} = \dfrac{\bar{L}}{V}cos\,\sigma + \left(\dfrac{V}{R} - \dfrac{1}{VR^2}\right)cos\,\gamma \\ \dot{\psi} = \dfrac{\bar{L}}{V}\dfrac{sin\,\sigma}{cos\,\gamma} + \dfrac{V}{R}sin\,\psi\,cos\,\gamma\,tan\,\lambda \end{cases} \quad \textbf{Equation 3-6}$$

Because the initial and terminal conditions are normalised, **Equation 3-6** is now a better formulation of the optimisation problem. The state variable is defined as

$$\boldsymbol{x} = [R, V, \theta, \lambda, \gamma, \psi] \quad \textbf{Equation 3-7}$$

3.2 Path constraints

To achieve the requirements of safety, there are path constraints on an entry trajectory. Typically, the aerodynamic load (a), dynamic pressure (q) and aerodynamic heating rate ($\dot{Q}$) are considered as path constraints. The models of path constraints are given by [39] [40]

Dynamic pressure

To maintain the structural integrity of the entry vehicle, it is necessary to set a constraint on the dynamic pressure *q*, which is calculated by the following equation

$$q = \frac{1}{2}\rho v^2 \qquad \textbf{Equation 3-8}$$

where ρ is defined as **Equation 3-4**

The dynamic pressure must be lower than the maximum tolerance value q_{max} during the entire landing process to guarantee the safety of the entry vehicle. Hence, the path constraints can be illustrated as the following equation

$$q = \frac{1}{2}\rho v^2 \leq q_{max} \qquad \textbf{Equation 3-9}$$

Aerodynamic load

The aerodynamic load model is defined as

$$a = \sqrt{L^2 + D^2} \qquad \textbf{Equation 3-10}$$

where *L* and *D* are lift and drag accelerations respectively (**Equation 3-3**)

Aerodynamic load must meet the requirement of the maximum tolerance aerodynamic load a_{max}, which is shown below

$$a = \sqrt{L^2 + D^2} \leq a_{max}$$ **Equation 3-11**

Heating rate

Heating rate model provided from [39] [41] is shown in the following

$$\dot{Q} = k_q(\rho/r_n)^N v^M$$ **Equation 3-12**

where k_q, N, M are the heating rate parameters.

The maximum allowable heating rate is defined as $\dot{Q}_{max}$. Therefore, the heating rate constraints is described as the following equation

$$\dot{Q} = k_q(\rho/r_n)^N v^M \leq \dot{Q}_{max}$$ **Equation 3-13**

Path Constraints formulation

Three path constraints are formulated as

$$\begin{cases} q = \frac{1}{2}\rho v^2 \leq q_{max} \\ a = \sqrt{L^2 + D^2} \leq a_{max} \\ \dot{Q} = k_q(\rho/r_n)^N v^M \leq \dot{Q}_{max} \end{cases}$$ **Equation 3-14**

3.3 Control limits

On the other hand, there are limits in bank angle control σ_c

$$\sigma_{c,min} \leq \sigma_c(t) \leq \sigma_{c,max}$$ **Equation 3-15**

where $\sigma_{c,min}$ is the minimum controllable bank angle and $\sigma_{c,max}$ is the maximum controllable bank angle.

3.4 Boundary conditions

The initial and terminal conditions are given by the following table

	Initial condition	**Terminal condition**
Time, t	t_0	t_f
Altitude, h	h_0	h_f
Distance, r	r_0	r_f
Velocity, v	v_0	v_f
Longitude, θ	θ_0	θ_f
Latitude, λ	λ_0	λ_f
Flight path angle, γ	γ_0	γ_f
Azimuth angle, ψ	ψ_0	ψ_f
Bank angle, σ	σ_0	σ_f

Table 3-1 Boundary conditions

The subscript *0* and *f* represent the initial time and terminal time respectively. Due to various objectives or purposes, these conditions may be different. The decision of the conditions will be discussed in the later section.

3.5 Mars atmospheric entry problem formulations

In this thesis, two main problems are studied. Each problem is divided into four subproblems with different methods and constraints.

3.5.1 Problem A: Minimum Terminal Velocity (MTV)

MTV is typically a concern and limitation for entry process. The vehicle may be damaged during landing process if the terminal velocity of the entry vehicle is too high. The lower terminal velocity (the velocity at parachutes deployment) can provide more time for the vehicle to decelerate before landing. This problem is divided into four subproblems (**Table 3-2**) and the cost function is defined as

$$J = v_f \qquad \textbf{Equation 3-16}$$

	Path-unconstrained	Path-constrained
IP method	**Problem A-1**	**Problem A-3**
SQP method	**Problem A-2**	**Problem A-4**

Table 3-2 Problem A: Minumum Terminal Velocity (MTV)

In the first two parts, the path constraints (**Equation 3-14**) are ignored.

- ***Problem A-1*: Path-unconstrained MTV problem with IP method**
  Find an optimal trajectory that minimises the terminal state v_f such that **Equation 3-6** and **Equation 3-15** are satisfied by using IP method.

- ***Problem A-2*: Path-unconstrained MTV problem with SQP method**
  Find an optimal trajectory that minimises the terminal state v_f such that **Equation 3-6** and **Equation 3-15** are satisfied by using SQP method.

Similar to problems A-1 and A-2, but the path constraints (**Equation 3-14**) are taken into account.

- ***Problem A-3*: Path-constrained MTV problem with IP method**
  Find an optimal trajectory that minimises the terminal state v_f such that **Equation 3-6**, **Equation 3-14** and **Equation 3-15** are satisfied by using IP method.

- ***Problem A-4*: Path-constrained MTV problem with SQP method**
  Find an optimal trajectory that minimises the terminal state v_f such that **Equation 3-6**, **Equation 3-14** and **Equation 3-15** are satisfied by using SQP method.

3.5.2 Problem B: Minimum Terminal Time (MTT)

MTT is a problem that minimises the time of flight of entry process. In some special cases, flight time is an important factor, so it is significant to study the MTT problem. The cost function is defined as

$$J = t_f \qquad \textbf{Equation 3-17}$$

Similarly, MTT problem is divided into four different cases (**Table 3-3**)

	Path-unconstrained	Path-constrained
IP method	**Problem B-1**	**Problem B-3**
SQP method	**Problem B-2**	**Problem B-4**

Table 3-3 Problem B: Minimum Terminal Time (MTT)

Path constraints are not considered in the first two problems

- ***Problem B-1*: Path-unconstrained MTT problem with IP method**

Find an optimal trajectory that minimises the terminal time t_f such that **Equation 3-6** and **Equation 3-15** are satisfied by using IP method.

- ***Problem B-2*: Path-unconstrained MTT problem with SQP method**
  Find an optimal trajectory that minimises the terminal time t_f such that **Equation 3-6** and **Equation 3-15** are satisfied by using SQP method.

In the following two problems, the path constraints are considered.

- ***Problem B-3*: Path-constrained MTT problem with IP method**
  Find an optimal trajectory that minimises the terminal time t_f such that **Equation 3-6**, **Equation 3-14** and **Equation 3-15** are satisfied by using IP method.

- ***Problem B-4*: Path-constrained MTT problem with SQP method**
  Find an optimal trajectory that minimises the terminal time t_f such that **Equation 3-6**, **Equation 3-14** and **Equation 3-15** are satisfied by using SQP method.

3.6 Structure of optimisation

The procedure of optimisation is illustrated in the following figure

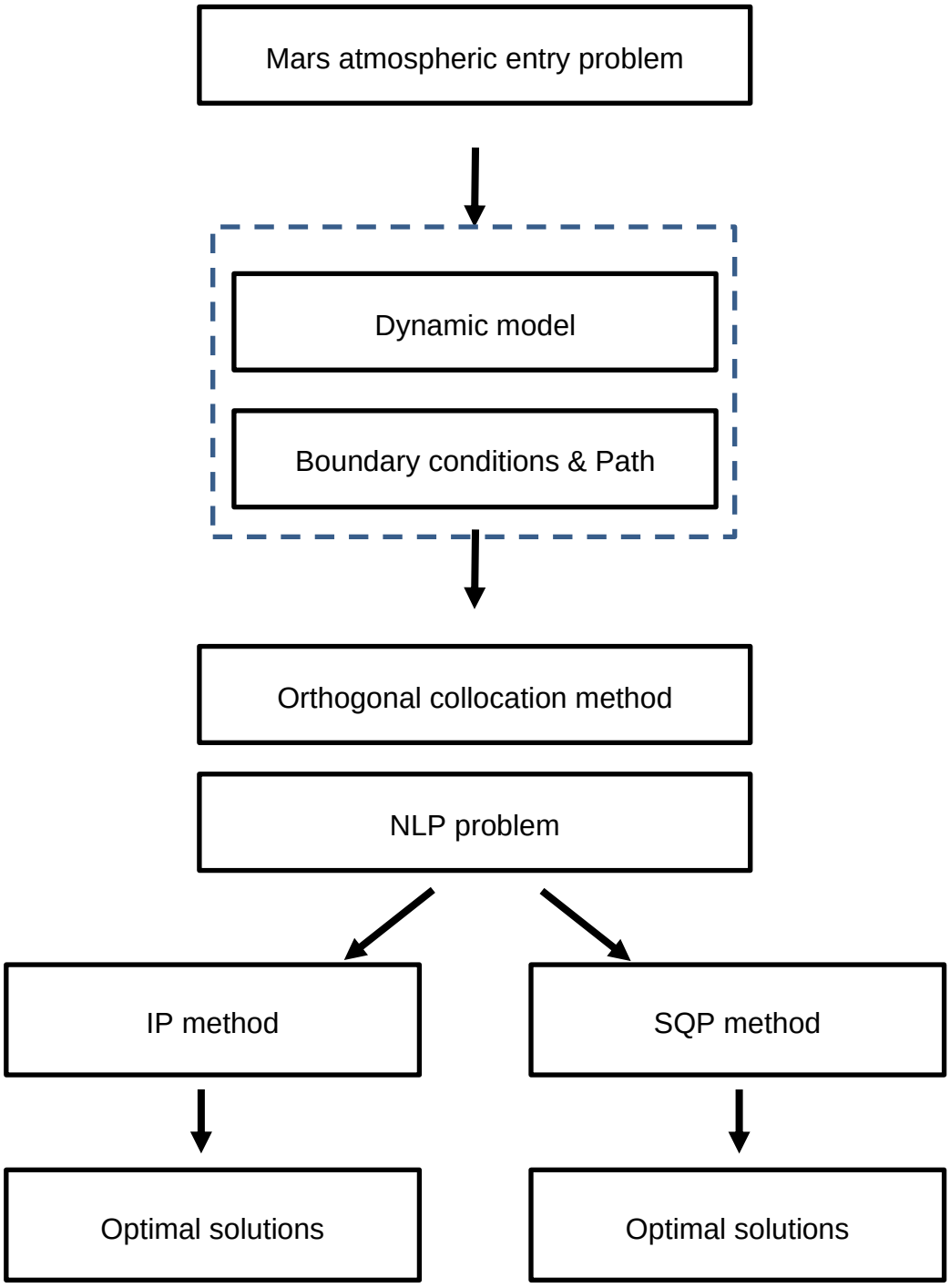

Figure 3-1 Structure of optimisation

4 Orthogonal collocation method

As earlier section mentioned, direction method, which transforms OCP into NLP problem, is chosen for the research. In this thesis, a Matlab package GPOPS-II is utilised and the orthogonal collocation method called *Radau pseudospectral method* is used for collocation. Radau pseudospectral method is a direct transcription method that transforms an OCP into a discrete NLP problem. Legendre-Gauss-Radau (LGR) points is used for collocation of the dynamic constraints, quadrature approximation of the integrated Lagrange cost term.

4.1 OCP description

Both problems mentioned above can be modelled as OCP. Consider an OCP scaled to the time domain $\tau \in [-1, +1]$ that minimises the cost function below

$$J = \phi\big(\boldsymbol{x}(-1), t_0, \boldsymbol{x}(+1), t_f, \big) + \frac{t_f - t_0}{2}\int_{-1}^{1} g\big(\boldsymbol{x}(\tau), \boldsymbol{u}(\tau), \tau;\ t_0, t_f\big)d\tau \qquad \textbf{Equation 4-1}$$

where $t \in [t_0, t_f]$, $\boldsymbol{x}(t) \in \mathbb{R}^n$ is state variable (**Equation 3-7**), $\boldsymbol{u}(t) \in \mathbb{R}^m$ is control variable (**Equation 3-15**), $\phi: \mathbb{R}^n \times \mathbb{R} \times \mathbb{R}^n \times \mathbb{R} \to \mathbb{R}$ and $g: \mathbb{R}^n \times \mathbb{R}^m \times \mathbb{R} \to \mathbb{R}$.

subject to the dynamic constraints

$$\dot{\boldsymbol{x}}(\boldsymbol{\tau}) = \frac{t_f - t_0}{2}\boldsymbol{f}(\boldsymbol{x}(\tau), \boldsymbol{u}(\tau), \tau; t_0, t_f) \qquad \textbf{Equation 4-2}$$

The boundary conditions

$$\phi\big(\boldsymbol{x}(-1), t_0, \boldsymbol{x}(+1), t_f, \big) = \boldsymbol{0} \qquad \textbf{Equation 4-3}$$

and the inequality path constraints

$$\frac{t_f - t_0}{2}\boldsymbol{C}(\boldsymbol{x}(\tau), \boldsymbol{u}(\tau), \tau; t_0, t_f) \leq \boldsymbol{0} \qquad \textbf{Equation 4-4}$$

4.2 Orthogonal collocation

Consider the *N* LGR points, $(\tau_1, \tau_2, \dots, \tau_N)$, where $\tau_1 = -1$ and $\tau_N < +1$. A new point is defined such that $\tau_{N+1} = 1$. It is important to note that $\tau_{N+1} = 1$ is utilised in approximation but is not a LGR point.

Let a Lagrange polynomials of degree *N*

$$L_i(\tau) = \prod_{i=1, j\neq i}^{N+1} \frac{\tau - \tau_j}{\tau_i - \tau_j}, \qquad i = 1,2, \dots, N+1 \qquad \textbf{Equation 4-5}$$

The state variable $\boldsymbol{x}(\tau)$ is approximated via **Equation 4-5** as follow

$$\boldsymbol{x}(\tau) \approx \boldsymbol{X}(\tau) = \sum_{i=1}^{N+1} \boldsymbol{X}_i L_i(\tau) \qquad \textbf{Equation 4-6}$$

Next, an approximation of the derivative of the state in τ domain is given by differentiating the approximation of **Equation 4-6**

$$\dot{\boldsymbol{x}}(\tau) \approx \dot{\boldsymbol{X}}(\tau) = \sum_{i=1}^{N+1} \boldsymbol{X}_i \dot{L}_i(\tau) \qquad \textbf{Equation 4-7}$$

Now the collocation conditions are formed by **Equation 4-2** and **Equation 4-7**

$$\sum_{i=1}^{N+1} \boldsymbol{X}_i \dot{L}_i(\tau_k) = \frac{t_f - t_0}{2} \boldsymbol{f}(\boldsymbol{X}_k, \boldsymbol{U}_k, \tau; t_0, t_f) \qquad \textbf{Equation 4-8}$$

where $k = 1, \dots, N$, $\boldsymbol{X}_k = \boldsymbol{X}(\tau_k)$ and $\boldsymbol{U}_k = \boldsymbol{U}(\tau_k)$

$$\sum_{i=1}^{N+1} \boldsymbol{X}_i D_{ki} = \frac{t_f - t_0}{2} \boldsymbol{f}(\boldsymbol{X}_k, \boldsymbol{U}_k, \tau; t_0, t_f) \qquad \textbf{Equation 4-9}$$

where $D_{ki} = \dot{L}_i(\tau_k)$

The collocation is done by *N* LGR points ($\tau_1, \dots, \tau_N$) and the approximation of state uses *N+1* points ($\tau_1, \dots, \tau_{N+1}$). Hence a non-square matrix ($N \times (N+1)$) called *Radau pseudospectral differentiation matrix* is defined as follow

$$\boldsymbol{D} = [D_{ki}], \;\; 1 \le k \le N, 1 \le i \le N+1 \qquad \textbf{Equation 4-10}$$

Let $\boldsymbol{X}^{LGR} = \begin{bmatrix} \boldsymbol{X}_1 \\ \vdots \\ \boldsymbol{X}_{N+1} \end{bmatrix}$. The collocated dynamics at the *N* LGR points collocation points in **Equation 4-9** can be written as

$$\boldsymbol{D}_k \boldsymbol{X}^{LGR} = \frac{t_f - t_0}{2} \boldsymbol{f}\left(\boldsymbol{X}_k, \boldsymbol{U}_k, \tau; t_0, t_f\right), \;\; k = 1, \dots, N \qquad \textbf{Equation 4-11}$$

and the path constraints in **Equation 4-4** at the *N* LGR collocation points are

$$\frac{t_f - t_0}{2} \boldsymbol{C}\left(\boldsymbol{X}_k, \boldsymbol{U}_k, \tau; t_0, t_f\right) \le \boldsymbol{0}, \;\; k = 1, \dots, N \qquad \textbf{Equation 4-12}$$

Lastly, the cost functional approximated by using LGR quadrature is described as

$$J = \phi(\boldsymbol{X}(\tau_1), \tau_1, \boldsymbol{X}(\tau_{N+1}), \tau_{N+1},) + \frac{t_f - t_0}{2} \sum_{k=1}^{N} w_k g(\boldsymbol{X}_k, \boldsymbol{U}_k, \tau; t_0, t_f) \qquad \textbf{Equation 4-13}$$

where w_k is the quadrature weight associated with k^{th} LGR collocation point

4.3 Mesh refinement

The mesh refinement method used in this research is *hp*-adaptive method. Assume that a trajectory is divided into several segments on the time interval $[t_0, t_f]$. The purpose of *hp*-adaptive method is to determine whether a segment should be divided into more segments and the locations of the new segments, or if the number of collocation points in a segment should be increased. This method improves accuracy with less computational cost and memory. The detail of this method is described in [42].

4.4 NLP problem

Now, the NLP problem corresponding to the *Radau pseudospectral method* is given as follows:

Minimise the cost function

$$J = \phi(\boldsymbol{X}(\tau_1), \tau_1, \boldsymbol{X}(\tau_{N+1}), \tau_{N+1},) + \frac{t_f - t_0}{2} \sum_{k=1}^{N} w_k g(\boldsymbol{X}_k, \boldsymbol{U}_k, \tau; t_0, t_f) \qquad \textbf{Equation 4-14}$$

Subject to the dynamic constraints

$$\boldsymbol{D}_k \boldsymbol{X}^{LGR} - \frac{t_f - t_0}{2} \boldsymbol{f}(\boldsymbol{X}_k, \boldsymbol{U}_k, \tau; t_0, t_f) = \boldsymbol{0} \qquad \textbf{Equation 4-15}$$

The boundary conditions

$$\phi(\boldsymbol{X}(\tau_1), \tau_1, \boldsymbol{X}(\tau_{N+1}), \tau_{N+1},) = \boldsymbol{0} \qquad \textbf{Equation 4-16}$$

and the path constraints

$$\frac{t_f - t_0}{2} \boldsymbol{C}(\boldsymbol{X}_k, \boldsymbol{U}_k, \tau; t_0, t_f) \leq \boldsymbol{0} \qquad \textbf{Equation 4-17}$$

where $k = 1, \dots, N$; the NLP variables are $(\boldsymbol{X}_1, \dots, \boldsymbol{X}_{N+1})$, $(\boldsymbol{U}_1, \dots, \boldsymbol{U}_N)$, t_0 and t_f

Now the discrete Radau pseudospectral approximation of OCP defined in **Equation 4-1** - **Equation 4-4** is transformed into NLP problem defined by **Equation 4-14** - **Equation 4-17.**

Several significant properties of the Radau pseudospectral method given by [43] are addressed in the follows

- The state is approximated using the Lagrange polynomials of degree *N*
- The discretisation points are *N* LGR points plus the final point
- Only *N* LGR points are used for collocation of state dynamics
- Radau pseudospectral differentiation matrix is a non-square matrix

5 Results and Conclusion

From the previous section, the OCP problem is transformed into NLP problem by using orthogonal collocation method. In this chapter, the simulation and the results of solving NLP problem with IP method and SQP method is discussed. This chapter is organised as follows: Parameters and conditions setting for simulations in Matlab. Next, the results of problem A is addressed, and then the comparison of problem A1-4. Later, the results and comparison of problem B is discussed. Finally, the last section contains conclusion.

5.1 Parameters and conditions setting

In this section, the parameters and boundary conditions will be determined for each problem.

Parameters of entry vehicle

Parameters	Value
Entry vehicle mass, m	*2920 kg*
Reference area of entry vehicle, S	*15.9 m^2*
Entry vehicle nose radius. r_n	*0.6 m*

Table 5-1 Parameters of entry vehicle

Parameters of Mars

Parameters	Value
Radius, r_M	*3396.2 km*
Gravitational constant, μ_M	*4.284×10^{13} m^3/s^2*
Density scale height, h_s	*9354 m*
Sea level atmospheric density, ρ_0	*0.0158 kg/m^3*

Table 5-2 Parameters of Mars

Boundary conditions

	Initial condition	Terminal condition
Time, t	*0 s*	*1000 s*
Altitude, h	*125 km*	*7.5 km*
Distance, r	*125+r_M km*	*7.5+r_M km*
Velocity, v	*6000 m/s*	*v_f m/s*
Longitude, θ	*0 deg*	*0 deg*
Latitude, λ	*0 deg*	*0 deg*
Flight path angle, γ	*0 deg*	*0 deg*
Azimuth angle, ψ	*0 deg*	*0 deg*
Bank angle, σ	*-30 deg*	*+30 deg*

Table 5-3 Boundary conditions

v_f is different in each problem and will be determined in the beginning of each problems.

Path constraints and control limit

Parameters	Value
Bank angle Control, σ_c	*$-30 \sim 30$ deg*
Dynamic pressure tolerance, q_{max}	*10000 Pa*
Aerodynamic load factor tolerance, a_{max}	*5 g_{earth}*
Heating rate, $\dot{Q}_{max}$	*70 W/cm^2*

Table 5-4 Path constraints and control limit

where g_{earth} is the earth gravitational acceleration

Parameters of the heating rate model (Equation 3-14)

Parameters	Value
k_q	1.9027×10^{-4}
N	0.5
M	3

Table 5-5 Parameters of the heating rate model

5.2 Results of Problem A (MTV problem)

For MTV problem, v_f is chosen to be a range of 1 m/s and 500 m/s. The minimised objective is terminal velocity v_f, which means that the velocity is reduce to the minimum while the other boundary conditions are satisfied. In the meantime, the value of terminal velocity is lower than the upper bound of v_f. In this section, only part of results is shown. See **5.5Appendix A** for full results and profiles.

5.2.1 Problem A-1 and A-2

The following figures show the results of ***Problem A-1*** and ***Problem A-2***, which are the results of MTV problem without path constraints and are solved by IP method and SQP method respectively.

Results of Problem A-1

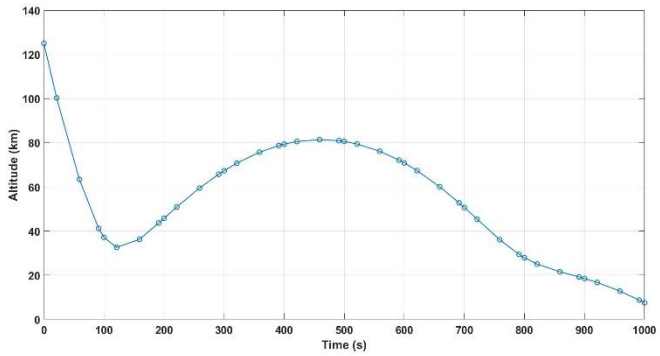

(a)Altitude

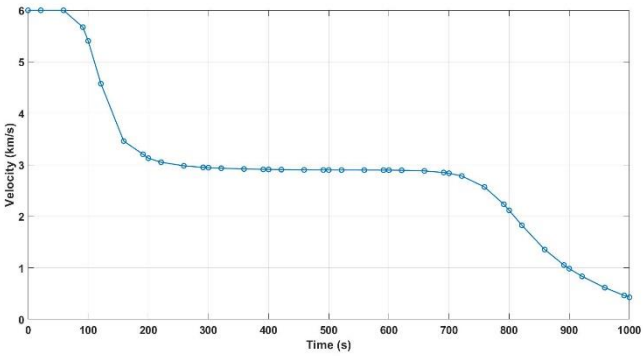

(b) Velocity

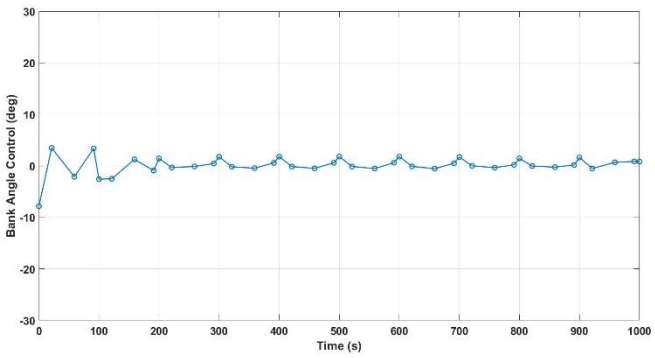

(c) Bank angle control

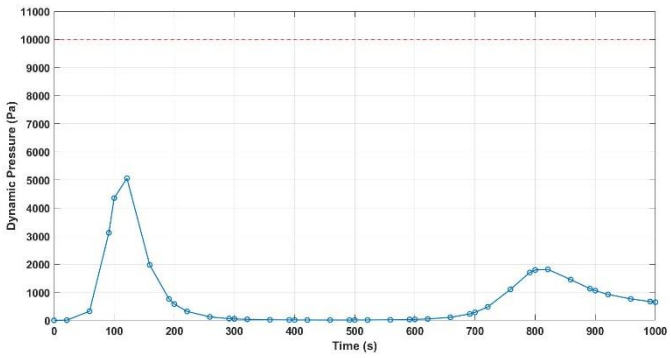

(d) Dynamic Pressure

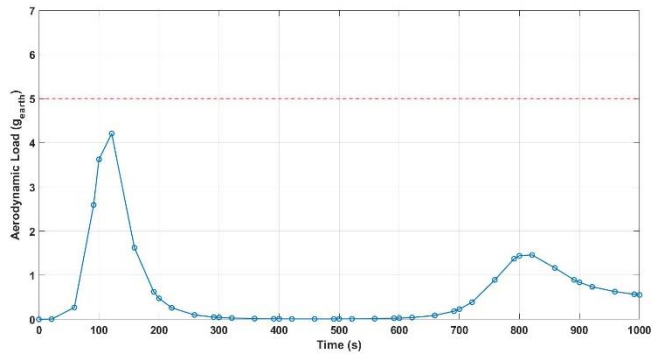

(e) Aerodynamic Load

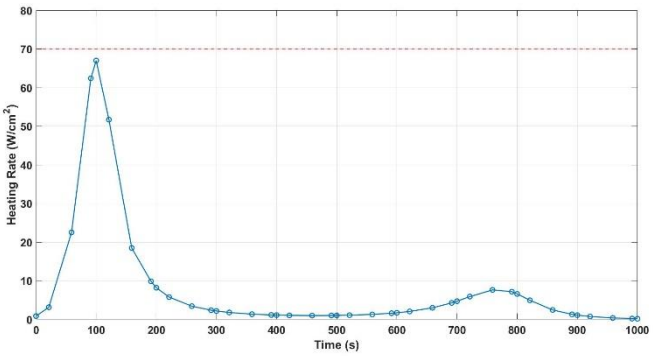

(f) Heating rate

Figure 5-1 Results of Problem A-1

Firstly, **Figure 5-1** is solved by IP method. The terminal conditions are satisfied at terminal time equals to *1,000 seconds*, which is the upper bound of the time variable. This means that the solution is a local optimal solution. The trajectory during the entire entry process is shown in **Figure 5-1(a)** and the terminal altitude *7.5 km* is achieved at *1000 seconds*. The optimal objective, terminal velocity *427.54 m/s,* is within the given range of v_f. This trajectory is performed by a small bank angle control (**Figure 5-1(c)**), with the maximum angle of *3.46 degrees* and minimum angle of *-7.83 degrees*. In terms of the path constraints, which is not involved in the calculation process, all three values are lower than the maximum tolerance values. The peak values of dynamic pressure, aerodynamic load and heating rate are *5,057 Pa*, *4.2* g_{earth} and *67* W/cm^2, respectively. The first two values are way below the maximum tolerance values, while the last one is close to the maximum tolerance value.

Results of Problem A-2

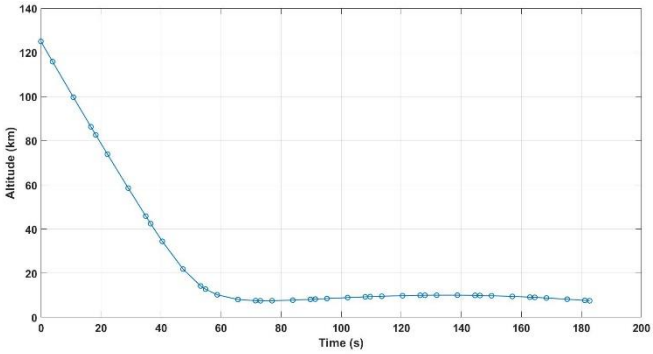

(a)Altitude

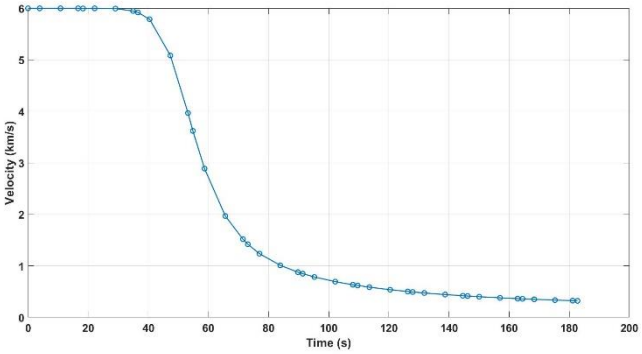

(b) Velocity

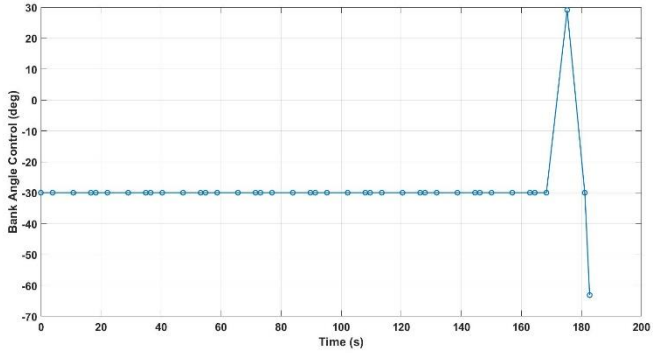

(c) Bank angle control

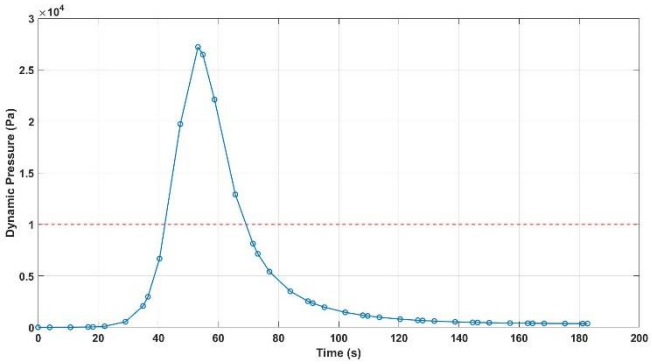

(d) Dynamic Pressure

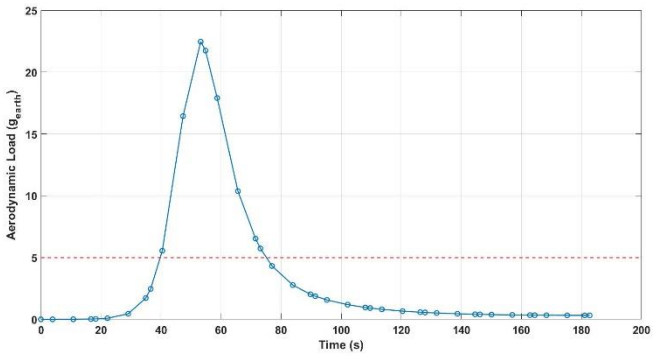

(e) Aerodynamic Load

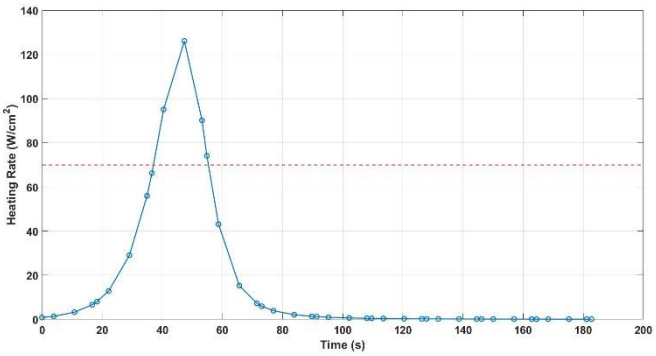

(f) Heating rate

Figure 5-2 Results of Problem A-2

Next, **Figure 5-2** shows that the results of ***Problem A-2*** is a global optimal solution. Time of flight of *182.7 seconds* is performed, with terminal velocity of *320.6 m/s* (**Figure 5-2(b)**). The altitude rapidly decreases by *110 km* in the first

60 seconds. The control mode (**Figure 5-2(c)**) maintains almost 0 bank angle control at the beginning of entry process. At *175 seconds*, about *30 degrees* of control is utilised and followed by a *-63 degrees* control, which is out of the boundary condition of control. Moreover, the values of three path constraints are not satisfied. Although the terminal is minimised, the trajectory is unacceptable due to the three path constraints.

Comparison of Problem A-1 and Problem A-2

Comparing these two results, ***Problem A-1*** solved with IP method converges to a local optimum, and ***Problem A-2*** solved with SQP method converges to a global optimum. Although SQP performs a better solution in the aspect of terminal velocity and terminal time, the dynamic pressure, aerodynamic load and heating rate are way beyond the tolerance values. On the other hand, IP method produces a trajectory that requires longer entry time and is less smooth. However, it satisfies all the path constraints and boundary conditions. Hence, IP method is more suitable in this case.

5.2.2 Problem A-3 and A-4

In this section, a comparison between ***Problem A-3*** and ***Problem A-4*** is addressed. **Figure 5-3** and **Figure 5-4** show a part of the results of ***Problem A-3*** and ***Problem A-4*** respectively.

Results of Problem A-3

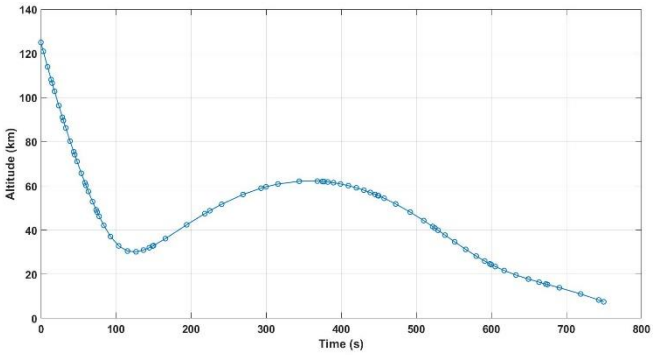

(a)Altitude

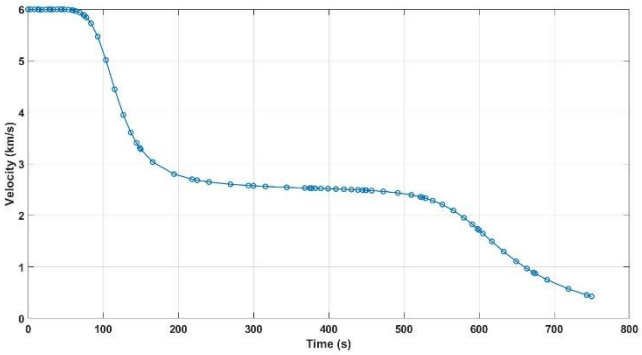

(b) Velocity

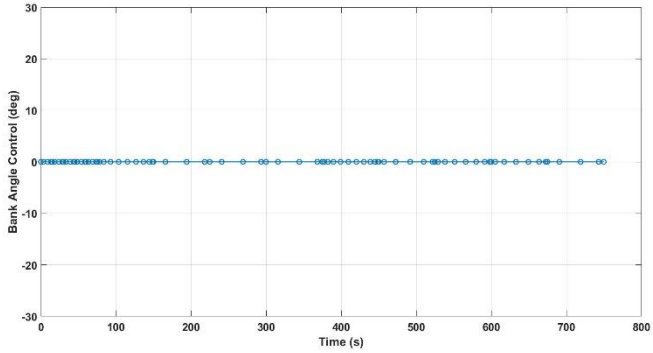

(c) Bank angle control

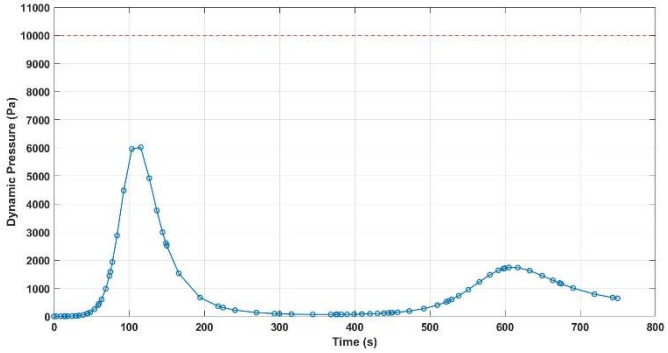

(d) Dynamic Pressure

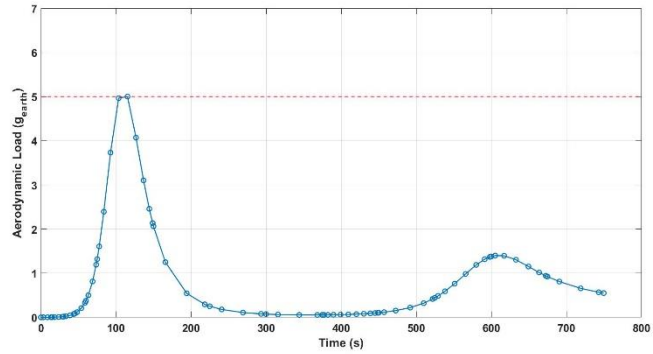

(e) Aerodynamic Load

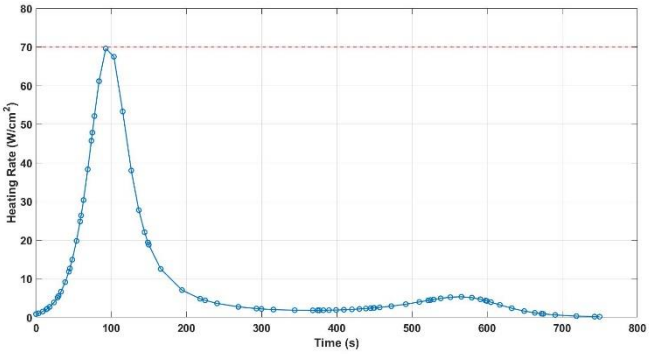

(f) Heating rate

Figure 5-3 Results of Problem A-3

In the ***Problem A-3***, IP method is utilised and converges to a global optimal solution. The terminal altitude is *7.5 km* and the terminal time is *749.6 second*. In terms of terminal velocity, *425.8 m/s* is achieved. Bank angle control is given in **Figure 5-3(c)** which is nearly *0 degree*. According to this control, the bank angle

during the entire entry process is barely changed (**5.5A.3**). On the other hand, we can see that all the path constraints (**Figure 5-3(e)(f)(g)**) are satisfied. The peak value of the dynamic pressure is *6,013 Pa* at *115.3 seconds*. Although the peak values of the heating rate (*69.6 W/cm^2*) is marginally below the constraints, it is in the tolerance range. However, the aerodynamic load reaches *5 g_{earth}* at *115.3 seconds*, this may be a potential risk during the entry process.

Results of Problem A-4

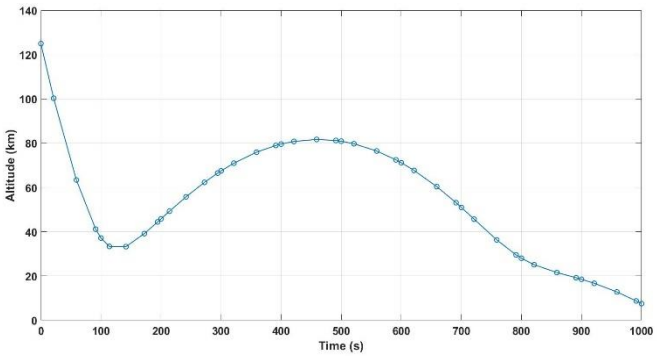

(a)Altitude

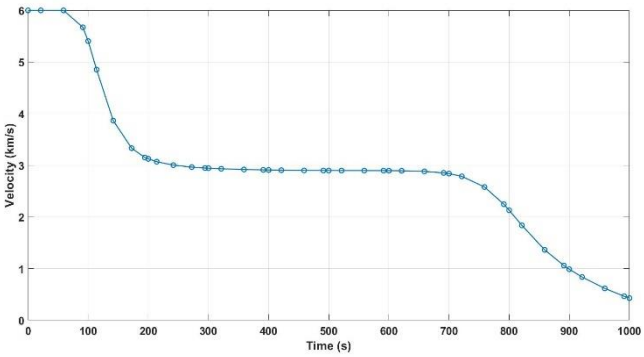

(b) Velocity

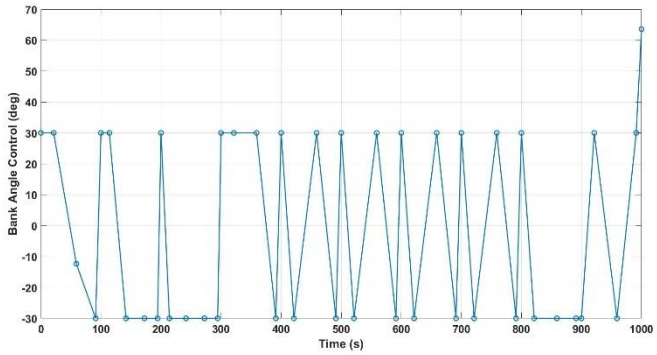

(c) Bank angle control

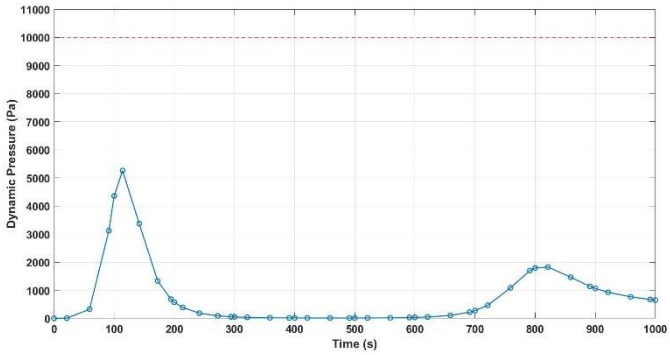

(d) Dynamic Pressure

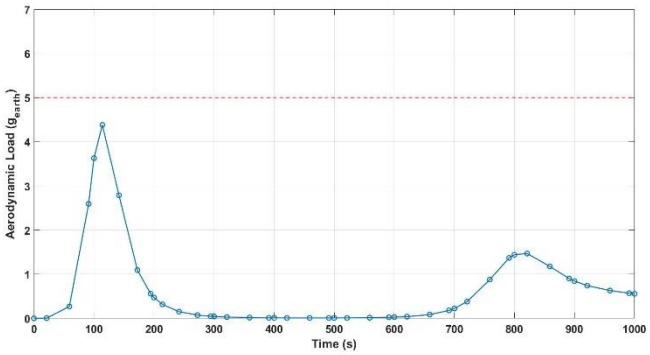

(e) Aerodynamic Load

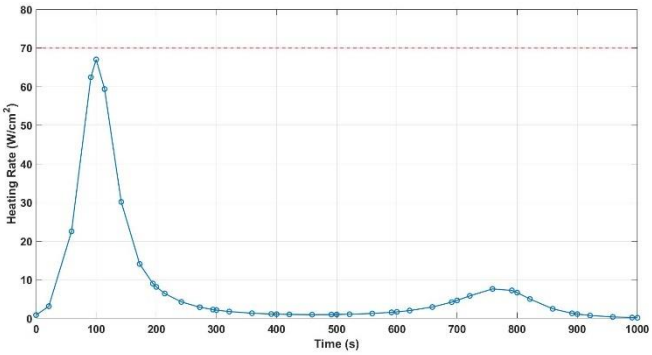

(f) Heating rate

Figure 5-4 Results of Problem A-4

Figure 5-4 shows the results of ***Problem A-4***. The results converge to a local optimal solution, since the terminal time is *1,000 second*. The objective, terminal velocity, 428 m/s is shown in **Figure 5-4(b)**. To achieve this trajectory, Bang-Bang Control is performed and illustrated in **Figure 5-4(c)**. However, at the end of the entry process, a control of 63.5 degrees is required. The path constraints are all satisfied the tolerance values. The peak value of q (*5,260 Pa*) is largely below the tolerance value. The greatest aerodynamic load during entry process is *4.38* g_{earth} while the maximal heating rate is *67* W/cm^2. Another key point is that this solution is similar to the solution of ***Problem A-1***.

Comparison of Problem A-3 and Problem A-4

Comparing ***Problem A-3*** with ***Problem A-4***, the former is solved with IP method and converges to a global optimal solution, while the latter is solved with SQP method and converges to a local optimum. The entry trajectory of IP method is marginally smoother than that of SQP method. In terms of the objective terminal velocity, IP method produces a slightly lower terminal velocity than SQP method, approximately 2 m/s difference. Furthermore, the terminal time of IP method is largely shorter than SQP method. Even though the values of q, a and $\dot{Q}$ of the IP method are higher than those of SQP method, they are still in an acceptable range. In this case, IP method produces a better solution than SQP method in

terms of terminal velocity and terminal time. However, SQP produced a safer trajectory due to the heating rate and aerodynamic load.

5.2.3 Comparison of Problem A

Among all the results of ***Problem A***, it is clear that the terminal velocities are around *430 m/s,* except for ***Problem A-2***. However, the time of flight are totally different in each problem. Two of them converge to local optimal solutions, and the others converge to global optimal solutions. With regards to bank angle control, the results show the similar control modes apart from the last problem. Both control results of SQP method require a large angle control at the end of the entry process. On the other hand, a comparison of four results in terms of path constraints are shown below (see **5.5A.5** for full results). It is noticeable that all the peaks of constraints are reached around *120 seconds*. As former section mentioned, the values of path constraints of ***Problem A-1*** and ***Problem A-4*** are nearly identical. Concerning all the path constraints and boundary conditions, only the solution of ***Problem A-2*** is not feasible. The aerodynamic load of ***Problem A-3*** may be a risk, while the bank angle control of ***Problem A-4*** does not satisfy the bank control condition at the end of entry process. Hence, the solution obtained from ***Problem A-1*** is more feasible than the others.

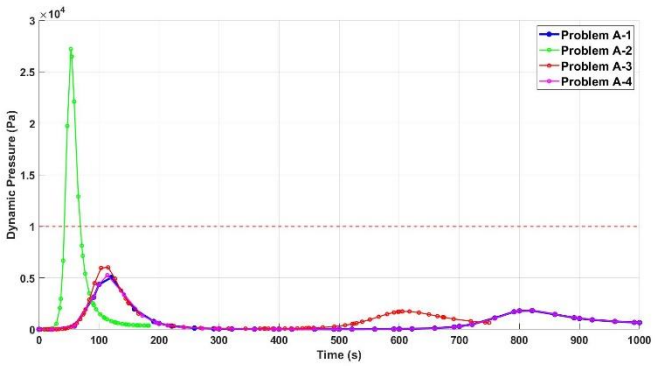

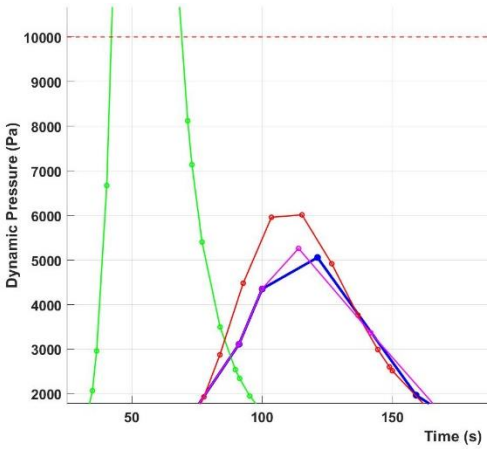

(e) Dynamic Pressure

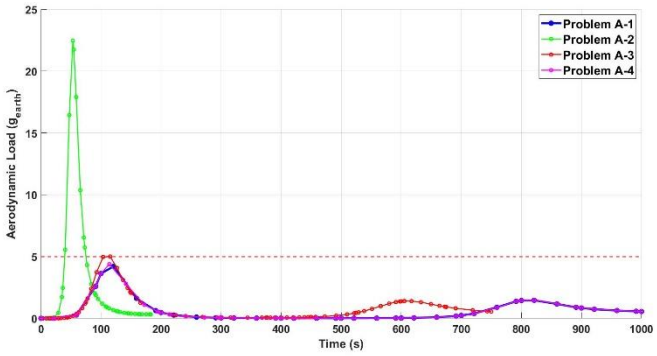

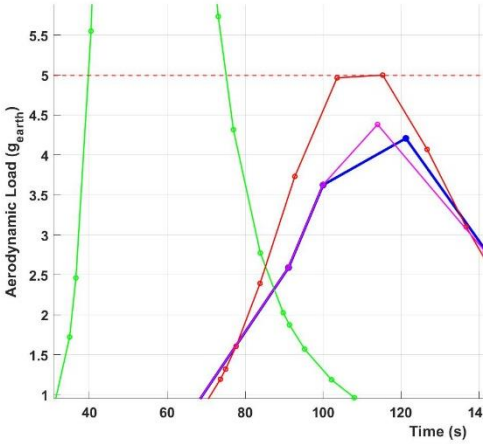

(f) Aerodynamic Load

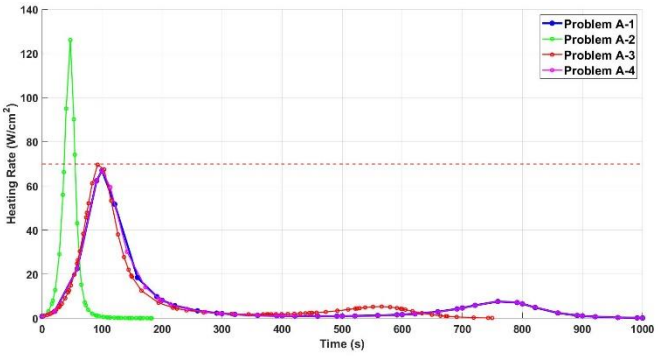

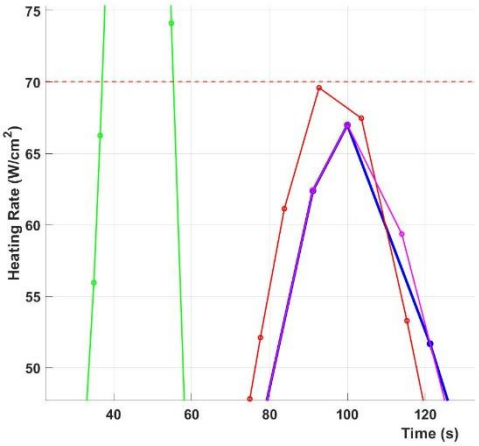

(g) Heating rate

Figure 5-5 Comparison of path constraints of Problem A

5.3 Results of Problem B (MTT problem)

In this section, the MTT problem is discussed. The minimised objective is terminal time t_f. Similarly, the value of terminal time is reduced to the minimum and is lower than the given t_f, which means that vehicle spends the least time to achieve all terminal conditions. The purpose of this problem is to find the minimal time that vehicle reaches the given v_f. In this case, the value of v_f is chosen to be *400 m/s*. In other words, the problem is to minimise the time that vehicle deaccelerates from *6000 m/s* to *400 m/s* while all conditions and constraints are satisfied. In this section, only part of results is shown. See **5.5Appendix B** for full results and profiles.

5.3.1 Problem B-1 and B-2

The following figures show the results of ***Problem B-1*** and ***Problem B-2***, which are solved without path constraints.

Results of Problem B-1

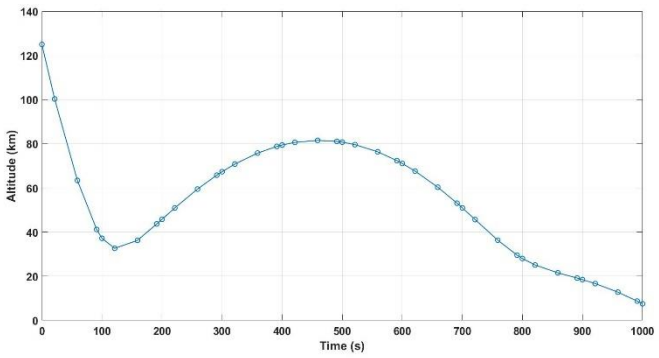

(a)Altitude

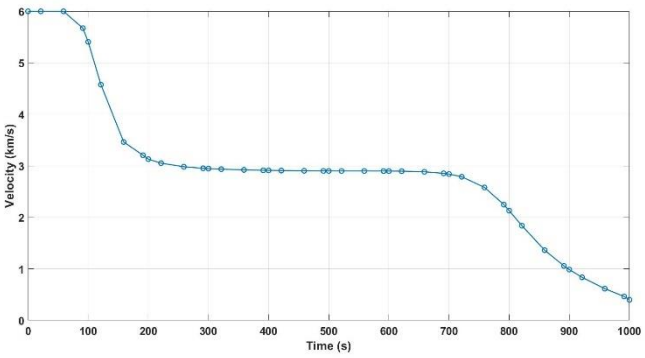

(b) Velocity

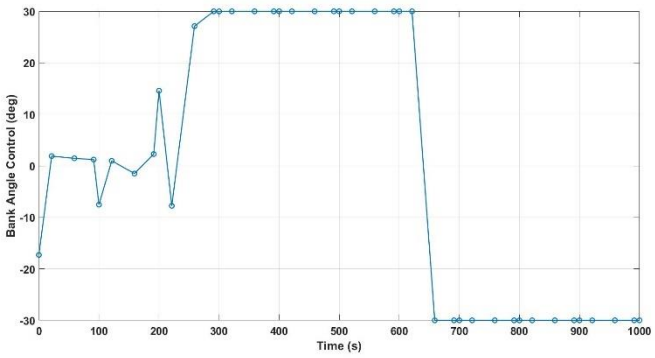

(c) Bank angle control

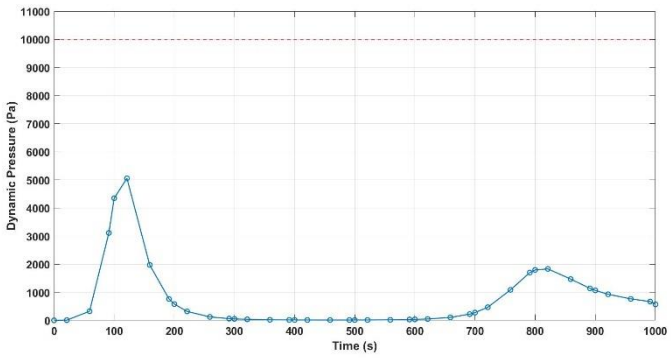

(d) Dynamic Pressure

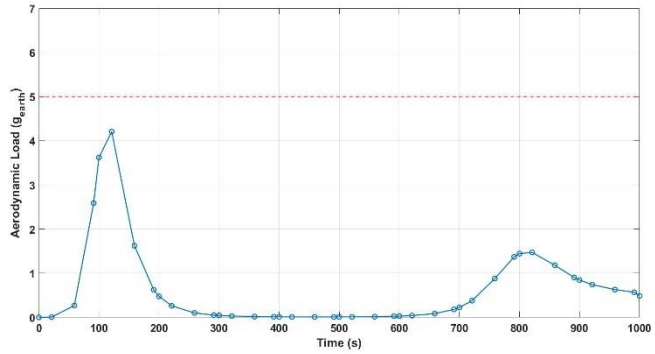

(e) Aerodynamic Load

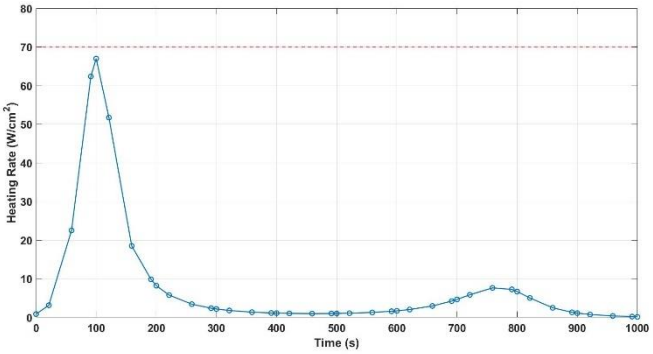

(f) Heating rate

Figure 5-6 Results of Problem B-1

According to **Figure 5-6**, a local optimal solution is achieved. The velocity of vehicle reduces to *400 m/s* at the upper bound of terminal time *1000 seconds*, while all other conditions are satisfied. The velocity of entry vehicle (**Figure 5-6(b)**) maintains around *3000 m/s* in the middle of entry process, and the corresponding bank angle control is shown in **Figure 5-6(c)**. There is a fluctuation of bank control at the beginning of entry process, and it turns into more stable mode after *291 seconds*. This is about the time that vehicle decreases deceleration, while the altitude is increasing. In the meantime, all three path constraints are satisfied in this problem.

Results of Problem B-2

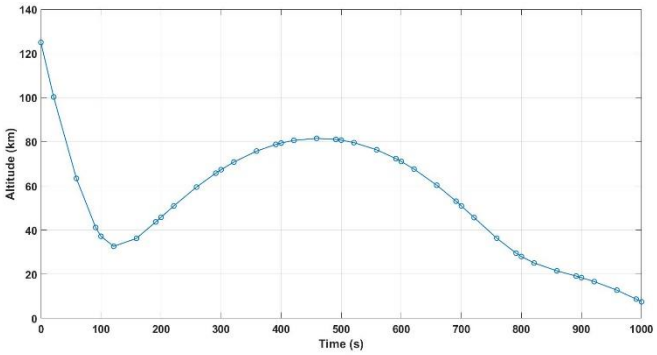

(a)Altitude

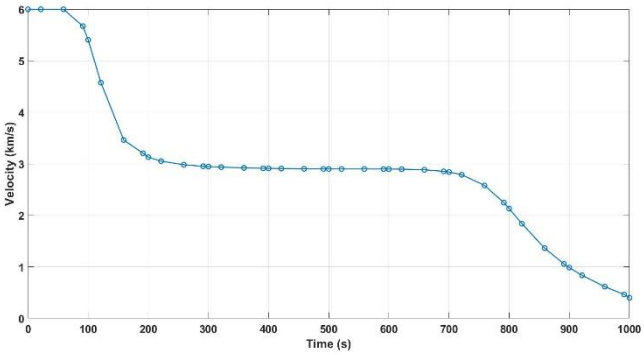

(b) Velocity

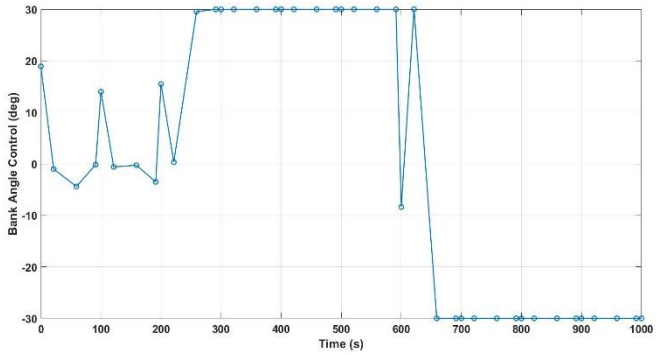

(c) Bank angle control

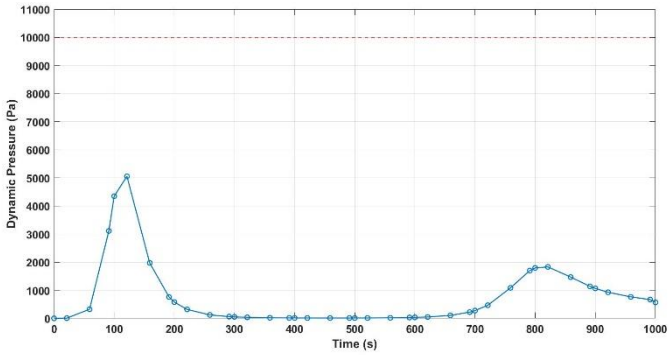

(d) Dynamic Pressure

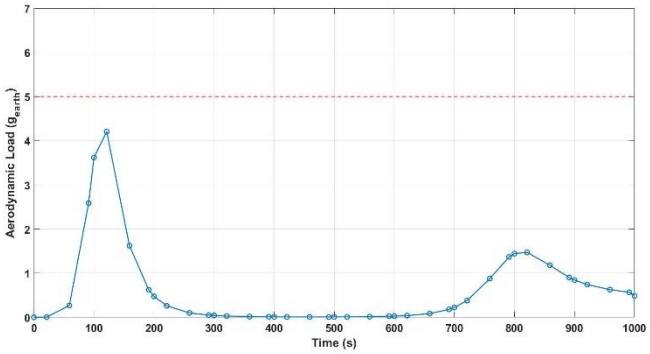

(e) Aerodynamic Load

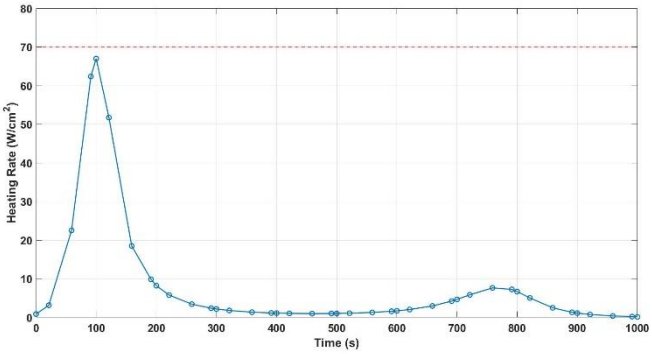

(f) Heating rate

Figure 5-7 Results of Problem B-2

Figure 5-7 is the results of ***Problem B-2***. We can see that these figures are extremely similar to **Figure 5-6**, except bank angle control (**Figure 5-7(c)**). However, a similar pattern can be seen. The peak values of dynamic pressure,

aerodynamic load and heating rate are approximately *5,055 Pa*, *4.2* g_{earth} and *67* W/cm^2 respectively, which are all allowable.

Comparison of Problem B-1 and Problem B-2

A comparison of ***Problem B-1*** and ***Problem B-2*** is shown in the figures below. The difference of these two problems is that the methods used are different. However, the solutions of these two problems are almost identical. The most obvious differences are bank angle control (**Figure 5-8(a)**), which leads the variety in bank angle (**Figure 5-8(b)**).

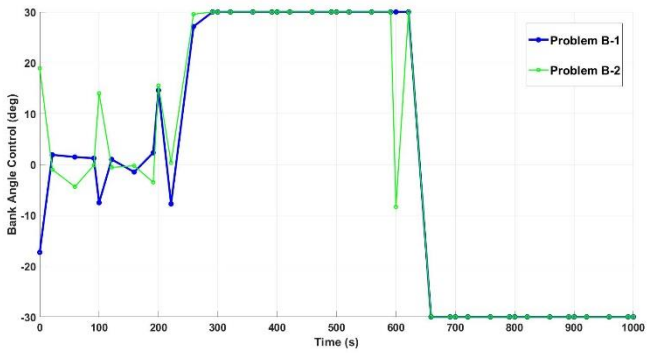

(a) Bank angle control

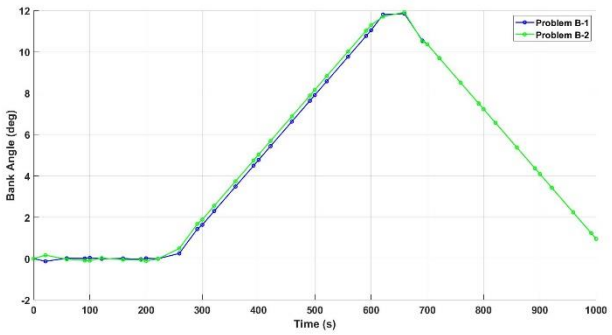

(b) Bank angle

Figure 5-8 Comparison of bank angle and control of Problem B-1 and B-2

At the beginning, it is clear that the bank controls are performed in contrary directions, but the same pattern is shown from *291 seconds*. However, at *600 seconds*, SQP method performs an opposite direction control and then returns to the same as IP method. This causes a slightly difference in the bank angle during the latter entry process.

In this case, both IP method and SQP method produce feasible solutions. The terminal times, trajectories, velocities and path constraints during the entire entry process are almost identical. The variety of bank angles do not have any significant effect on the final results.

5.3.2 Problem B-3 and B-4

Results of Problem B-3

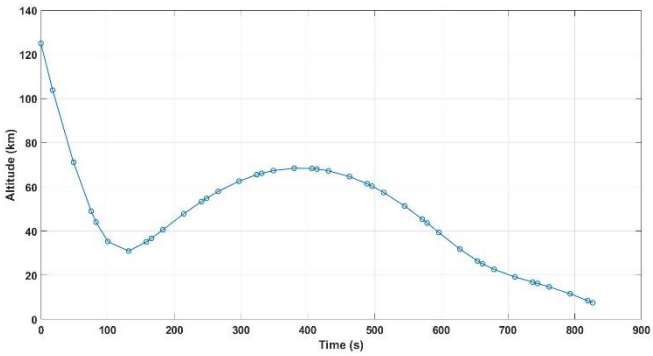

(a)Altitude

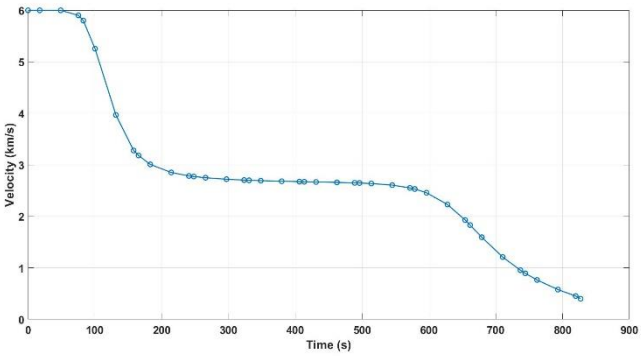

(b) Velocity

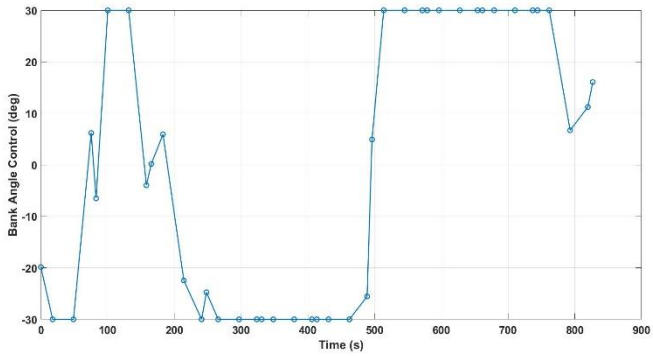

(c) Bank angle control

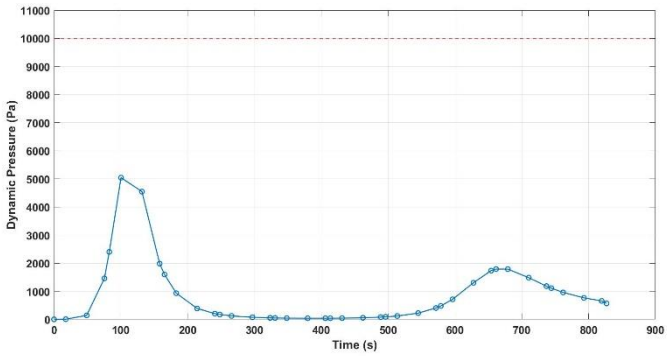

(d) Dynamic Pressure

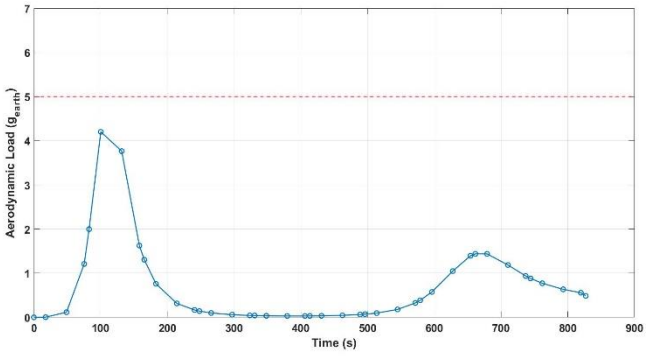

(e) Aerodynamic Load

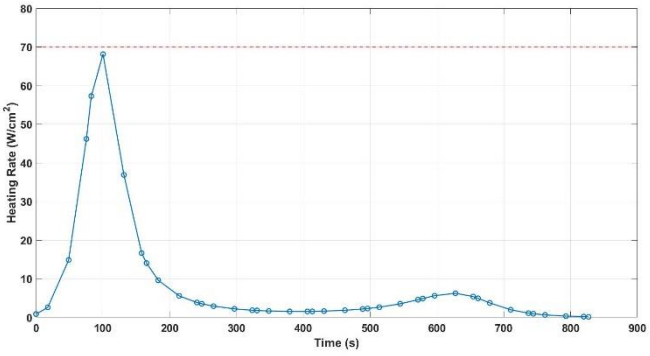

(f) Heating rate

Figure 5-9 Results of problem B-3

Figure 5-9 shows the results of ***Problem B-3***, which is a global optimal solution. The objective terminal time is minimised to *826.8 seconds,* while the other conditions are satisfied. According to **Figure 5-9(b)**, the velocity maintains around *2600 m/s*, which is slightly lower than the velocities obtained from ***Problem B-1*** and ***Problem B-2***, from *266* to *579 seconds*. In terms of bank angle control mode, Bang Bang control is utilised with some small fluctuations. All the path constraints are satisfied in this case. The peak values of dynamic pressure (*5042.2 Pa*) and aerodynamic load (*4.2* g_{earth}) are largely below the maximal tolerance values, while heating rate (*68.1* W/cm^2) is close to the maximal allowable value.

Results of Problem B-4

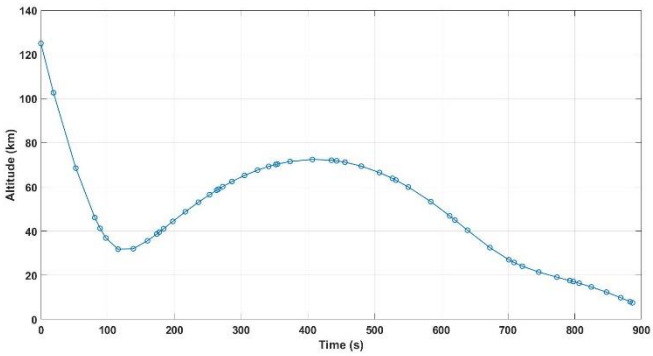

(a)Altitude

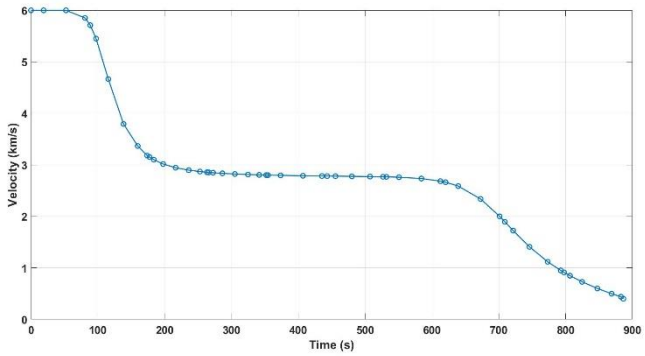

(b) Velocity

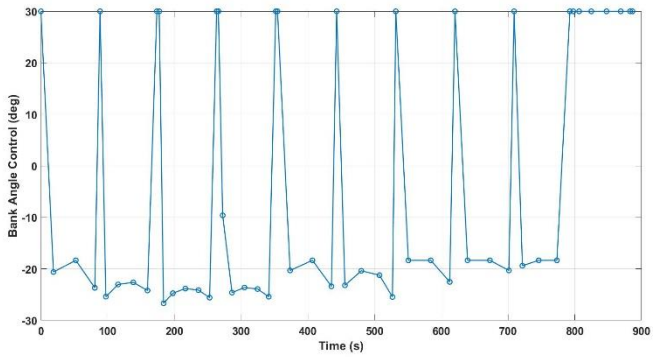

(c) Bank angle control

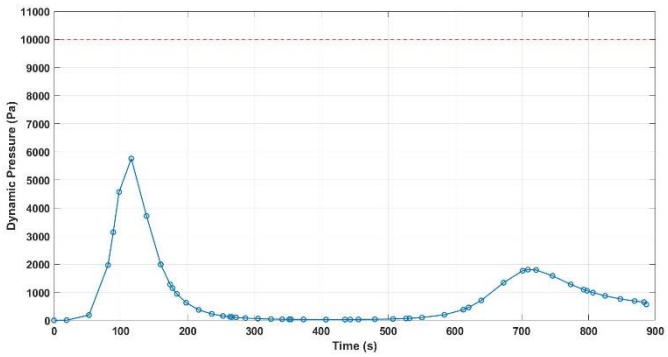

(d) Dynamic Pressure

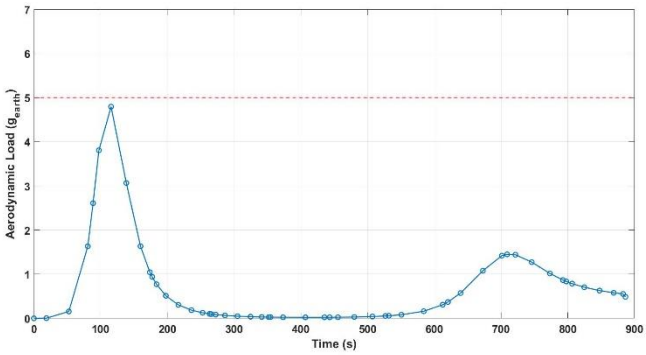

(e) Aerodynamic Load

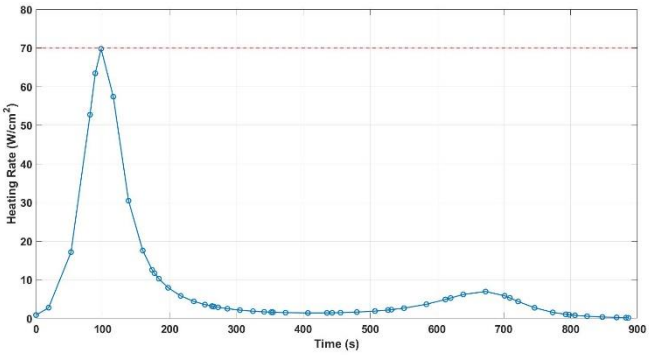

(f) Heating rate

Figure 5-10 Results of Problem B-4

The results of ***Problem B-4*** are shown in **Figure 5-10**, and a global optimal solution is achieved. All the terminal conditions are met at *886.4 seconds*. The velocity maintains the same pattern as the previous ones. In terms of bank angle control, Bang Bang control is performed during the entire entry process, which is completely different from the control in ***Problem B-3***. Concerning the path constraints, a low dynamic pressure value of *5,759 Pa* can be seen from **Figure 5-10(d)**. However, the *4.8* g_{earth} of aerodynamic load and *69.8 W/cm*^{2} of heating rate almost reach the maximal tolerance values.

Comparison of Problem B-3 and Problem B-4

Both solutions of these problems are global optimal solutions. In the aspect of terminal time, IP method performs better than SQP method, approximately *60 second* shorter. From **Figure 5-9(a)** and **Figure 5-10(a)**, the trajectory obtained from the former one is slightly smoother than the latter, as well as the curve of velocity. On top of that, all three peak values of the path constraints of ***Problem B-3*** are evidently lower than another. Hence, IP method produces a better solution in this case.

5.3.3 Comparison of Problem B

As the previous section mentioned, the results obtained from ***Problem B-1*** and ***Problem B-2*** converge to local optimal solutions and are nearly identical, while the other two converge to global optimal solutions. In terms of trajectory, **Figure 5-11(a)** shows that the trajectory of ***Problem B-3*** is the smoothest among all problems. Moreover, the terminal time is the shortest. According **Figure 5-11(b)**, the velocity of ***Problem B-3*** are the lowest during the middle of entry process. Unlike ***Problem A***, small angle control is not shown in this problem. All the control modes are similar to Bang Bang control, and some fluctuations can be seen in the controls. **Figure 5-11(c)(d)(e)** shows a comparison of the three path constraints, all the constraints are satisfied in each problem. The peak values of path constraints of ***Problem B-1***, ***B-2*** and ***B-3*** are close, while the peak values of ***Problem B-4*** are much higher than the others. Hence, the solution of ***Problem B-3*** is the most feasible in this case due to the terminal time, as well as the other conditions.

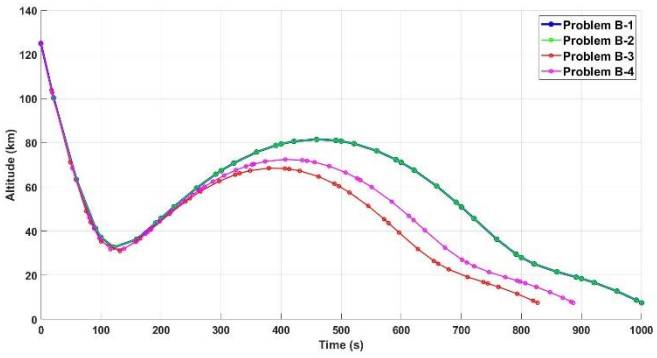

(a)Altitude

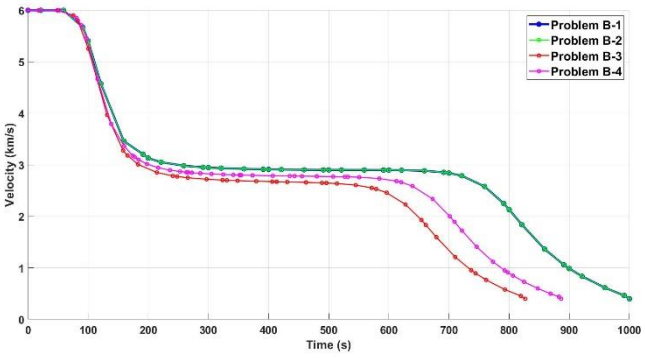

(b) Velocity

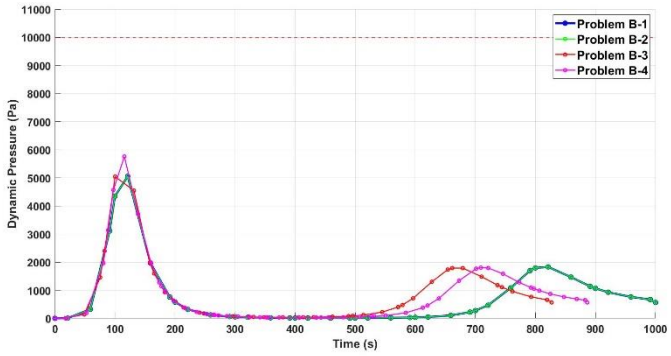

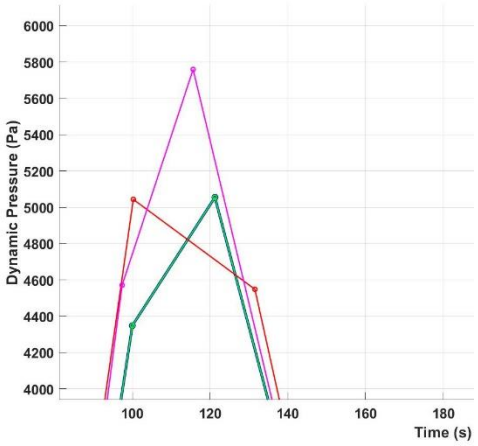

(c) Dynamic Pressure

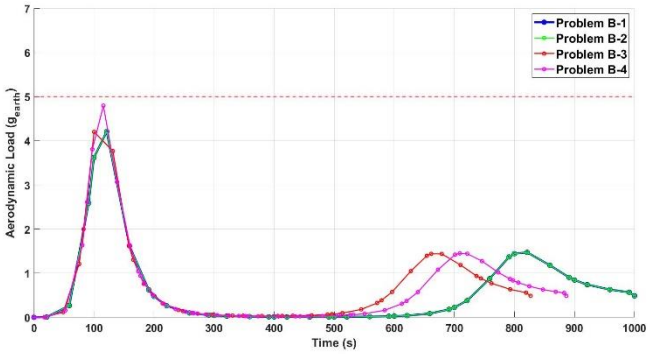

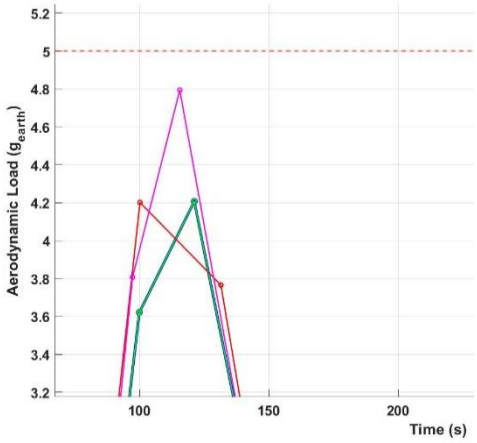

(d) Aerodynamic Load

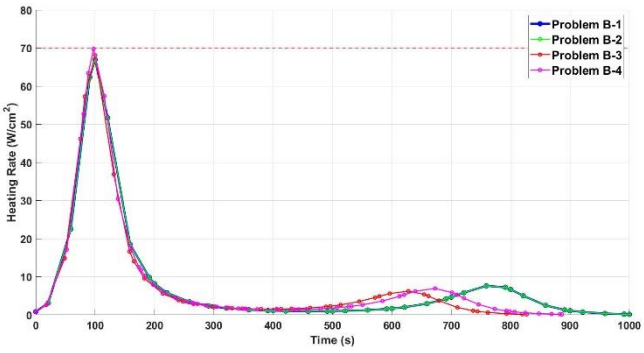

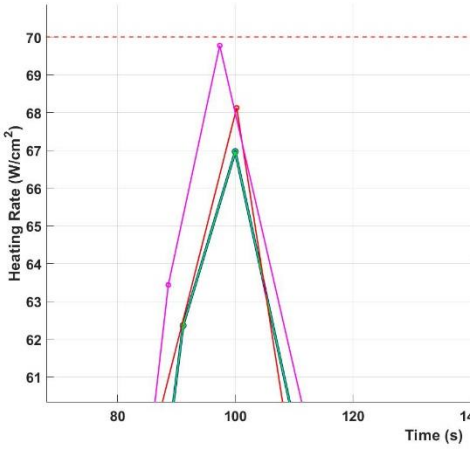

(e) Heating rate

Figure 5-11 Comparison of Problem B

5.4 Conclusion

In this thesis, Mars atmospheric entry trajectory optimisation problems with minimum terminal and minimum terminal time are investigated. The optimisation problems are transformed into NLP problems and are solved by IP method and SQP method respectively. The tables below show the brief results of all problems.

	Problem A-1	***Problem A-2***	***Problem A-3***	***Problem A-4***
terminal time (s)	1,000	182.7	749.6	1,000
terminal velocity (m/s)	427.54	320.6	425.8	428
control mode	small angle control	small angle control	small angle control	Bang Bang Control
dynamic pressure (Pa)	5,057	27,215	6,013	5,260
aerodynamic load (g_{earth})	4.2	22.5	5	4.38
heating rate (W/cm^2)	67	126	69.6	67

Table 5-6 Data of Problem A

	Problem B-1	***Problem B-2***	***Problem B-3***	***Problem B-4***
terminal time (s)	1000	1000	826.8	886.4
terminal velocity (m/s)	400	400	400	400
control mode	Bang Bang Control with fluctuation	Bang Bang Control with fluctuation	Bang Bang Control with fluctuation	Bang Bang Control
dynamic pressure (Pa)	5,054.79	5,054.78	5,042.2	5,759
aerodynamic load (g_{earth})	4.2	4.2	4.2	4.8
heating rate (W/cm^2)	67	67	68.1	69.8

Table 5-7 Data of Problem B

Although the objectives of ***Problem A*** and ***B*** are different, similar results can be seen in each problem, especially the curves of trajectories, velocities and path constraints. It is noticeable that the path constraints are satisfied in some path-unconstrained problems. In addition, the solutions in path-unconstrained problems may be better than path-constrained ones. Both IP method and SQP method provide feasible solutions in each problem. The terminal time in ***Problem B-3*** is relatively short, and the velocity is also satisfied the parachute deployment velocity. Moreover, the path constraints are way below the maximal tolerance values. Hence, the most suitable solution is the results of ***Problem B-3*** in the aspect of terminal time and velocity.

5.5 Future work

There are several ways to continue this work. The analysis of minimum terminal velocity and minimum terminal time with two different NLP solver has been completed. However, the other terminal conditions or path constraints can also be optimised objective, which is not studied in this thesis. The changing of the boundary conditions may influence the resulting trajectory largely. The control limit of bank angle is a crucial point to study, because of the variety of control systems. Also, control of angle of attack is an alternative way to achieve mission requirements. This has not been studied a lot. On the other hand, the resulting trajectory can be used in guidance system design. The feasibility of reference trajectories provided in this thesis has not been tested yet. In terms of OCP, there are still number of methods to solve OCP. Comparing different methods is also an important work. A new method may be developed during this study.

REFERENCES

[1] Li, Shuang, Jiang, Xiuqiang, "Review and prospect of guidance and control for Mars atmospheric entry," *In Progress in Aerospace Sciences,* 2014.

[2] Martin, Miguel San, Mendeck, Gavin F., Brugarolas, Paul B., Singh, Gurkirpal, Serricchio, Frederick, Lee, Steven W., Wong, Edward C., Essmiller, John C., "In-flight experience of the Mars Science Laboratory Guidance, Navigation, and Control system for Entry, Descent, and Landing," *An Official Journal of the Council of European Aerospace Societies,* vol. 7, no. 2, pp. 119-142, 2015.

[3] Wong, T. J., and Slye, R. E., ""The Effect of Lift on Entry Corridor Depth and Guidance Requirements for the Return Lunar Flight," NASATR-R-80, Ames Research Center, 1961.

[4] Robert D. Braun, Robert M. Manning, "Mars Exploration Entry, Descent, and Landing Challenges," *Journal of Spacecraft and Rockets,* pp. 310-323, 2007.

[5] Zhao, Jisong and Li, Shuang, "Mars atmospheric entry trajectory optimization with maximum parachute deployment altitude using adaptive mesh refinement," *Acta Astronautica,* pp. 401-413, 2019.

[6] Cerimele, Christopher J, Lafleur, Jarret M, "Angle of Attack Modulation for Mars Entry Terminal State Optimization," in *AIAA Atmospheric Flight Mechanics Conference*, Chicago, 2009.

[7] G.L. Jacob, G. Neeler, R.V. Ramanan, "Mars entry mission bank profile optimization," *Journal of Guidance, Control, and Dynamics,* vol. 37, no. 4, pp. 1305-1316, 2014.

[8] J. T. Betts, "Survey of numerical methods for trajectory," *Journal of Guidance, Control, and Dynamics.,* pp. 193-207, 1998.

[9] J.M. Lafleur, C.J. Cerimele, "Mars entry bank profile design for terminal state optimization," *Spacecr. Rocket,* vol. 48, no. 6, pp. 1012-1024, 2011.

[10] M.J. Grant, G.F. Mendeck, "Mars Science Laboratory entry optimization using particle," *AIAA Atmospheric Flight Mechanics Conference and Exhibit,* 2007.

[11] B. A. Conway, "A Survey of Methods Available for the Numerical Optimization of Continuous Dynamic Systems," *JOURNAL OF OPTIMIZATION THEORY AND APPLICATIONS. 152(2):271-306,* 2012.

[12] Philip E. Gill, Walter Murray, Michael A. Saunders, "SNOPT: An SQP Algorithm for Large-Scale Constrained Optimization," *SIAM Review,* vol. 47, no. 1, pp. 99-131, 2005.

[13] Wächter, Andreas, Biegler, Lorenz T., "On the Implementation of an Interior-Point Filter Line-Search Algorithm for Large-Scale Nonlinear Programming," *Mathematical Programming,* vol. 106, no. 1, pp. 25-57, 2006.

[14] Jiang, Xiuqiang and Li, Shuang, "Mars atmospheric entry trajectory optimization via particle swarm optimization and Gauss pseudo-spectral method," *Journal of Aerospace Engineering,* pp. 2320-2329, 2016.

[15] Michael Grant, Gavin Mendeck, "Mars Science Laboratory Entry Optimization Using Particle Swarm Methodology," *AIAA Atmospheric Flight Mechanics Conference and Exhibit,* 2007.

[16] Rahimi, Afshin, Kumar, Krishna Dev, Alighanbari, Hekmat, "Particle Swarm Optimization Applied to Spacecraft Reentry Trajectory," *Journal of Guidance, Control & Dynamics,* vol. 36, no. 1, pp. 307-310, 2013.

[17] Benson A, Thorvaldsen T and Rao V., "Direct trajectory optimization and co-state estimation via an orthogonal collocation method," *Journal of Guidance, Control, and Dynamics,* vol. 29, pp. 1435-1440, 2006.

[18] H. GT, "Advancement and analysis of a Gauss," *PhD Dissertation,* 2007.

[19] Jain, S., Tsiotras, P., Zhou, H.-M., "A Hierarchical Multiresolution Adaptive Mesh Refinement for the Solution of Evolution PDEs," *SIAM JOURNAL ON SCIENTIFIC COMPUTING,* vol. 31, no. 2, pp. 1221-1248, 2010.

[20] J. Zhao, S. Li, "Modified multiresolution technique for mesh refinement in numerical optimal control," *Journal of Guidance, Control, and Dynamics,* vol. 40, no. 12, pp. 3328-3338, 2017.

[21] R. Fletcher and S. Ley, "Nonlinear programming without a penalty function," *Mathematical Programming,* vol. 91, no. 2, pp. 239-269, 2002.

[22] A. W• achter and L. T. Biegler., "Line search filter methods for nonlinear programming: Motivation and global convergence," Department of Chemical Engineering, Carnegie Mellon University, 2003.

[23] A. Forsgren, P. E. Gill, and M. H. Wright, "Interior methods for nonlinear optimization," *SIAM Review,* vol. 44, no. 4, pp. 525-597, 2002.

[24] H. Y. Benson, D. F. Shanno, and R. J. Vanderbei, "Interior-point methods for nonconvex nonlinear programming: Filter methods and merit functions," Operations Research and Financial Engineering, Princeton University, 2000.

[25] R. B. Wilson, "A Simplicial Method for Convex Programming," Ph.D. thesis, Harvard University, 1963.

[26] C. Zhu, R. H. Byrd, P. Lu, and J. Nocedal, "L-BFGS-B—Fortran subroutines for large-scale bound constrained optimization," *ACM Trans.Math.Soft ware,* pp. 550-560, 1997.

[27] L. T. Biegler, J. Nocedal, and C. Schmid, "A reduced Hessian method for large-scale constrained optimization," *SIAM Journal on Optimization ,* pp. 314-347, 1995.

[28] S. K. Eldersveld, "Large-Scale Sequential Quadratic Programming Algorithms," Ph.D. thesis, Department of Operations Research, Stanford University, Stanford, 1991.

[29] I.-B. Tjoa, L. T. Biegler, "Simultaneous solution and optimization strategies for parameter estimation of differential algebraic equation systems," *Industrial & Engineering Chemistry Research,* vol. 30, pp. 376-385, 1991.

[30] R. S. Dembo, S. C. Eisenstat, andT. Steihaug, "Inexact Newton methods," *SIAM Journal on Numerical Analysis,* vol. 19, pp. 400-408, 1982.

[31] A. Bondarenko, D. Bortz, and J. J. Mor´e,, "COPS: Large-Scale Nonlinearly Constrained Optimization Problems," Technical Report ANL/MCS-TM-237, Mathematics and Computer Science division, Argonne National Laboratory, 1998.

[32] I. Bongartz, A. R. Conn, N. I. M. Gould, and Ph. L. Toint,, "CUTE: Constrained and unconstrained testing environment," *ACM Trans.Math.Soft ware,* vol. 21, pp. 123-160, 1995.

[33] Cui, Pingyuan, Zhao, Zeduan, Yu, Zhengshi, Dai, Juan, "Terminal altitude maximization for Mars entry considering uncertainties," *Acta astronautica,* vol. 145, pp. 446-455, 2018.

[34] Li, Shuang, Peng, Yuming, "Mars entry trajectory optimization using DOC and DCNLP," *In Advances in Space Research ,* vol. 47, no. 3, pp. 440-452, 2011.

[35] M.A. Patterson, A.V. Rao,, "a MATLAB software for solving multiple-phase optimal control problems using hp-Adaptive Gaussian quadrature collocation methods and sparse nonlinear programming," *ACM Trans. Math Software,* vol. 41, no. 1, pp. 1-37, 2014.

[36] A.D. Steltzner, A.M.S. Martin, T.P. Rivellini, A. Chen, D. Kipp, Mars Science, "Mars Science Laboratory entry, descent, and landing system development challenges," *spacecraft and rockets,* vol. 51, no. 4, pp. 994-1003, 2014.

[37] M. Smirnova, "Mars transportation vehicle concept," *Acta Astronaut,* vol. 103, pp. 250-256, 2014.

[38] N. X. Vinh, "Optimal Trajectories in Atmospheric Flight," Elsevier, 1981.

[39] Yiyu Zheng, Hutao Cui, Yuanhang Ai, "Indirect Trajectory Optimization for Mars Entry with Maximum Terminal Altitude," *JOURNAL OF SPACECRAFT AND ROCKETS,* vol. 54, no. 5, 2017.

[40] Joel Benito, Kenneth D. Mease, "Reachable and Controllable Sets for Planetary Entry and Landing," *JOURNAL OF GUIDANCE, CONTROL, AND DYNAMICS,* vol. 33, no. 3, 2010.

[41] Sutton, K., Graves, R. A.,, "AGeneral Stagnation-Point Convective-Heating Equation for Arbitrary Gas Mixtures," NASA, 1971.

[42] Darby, C. L., Hager, W. W., and Rao, A. V., "An hp–Adaptive Pseudospectral Method for Solving," vol. 32, no. 4, pp. 476-502, 2011.

[43] D. GARG, "ADVANCES IN GLOBAL PSEUDOSPECTRAL METHODS FOR OPTIMAL CONTROL," 2011.

[44] NASA Ames Research Center and ELORET Corporation, Co-Optimization of Mid Lift to Drag Vehicle Concepts for Mars Atmospheric Entry, Chicago, 2010.

APPENDICES

Appendix A Full results of Problem A

A.1 Full results of Problem A-1

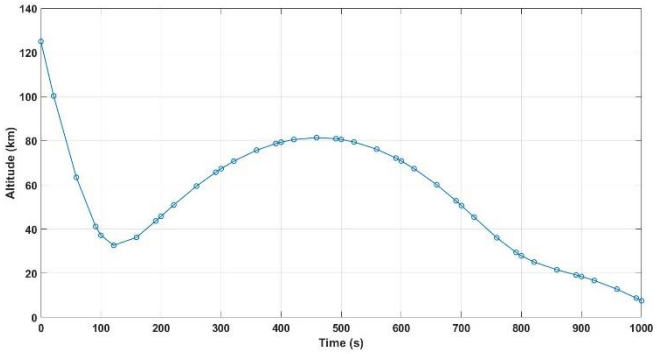

(a)Altitude

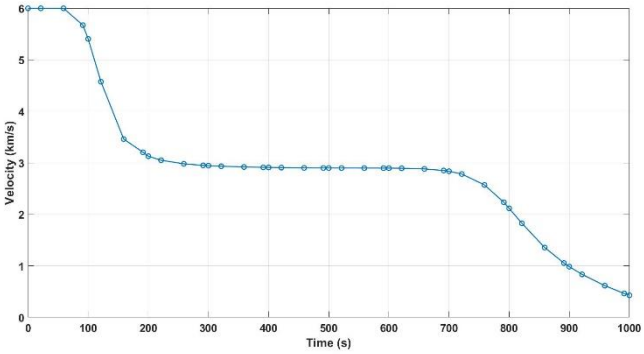

(b) Velocity

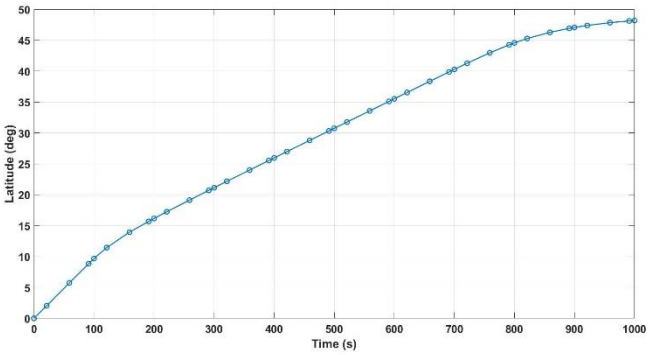

(c) Latitude

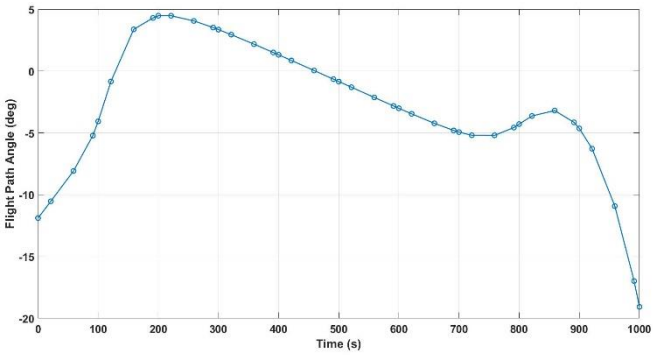

(d) Flight path angle

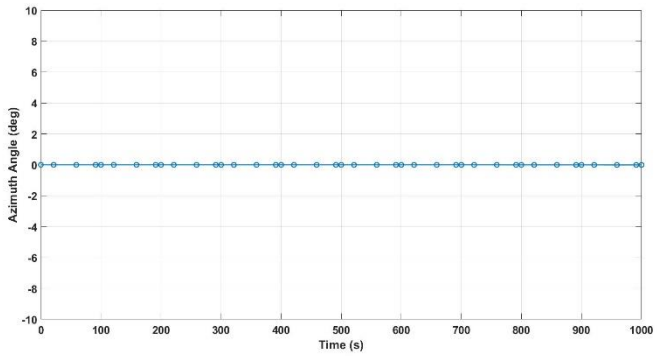

(e)Azimuth angle

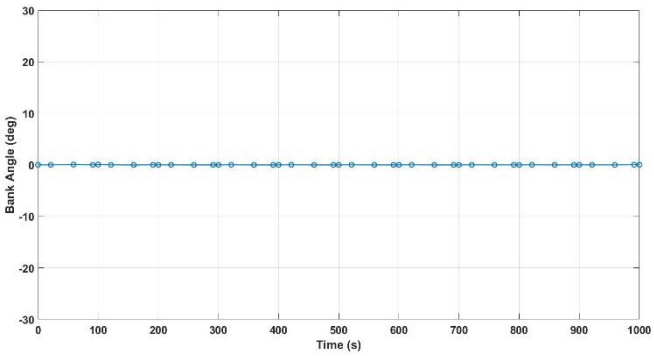

(f) Bank angle

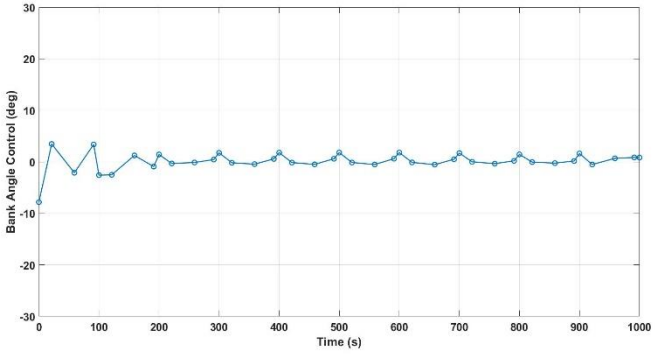

(g) Bank angle control

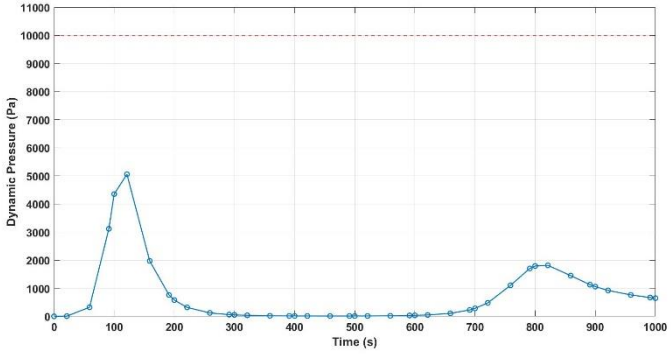

(h) Dynamic Pressure

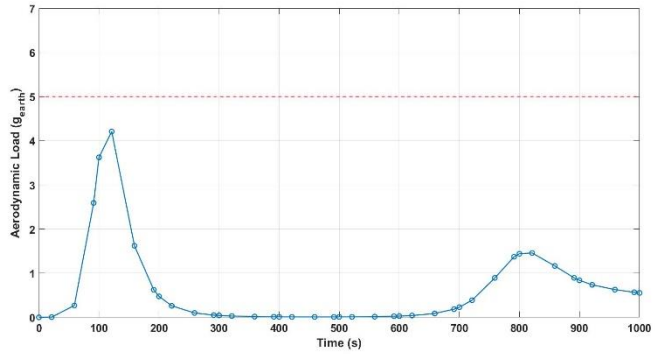

(i) Aerodynamic Load

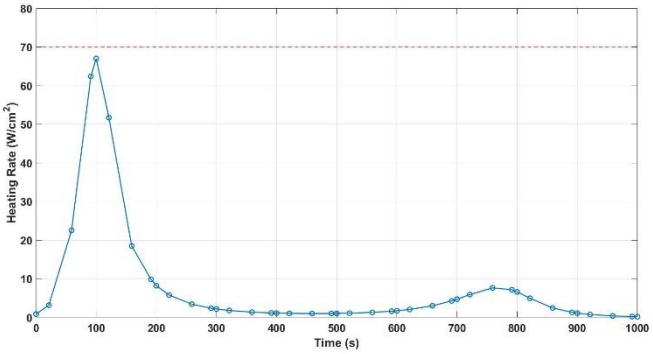

(j) Heating rate

Figure A-1 Full results of Problem A-1

t (sec)	h (km)	v (km/s)	λ (deg)	γ (deg)	ψ (deg)	σ (deg)	σ_c (deg)	q (Pa)	a (g_{earth})	$\dot{Q}$ (W/cm^2)
0	125	6	0	-11.8883	0	0	-7.83025	0.44703	0.000372	0.836143
21.23405	100.274	6	2.038777	-10.5287	-1.3E-05	-0.01513	3.457805	6.285391	0.005212	3.135294
59.05331	63.39615	6	5.737778	-8.07437	0.000109	0.053154	-2.11602	323.9856	0.268556	22.50998
91.1412	41.17685	5.672759	8.84876	-5.21138	0.000163	-0.00666	3.369608	3114.773	2.591188	62.38951
100	37.14686	5.40629	9.671041	-4.06421	6.16E-05	0.059518	-2.58499	4352.55	3.624732	66.98542
121.2341	32.61614	4.574026	11.4363	-0.83744	0.000811	-0.00346	-2.5208	5057.058	4.208764	51.68397
159.0533	36.21048	3.461354	13.9396	3.376869	-0.00033	-0.02747	1.240987	1972.022	1.621907	18.48237
191.1412	43.666	3.204867	15.68219	4.300841	-0.00077	0.005298	-0.92275	761.8856	0.624765	9.848604
200	45.76704	3.128265	16.15926	4.479871	-0.00073	-0.01496	1.420512	579.866	0.475027	8.186164

221.2341	50.90575	3.049884	17.24586	4.47982	-0.00079	-0.0064	-0.32284	318.2028	0.260584	5.76406
259.0533	59.44993	2.980988	19.1302	4.0602	-0.00085	-0.02379	-0.1255	121.9444	0.09991	3.408876
291.1412	65.74963	2.95063	20.70305	3.52587	-0.00092	-0.01517	0.43478	60.92337	0.049941	2.360648
300	67.32199	2.945263	21.13407	3.359547	-0.00092	-0.01185	1.739973	51.30974	0.042066	2.158528
321.2341	70.75864	2.934014	22.16449	2.949742	-0.00092	0.002318	-0.18184	35.26279	0.028916	1.775793
359.0533	75.71993	2.920076	23.99036	2.181556	-0.00094	-0.01978	-0.44284	20.55105	0.016855	1.342812
391.1412	78.73362	2.912024	25.53289	1.507818	-0.00096	-0.01793	0.565233	14.80859	0.012145	1.133591
400	79.37005	2.910275	25.95793	1.319315	-0.00097	-0.01168	1.78227	13.81794	0.011332	1.093703
421.2341	80.54743	2.906697	26.97565	0.864758	-0.00097	0.003504	-0.14557	12.15376	0.009967	1.02321
459.0533	81.42345	2.902259	28.78538	0.047695	-0.00099	-0.0189	-0.48963	11.03344	0.009047	0.971935
491.1412	80.93467	2.900045	30.3191	-0.64986	-0.00101	-0.01805	0.594875	11.60757	0.009518	0.995382
500	80.60007	2.899639	30.74238	-0.8428	-0.00102	-0.0112	1.793908	12.02693	0.009862	1.012919
521.2341	79.44614	2.898934	31.75688	-1.30531	-0.00103	0.004334	-0.1325	13.59939	0.01115	1.07658
559.0533	76.1622	2.898225	33.56395	-2.12729	-0.00105	-0.01836	-0.5159	19.30971	0.01583	1.282217
591.1412	72.14906	2.897156	35.09763	-2.81885	-0.00108	-0.01816	0.60253	29.63336	0.024284	1.587245
600	70.84457	2.896574	35.5211	-3.00805	-0.00109	-0.01108	1.791678	34.05428	0.027903	1.700846
621.2341	67.37813	2.894	36.53598	-3.45619	-0.0011	0.004771	-0.10998	49.2427	0.040327	2.041633
659.0533	60.05135	2.881598	38.34129	-4.2228	-0.00115	-0.01774	-0.54347	106.8526	0.087369	2.981735
691.1412	52.8023	2.850864	39.86388	-4.79786	-0.00124	-0.01974	0.499786	227.0052	0.1852	4.253836
700	50.66355	2.836281	40.28108	-4.93439	-0.00128	-0.01369	1.696941	282.4105	0.230217	4.696223
721.2341	45.37893	2.78262	41.27071	-5.19148	-0.0013	0.002439	0.001035	478.2423	0.38895	5.882223
759.0533	36.07176	2.570336	42.96006	-5.1974	-0.00147	-0.01231	-0.34926	1103.673	0.892408	7.624473
791.1412	29.37841	2.233912	44.25055	-4.56673	-0.00204	-0.01426	0.195614	1705.126	1.371989	7.158466
800	27.89909	2.115881	44.57169	-4.28345	-0.00225	-0.01223	1.438956	1791.801	1.44058	6.583201
821.2341	25.02025	1.82543	45.27028	-3.6292	-0.0024	0.000624	-0.04899	1814.257	1.458185	4.930484
859.0533	21.55021	1.355323	46.27174	-3.19154	-0.0028	-0.01213	-0.24931	1449.318	1.163609	2.429279
891.1412	19.20176	1.053906	46.91348	-4.1426	-0.00389	-0.0123	0.156695	1126.463	0.894372	1.295006
900	18.50401	0.983376	47.06505	-4.63724	-0.00409	-0.01102	1.617754	1056.693	0.83779	1.092002

921.2341	16.69739	0.834294	47.38687	-6.27613	-0.00442	-0.00489	-0.51965	922.6272	0.736305	0.734447
959.0533	12.77574	0.614996	47.83951	-10.9179	-0.00554	-0.01202	0.677768	762.448	0.627805	0.362793
991.1412	8.717634	0.463785	48.12114	-16.9809	-0.00534	0.024707	0.852028	669.1316	0.567231	0.193285
1000	7.5	0.427543	48.1842	-19.0731	-0.00416	0.028841	0.833234	647.6955	0.553311	0.161605

Table A-1 Profile of Problem A-1

A.2 Full results of Problem A-2

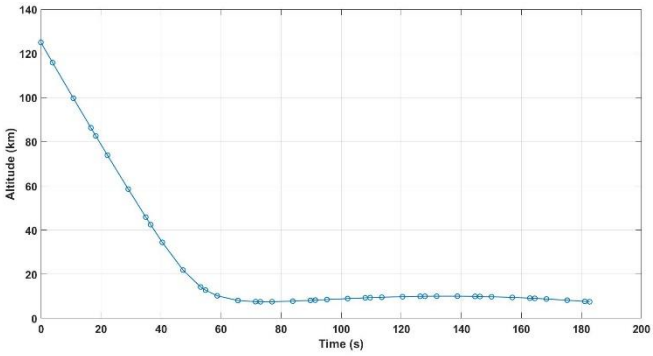

(a)Altitude

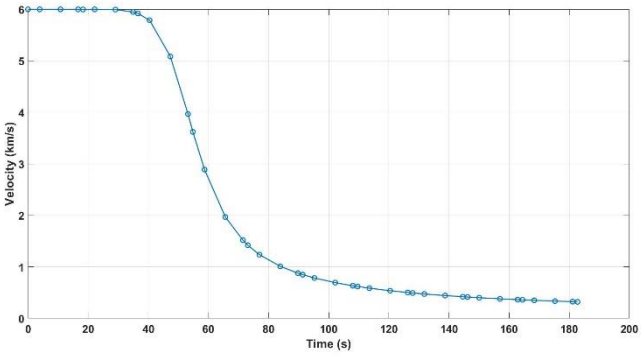

(b) Velocity

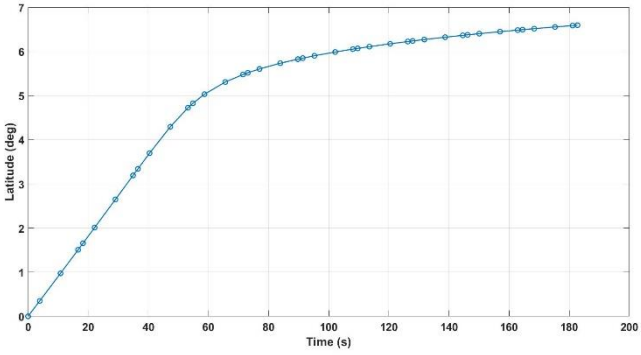

(c) Latitude

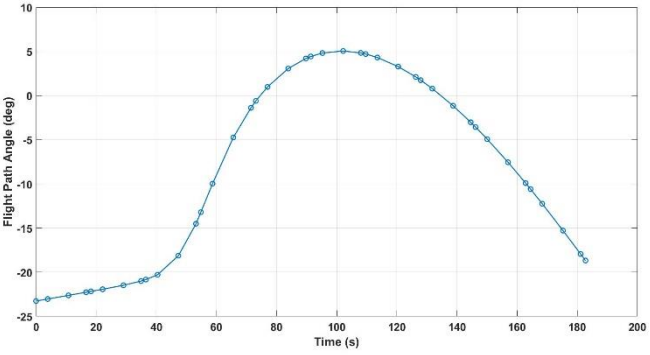

(d) Flight path angle

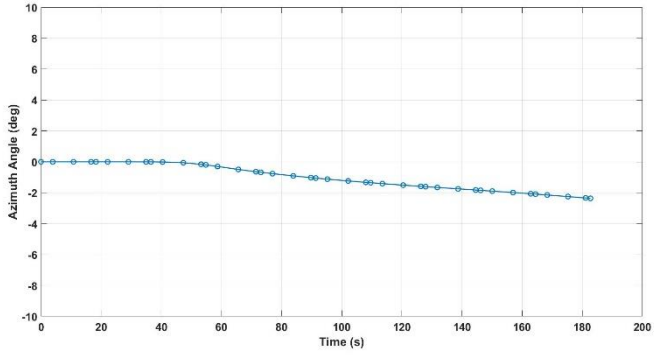

(e)Azimuth angle

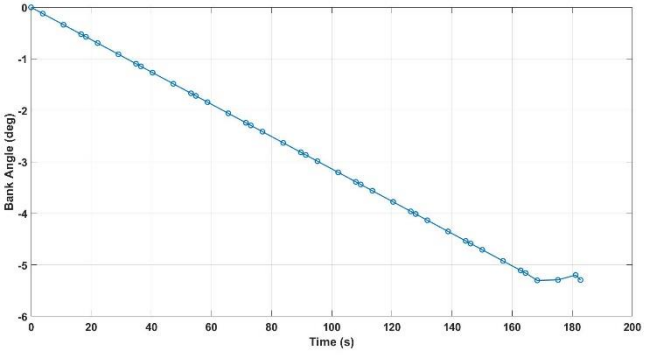

(f) Bank angle

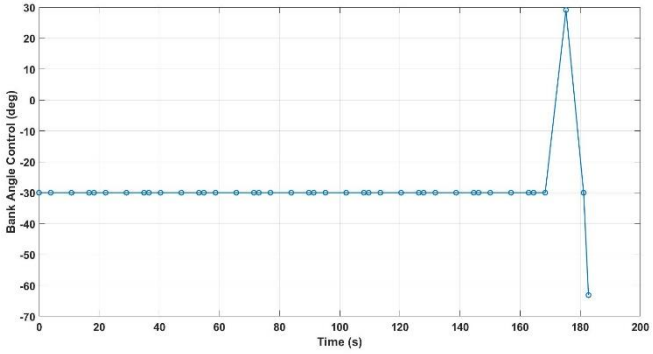

(g) Bank angle control

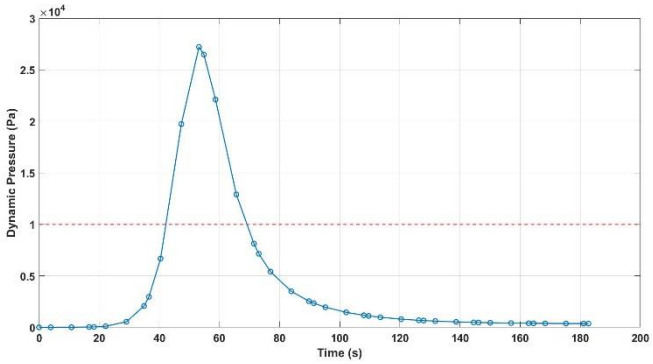

(h) Dynamic Pressure

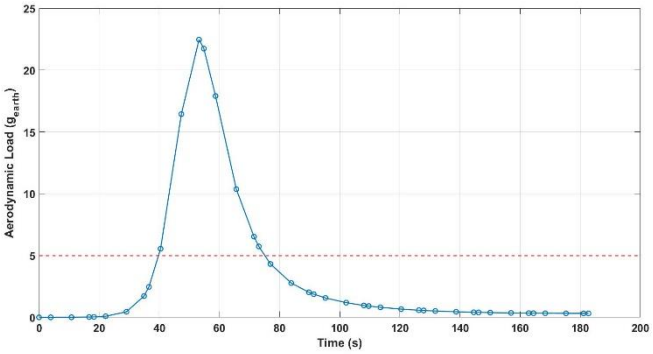

(i) Aerodynamic Load

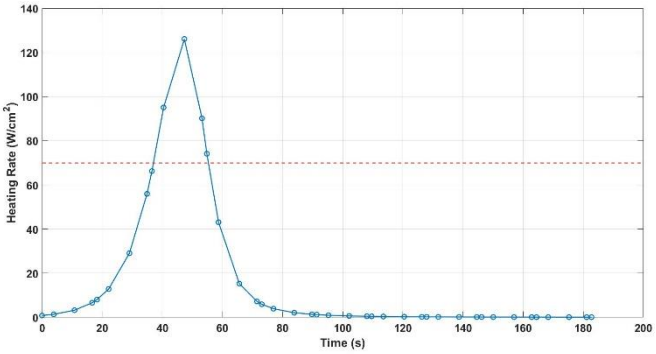

(j) Heating rate

Figure A-2 Full results of Problem A-2

t (sec)	h (km)	v (km/s)	λ (deg)	γ (deg)	ψ (deg)	σ (deg)	σ_c (deg)	q (Pa)	a (g_{earth})	$\dot{Q}$ (W/cm^2)
0	125	6	0	-23.2673	0	0	-30	0.44703	0.000372	0.836143
3.879948	115.8471	6	0.348747	-23.0365	-2.2E-07	-0.12173	-30	1.189306	0.000989	1.363826
10.79039	99.75953	6	0.973615	-22.6235	-1.6E-06	-0.33853	-30	6.640794	0.005507	3.222717
16.65358	86.32711	6	1.507516	-22.27	-1.6E-05	-0.52247	-30	27.91708	0.023123	6.607653
18.27229	82.65415	5.997201	1.655516	-22.1717	-2.6E-05	-0.57326	-30	41.30435	0.034208	8.029801
22.15224	73.91647	6	2.011225	-21.9323	-0.0001	-0.69498	-30	105.2157	0.087153	12.82781
29.06268	58.576	5.9955	2.648701	-21.4825	-0.00057	-0.91178	-30	541.5866	0.449143	29.05992
34.92587	45.87303	5.948351	3.191341	-21.0017	-0.00303	-1.09573	-30	2072.971	1.721818	55.96282
36.54458	42.44145	5.919358	3.340826	-20.8329	-0.00453	-1.14651	-30	2962.602	2.461926	66.25148

40.42453	34.43007	5.788456	3.696406	-20.2852	-0.01175	-1.26824	-30	6671.257	5.550567	95.06901
47.33497	21.85344	5.083169	4.295075	-18.1325	-0.05849	-1.48504	-30	19736.42	16.44152	126.0994
53.19816	14.20581	3.966172	4.725578	-14.5147	-0.15784	-1.66899	-30	27215.24	22.46486	90.14858
54.81687	12.75339	3.620413	4.825193	-13.2037	-0.19753	-1.71977	-30	26486.19	21.73791	74.10299
58.69682	10.21553	2.888371	5.032203	-9.98036	-0.30134	-1.8415	-30	22112.54	17.90566	43.09579
65.60726	8.076504	1.967992	5.307665	-4.73943	-0.49265	-2.0583	-30	12903.03	10.36978	15.28277
71.47045	7.542301	1.517557	5.477093	-1.38469	-0.6399	-2.24224	-30	8123.392	6.530612	7.210548
73.08916	7.5	1.419423	5.517344	-0.6036	-0.67836	-2.29303	-30	7138.96	5.732974	5.913582
76.96911	7.517219	1.236115	5.603786	0.982288	-0.76563	-2.41475	-30	5404.18	4.317177	3.902045
83.87955	7.795544	1.009416	5.733267	3.063947	-0.90982	-2.63156	-30	3498.08	2.773421	2.093459
89.74274	8.146318	0.877092	5.825869	4.206078	-1.02286	-2.8155	-30	2543.865	2.025974	1.347867
91.36145	8.252101	0.847186	5.849251	4.43017	-1.05264	-2.86628	-30	2346.657	1.873471	1.207791
95.2414	8.507733	0.783605	5.902251	4.823043	-1.12176	-2.98801	-30	1953.519	1.570121	0.942784
102.1518	8.949883	0.693074	5.987521	5.054783	-1.23742	-3.20481	-30	1457.656	1.186208	0.637084
108.015	9.286255	0.632509	6.05255	4.83259	-1.32902	-3.38876	-30	1171.145	0.962278	0.475607
109.6337	9.370518	0.617833	6.069506	4.709771	-1.35339	-3.43954	-30	1107.41	0.912151	0.441272
113.5137	9.554615	0.585526	6.108626	4.314985	-1.4104	-3.56127	-30	975.2376	0.80777	0.371926
120.4241	9.813963	0.536429	6.173577	3.285818	-1.50772	-3.77807	-30	796.1622	0.665318	0.282056
126.2873	9.958652	0.501422	6.224638	2.115175	-1.58701	-3.96201	-30	684.9628	0.576199	0.228587
127.906	9.985807	0.492648	6.238157	1.747523	-1.6085	-4.0128	-30	659.2821	0.555541	0.21648
131.786	10.0277	0.472958	6.269636	0.792733	-1.65947	-4.13452	-30	604.9207	0.511721	0.191119
138.6964	10.01985	0.441994	6.32274	-1.14883	-1.74901	-4.35133	-30	528.7512	0.450123	0.156052
144.5596	9.929207	0.419171	6.365133	-3.01719	-1.82459	-4.53527	-30	480.185	0.410762	0.133751
146.1783	9.890545	0.413353	6.376442	-3.56592	-1.84552	-4.58605	-30	468.8832	0.4016	0.128524
150.0583	9.773871	0.400171	6.402898	-4.93511	-1.89595	-4.70778	-30	444.9694	0.382224	0.117345
156.9687	9.482738	0.379089	6.44787	-7.54689	-1.98739	-4.92458	-30	411.9427	0.355546	0.101323
162.8319	9.153244	0.363289	6.484024	-9.91524	-2.06759	-5.10853	-30	391.8834	0.339485	0.090759
164.4506	9.049176	0.359226	6.493699	-10.5906	-2.0903	-5.15931	-30	387.4549	0.335974	0.088238

168.3306	8.777067	0.349968	6.516372	-12.2429	-2.14618	-5.30129	-30	378.5948	0.329026	0.082785
175.241	8.215133	0.334988	6.555009	-15.2843	-2.24905	-5.293	29.12686	368.3546	0.321315	0.074817
181.1042	7.663784	0.323585	6.586114	-17.939	-2.33822	-5.19765	-30	364.5715	0.318939	0.069451
182.7229	7.5	0.32062	6.594439	-18.6803	-2.36323	-5.29398	-63.1257	364.2448	0.318897	0.068153

Table A-2 Profile of Problem A-2

A.3 Full results of Problem A-3

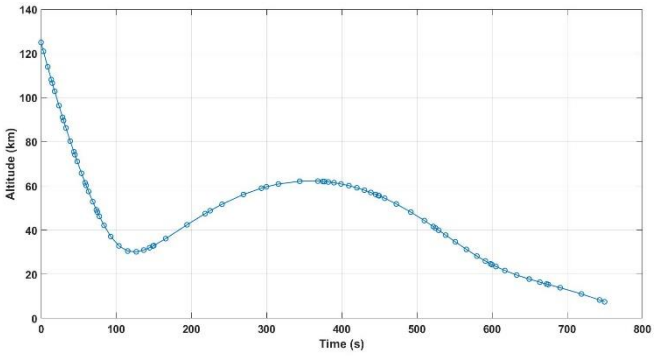

(a)Altitude

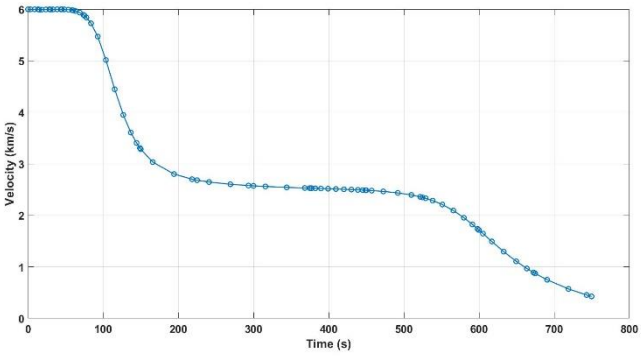

(b) Velocity

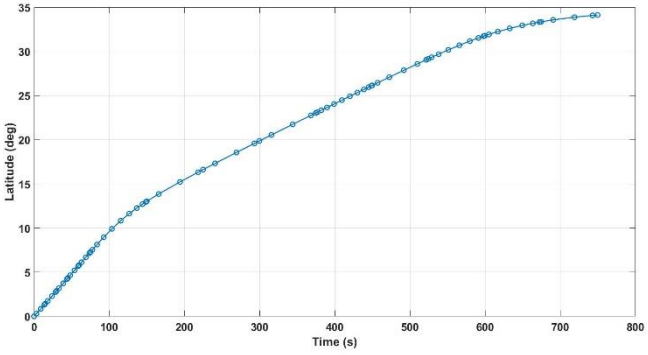

(c) Latitude

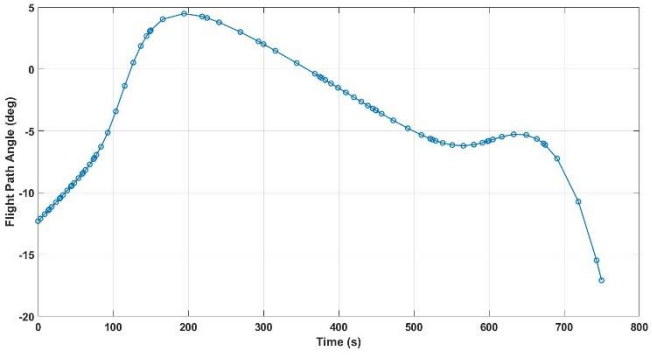

(d) Flight path angle

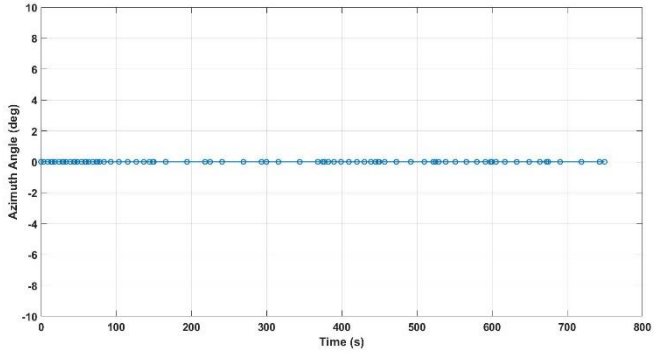

(e)Azimuth angle

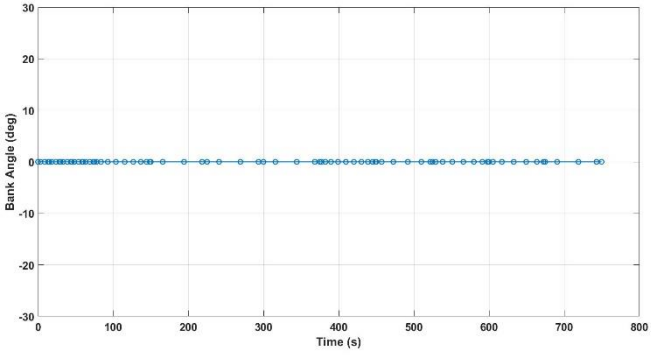

(f) Bank angle

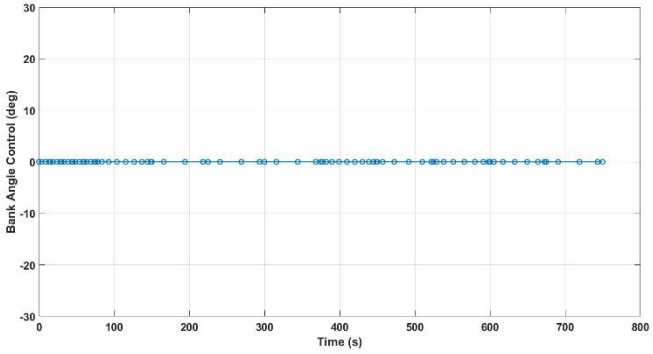

(g) Bank angle control

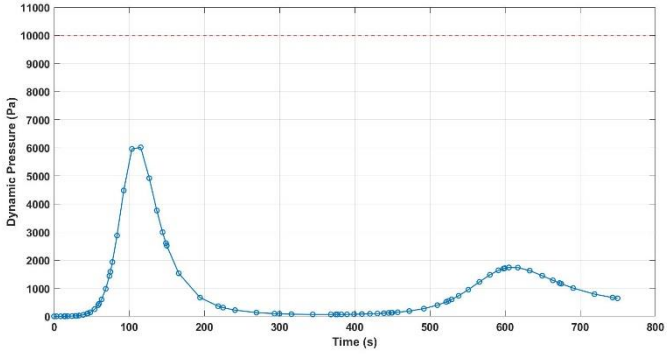

(h) Dynamic Pressure

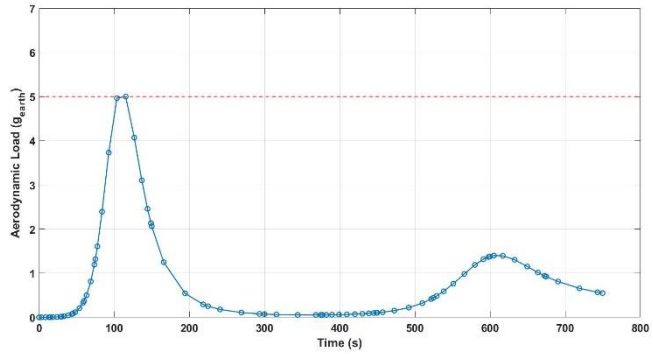

(i) Aerodynamic Load

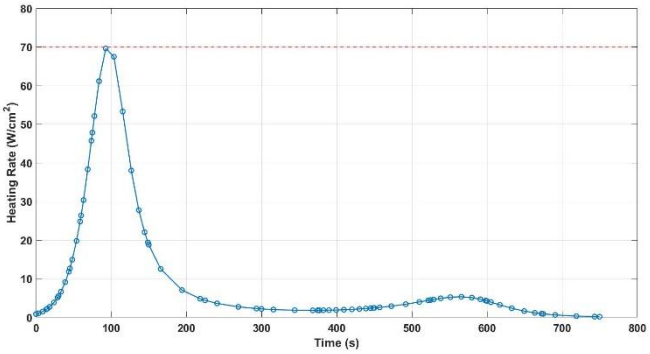

(j) Heating rate

Figure A-3 Full results of Problem A-3

t (sec)	h (km)	v (km/s)	λ (deg)	γ (deg)	ψ (deg)	σ (deg)	σ_c (deg)	q (Pa)	a (g_{earth})	$\dot{Q}$ (W/cm^2)
0	125	6	0	-12.2951	0	0	-7.9E-17	0.44703	0.000372	0.836143
3.183411	120.9654	6	0.303958	-12.0939	-1.1E-24	-4.4E-18	-2E-15	0.688112	0.000573	1.037389
8.853276	113.9421	6	0.846747	-11.7349	-2.1E-23	-1.4E-17	-8.7E-16	1.457948	0.001212	1.510022
13.66389	108.147	6	1.308676	-11.4295	-7.2E-23	-1.7E-17	-7.8E-16	2.708946	0.002249	2.058318
14.99201	106.5737	5.991826	1.436427	-11.3451	-9.4E-23	-1.9E-17	-1.5E-15	3.196421	0.002653	2.22977
18.17542	102.8537	5.993896	1.74266	-11.1429	-1.8E-22	-2.1E-17	-5.9E-16	4.760757	0.00395	2.723116
23.84528	96.38914	5.997368	2.289659	-10.7817	-4.9E-22	-2.9E-17	-2.2E-15	9.513092	0.007885	3.853825
28.6559	91.06698	6	2.755301	-10.4738	-1.2E-21	-4.1E-17	-1.9E-15	16.81914	0.013934	5.128781
29.98401	89.62414	5.99687	2.884096	-10.3885	-1.5E-21	-4.3E-17	-3E-15	19.60378	0.01624	5.531322

33.16742	86.21484	5.998281	3.193028	-10.1838	-2.7E-21	-5.1E-17	-1.4E-15	28.238	0.023388	6.641715
38.83729	80.30787	6	3.744639	-9.81679	-6.4E-21	-4.9E-17	1.55E-15	53.1295	0.044001	9.115491
43.64791	75.46453	6	4.213932	-9.5021	-1.2E-20	-4.7E-17	-2.7E-15	89.16742	0.073855	11.80906
44.97602	74.15507	5.999989	4.343679	-9.41452	-1.4E-20	-5.3E-17	-3.3E-16	102.5655	0.084957	12.66518
48.15943	71.0657	5.998764	4.654987	-9.20295	-2E-20	-5.1E-17	1.23E-15	142.6459	0.118175	14.9301
53.82929	65.74016	5.993318	5.210309	-8.81866	-3.7E-20	-4.7E-17	-3.9E-16	251.6103	0.20853	19.79286
58.63991	61.4065	5.983733	5.682003	-8.48163	-6.2E-20	-5.4E-17	-2.4E-15	398.607	0.330498	24.83285
59.96802	60.24125	5.979979	5.812252	-8.38618	-7.2E-20	-5.8E-17	4.27E-16	450.9215	0.373922	26.37907
63.15143	57.50561	5.968451	6.124372	-8.15196	-1E-19	-6.4E-17	-3.3E-15	601.7789	0.499182	30.35648
68.8213	52.84581	5.936367	6.679414	-7.71022	-2.1E-19	-8.5E-17	-3E-15	979.7248	0.813209	38.31803
73.63192	49.12651	5.893048	7.148398	-7.30135	-3.8E-19	-9.3E-17	-1.1E-16	1436.895	1.193382	45.7301
74.96003	48.14117	5.877746	7.277371	-7.1814	-4.4E-19	-9.3E-17	-2.9E-16	1588.234	1.319299	47.8287
77.67792	46.18509	5.841125	7.540383	-6.92468	-5.9E-19	-9.7E-17	-1.8E-15	1933.321	1.606528	52.11403
83.81123	42.09792	5.727526	8.127684	-6.27919	-1.1E-18	-9.7E-17	9.62E-16	2877.449	2.393088	61.12906
92.73882	37.09449	5.47043	8.958512	-5.13872	-2.2E-18	-1.1E-16	-2.8E-15	4481.459	3.73152	69.59248
103.586	32.80344	5.015504	9.907452	-3.41964	-4.7E-18	-1.3E-16	-7.2E-16	5959.826	4.965539	67.46146
115.2907	30.47343	4.447936	10.83244	-1.35327	-8.6E-18	-1.4E-16	-1.5E-15	6013.135	5	53.29388
126.7074	30.13279	3.949985	11.63237	0.525239	-1.3E-17	-1.6E-16	-9.7E-16	4918.022	4.069914	38.00981
136.7183	30.93237	3.607617	12.26347	1.868624	-1.7E-17	-1.7E-16	-2.2E-15	3766.318	3.101611	27.74655
144.344	31.99585	3.40534	12.70958	2.670813	-1.9E-17	-1.8E-16	-9.9E-17	2995.165	2.458372	22.04656
148.8397	32.75049	3.306305	12.96131	3.057985	-2E-17	-1.8E-16	-2.4E-15	2604.646	2.134243	19.38072
149.9201	32.94308	3.284533	13.0207	3.142111	-2.1E-17	-1.9E-16	8.13E-16	2518.073	2.062539	18.80576
165.8371	36.11241	3.034784	13.85651	4.034234	-2.5E-17	-2.1E-16	-1.8E-15	1531.893	1.249543	12.52217
194.1864	42.37131	2.801473	15.22415	4.492306	-2.9E-17	-2.1E-16	1.67E-15	668.5796	0.543588	7.049513
218.2395	47.43606	2.70099	16.32183	4.264152	-3.1E-17	-1.8E-16	-1E-15	361.6399	0.293763	4.819408
224.8801	48.75346	2.682759	16.61788	4.142217	-3.1E-17	-2E-16	-1.6E-15	309.905	0.251716	4.401364
240.7971	51.69032	2.646553	17.32106	3.787927	-3.2E-17	-2.2E-16	-1.8E-15	220.3289	0.178936	3.611657
269.1465	56.11238	2.603135	18.55375	3.001321	-3.3E-17	-3E-16	-3.4E-15	132.8597	0.107897	2.713313

293.1996	58.96726	2.578147	19.58618	2.241885	-3.4E-17	-3.7E-16	-6.5E-16	96.04319	0.077998	2.262863
299.8401	59.60398	2.572561	19.86951	2.02183	-3.4E-17	-3.7E-16	-2.6E-15	89.33473	0.07255	2.172958
315.7572	60.85408	2.560611	20.54634	1.48238	-3.5E-17	-4.1E-16	-3E-15	77.43468	0.062883	2.004309
344.1065	62.10248	2.54328	21.74476	0.488326	-3.6E-17	-4.8E-16	-1.7E-15	66.84597	0.054276	1.837112
368.1596	62.16349	2.530966	22.75573	-0.37681	-3.7E-17	-5.4E-16	-3.3E-15	65.76983	0.053389	1.804661
374.8001	62.01774	2.527786	23.03399	-0.61802	-3.7E-17	-5.6E-16	-3.2E-15	66.63489	0.054086	1.811929
377.0511	61.95232	2.526717	23.12824	-0.69993	-3.7E-17	-5.7E-16	-2.7E-15	67.04586	0.054418	1.815971
382.1679	61.77344	2.5243	23.34232	-0.88641	-3.7E-17	-5.8E-16	2.32E-16	68.20964	0.055358	1.828162
389.7188	61.43298	2.520744	23.65788	-1.16213	-3.7E-17	-5.7E-16	4.65E-16	70.53883	0.057241	1.853878
399.0914	60.88366	2.516286	24.04896	-1.50497	-3.8E-17	-5.7E-16	8.76E-16	74.54094	0.060478	1.899009
409.5262	60.10739	2.511157	24.48355	-1.8869	-3.8E-17	-5.6E-16	7.34E-16	80.66112	0.065428	1.967386
420.178	59.13688	2.505587	24.92624	-2.27629	-3.9E-17	-5.4E-16	2.74E-15	89.08299	0.07224	2.058383
430.1836	58.06264	2.49987	25.34116	-2.64082	-3.9E-17	-5.1E-16	2.34E-15	99.46872	0.080638	2.165149
438.7327	57.02131	2.494455	25.6949	-2.95064	-4E-17	-5.1E-16	-2.7E-15	110.7007	0.089718	2.27424
445.1327	56.16818	2.489981	25.95921	-3.18117	-4E-17	-5.3E-16	-2.2E-15	120.8373	0.097911	2.367567
448.8668	55.64166	2.487169	26.11319	-3.31496	-4.1E-17	-5.3E-16	7.79E-16	127.5455	0.103332	2.426906
449.7602	55.51258	2.486472	26.15001	-3.34688	-4.1E-17	-5.3E-16	1.11E-15	129.2453	0.104705	2.441655
457.1464	54.3997	2.4803	26.45398	-3.6093	-4.1E-17	-5.2E-16	7.17E-16	144.8524	0.117313	2.572058
472.5882	51.81649	2.464412	27.08678	-4.14665	-4.2E-17	-5.2E-16	5.49E-16	188.486	0.152538	2.896516
491.8896	48.12992	2.436079	27.87098	-4.78487	-4.4E-17	-4.8E-16	2.42E-15	273.1479	0.220809	3.40715
509.8771	44.29523	2.396061	28.5919	-5.3237	-4.7E-17	-4.8E-16	-2.9E-15	398.154	0.321467	3.979523
521.7361	41.60095	2.358872	29.05963	-5.63294	-4.9E-17	-5.2E-16	-9.5E-16	514.7025	0.41519	4.385274
524.7202	40.90731	2.347773	29.17611	-5.70316	-5E-17	-5.2E-16	-5E-16	549.1163	0.442845	4.486979
528.9377	39.91877	2.330719	29.33978	-5.79636	-5.1E-17	-5.2E-16	-1.7E-16	601.4899	0.484917	4.62811
538.2311	37.71696	2.286816	29.6959	-5.9733	-5.4E-17	-5.2E-16	-5.3E-16	732.7206	0.590264	4.917466
551.153	34.64545	2.208908	30.17843	-6.14165	-5.9E-17	-5.2E-16	9.11E-16	949.3751	0.764013	5.222567
565.7349	31.2626	2.093616	30.70013	-6.20092	-6.7E-17	-5E-16	3.89E-16	1224.441	0.98445	5.328103
579.7566	28.20906	1.954036	31.1725	-6.11573	-7.7E-17	-5.1E-16	-1.5E-15	1478.363	1.188086	5.099941

591.0839	25.95567	1.823206	31.52879	-5.95623	-8.7E-17	-5.3E-16	-1.3E-15	1637.605	1.316194	4.672889
597.9952	24.69161	1.737529	31.73378	-5.83112	-9.4E-17	-5.4E-16	1.07E-15	1702.513	1.36867	4.327318
599.6802	24.3968	1.716164	31.78227	-5.79868	-9.6E-17	-5.3E-16	-1.8E-15	1714.084	1.378059	4.235878
605.1564	23.4752	1.64587	31.93572	-5.69097	-1E-16	-5.5E-16	-2.3E-15	1739.779	1.398983	3.925075
616.9785	21.67173	1.492618	32.24515	-5.46854	-1.2E-16	-5.7E-16	-8E-16	1735.135	1.395154	3.223843
632.7622	19.61832	1.294949	32.61212	-5.27622	-1.4E-16	-5.6E-16	9.37E-16	1626.591	1.303839	2.349385
649.3799	17.78735	1.107245	32.94501	-5.32233	-1.6E-16	-5.6E-16	-8.4E-16	1446.339	1.15048	1.619691
663.5403	16.39271	0.967691	33.19013	-5.6455	-1.9E-16	-5.8E-16	-2.4E-15	1282.353	1.016758	1.164895
672.4427	15.55579	0.889126	33.32811	-6.01352	-2E-16	-6.1E-16	-3.2E-15	1183.907	0.941184	0.944919
674.6403	15.35135	0.870741	33.36041	-6.12646	-2.1E-16	-6.2E-16	-2.2E-15	1160.544	0.923722	0.897261
690.5573	13.86801	0.748363	33.57501	-7.23749	-2.4E-16	-6.3E-16	1.57E-16	1004.563	0.810072	0.616627
718.9067	11.04753	0.571013	33.8838	-10.7258	-3E-16	-6.5E-16	-2E-15	790.6725	0.656375	0.318493
742.9597	8.317147	0.45368	34.08499	-15.468	-3.6E-16	-7E-16	-8.2E-16	668.3007	0.567735	0.18484
749.6003	7.5	0.425833	34.13214	-17.0907	-3.8E-16	-7E-16	2.96E-17	642.5249	0.549093	0.159674

Table A-3 Profile of Problem A-3

A.4 Full results of Problem A-4

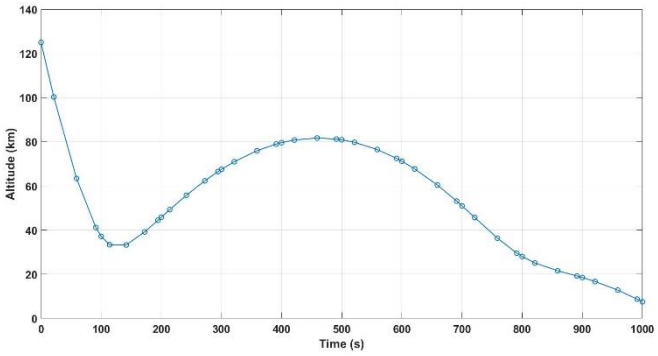

(a)Altitude

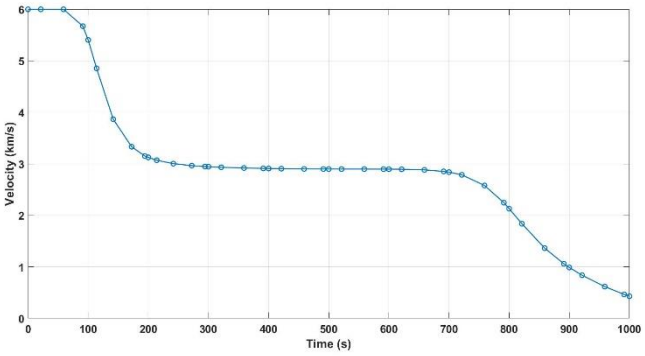

(b) Velocity

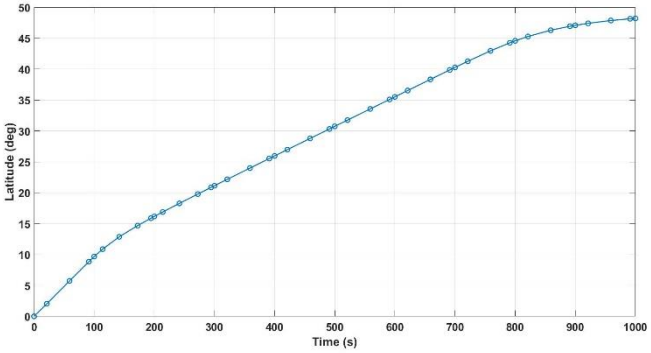

(c) Latitude

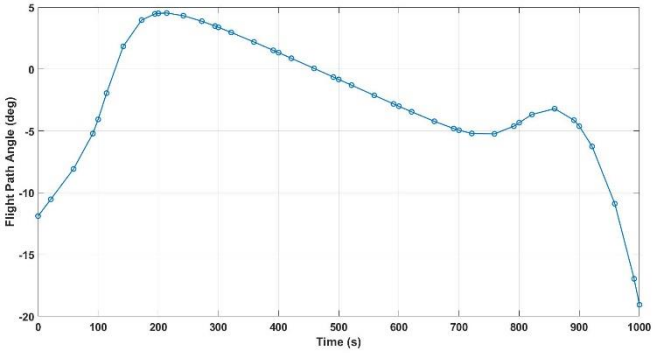

(d) Flight path angle

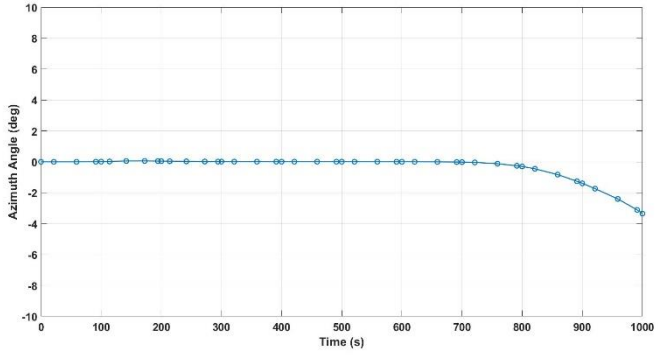

(e)Azimuth angle

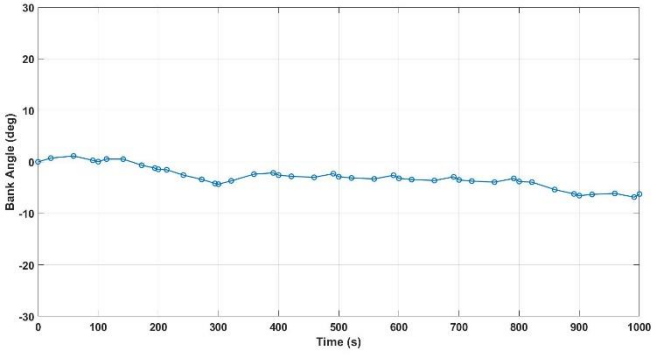

(f) Bank angle

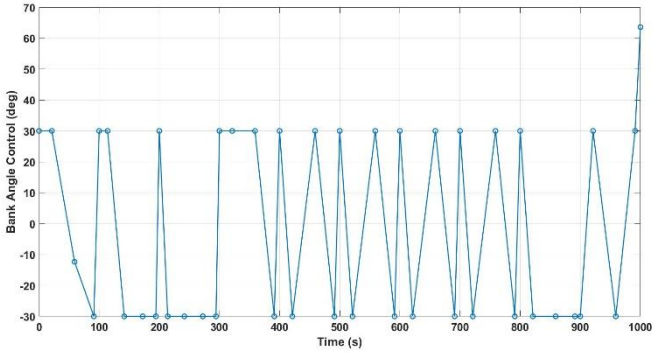

(g) Bank angle control

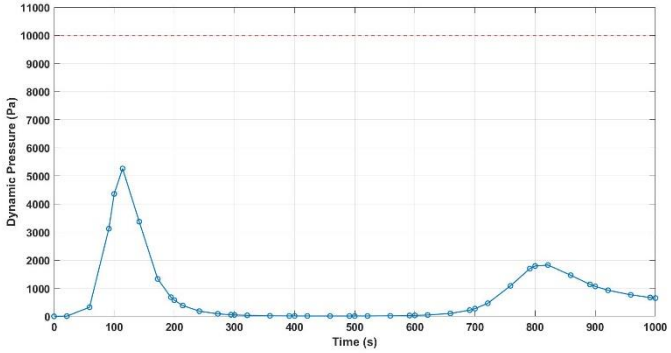

(h) Dynamic Pressure

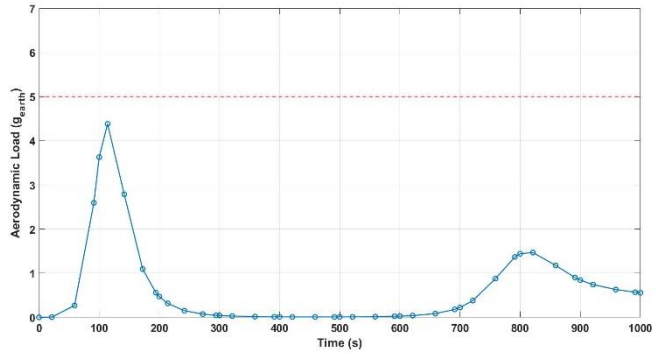

(i) Aerodynamic Load

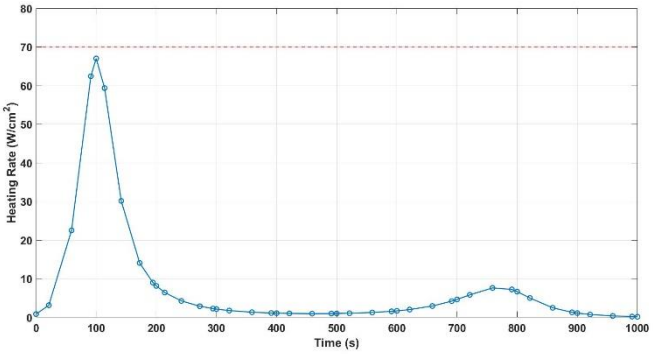

(j) Heating rate

Figure A-4 Full results of Problem A-4

t (sec)	h (km)	v (km/s)	λ (deg)	γ (deg)	ψ (deg)	σ (deg)	σ_c (deg)	q (Pa)	a (g_{earth})	$\dot{Q}$ (W/cm^2)
0	125	6	0	-11.8897	0	0	30	0.44703	0.000372	0.836143
21.23405	100.271	6	2.038765	-10.5301	-7.8E-05	0.721875	30	6.287447	0.005214	3.135807
59.05331	63.38724	6	5.737769	-8.07582	0.001789	1.13696	-12.3565	324.2943	0.268812	22.5207
91.1412	41.16467	5.672353	8.848671	-5.21195	0.008409	0.287033	-30	3118.384	2.594199	62.41673
100	37.13483	5.405569	9.670878	-4.06408	0.011367	0.034483	30	4356.988	3.628436	67.00169
113.976	33.35757	4.853715	10.86731	-1.94313	0.020788	0.537557	30	5260.48	4.382096	59.35687
141.641	33.26336	3.866004	12.86834	1.838509	0.053799	0.523425	-30	3371.128	2.78842	30.14546
172.3157	39.16536	3.331338	14.68291	3.969631	0.058954	-0.66684	-30	1331.882	1.093606	14.06954
194.2896	44.38893	3.151175	15.86795	4.467824	0.045054	-1.22362	-30	681.7887	0.558587	9.006987

200	45.81471	3.125306	16.16325	4.513834	0.042984	-1.45195	30	575.828	0.471697	8.14219
213.976	49.23561	3.069665	16.88086	4.536879	0.037047	-1.54086	-30	385.3553	0.315578	6.425727
241.641	55.74965	3.003665	18.27065	4.322719	0.028101	-2.57603	-30	183.8839	0.150611	4.249956
272.3157	62.30713	2.964634	19.78371	3.874436	0.020348	-3.41993	-30	88.86435	0.072823	2.878165
294.2896	66.47995	2.94753	20.85668	3.484651	0.01687	-4.19075	-30	56.22933	0.046096	2.263119
300	67.48634	2.943886	21.13451	3.378051	0.015952	-4.33826	30	50.36892	0.041294	2.136647
321.2341	70.9406	2.93275	22.1644	2.966503	0.013684	-3.69581	30	34.55367	0.028335	1.756333
359.0533	75.92971	2.918946	23.9894	2.195843	0.011837	-2.39823	30	20.07974	0.016468	1.326298
391.1412	78.96414	2.910972	25.53125	1.520369	0.011188	-2.15317	-30	14.43768	0.011841	1.118496
400	79.60588	2.909241	25.9561	1.331425	0.011048	-2.58427	30	13.46436	0.011042	1.078852
421.2341	80.79535	2.905705	26.97339	0.875854	0.010666	-2.81906	-30	11.82779	0.0097	1.008706
459.0533	81.6907	2.901337	28.78239	0.057108	0.010009	-3.00789	30	10.71585	0.008787	0.957236
491.1412	81.21626	2.899188	30.31552	-0.64179	0.009519	-2.30065	-30	11.25669	0.00923	0.979643
500	80.8853	2.898803	30.73864	-0.83509	0.009418	-2.89365	30	11.65901	0.00956	0.996731
521.2341	79.7395	2.898154	31.75278	-1.29846	0.008993	-3.12843	-30	13.17241	0.0108	1.058974
559.0533	76.46795	2.897581	33.55924	-2.12203	0.007867	-3.31727	30	18.68045	0.015314	1.260592
591.1412	72.46293	2.896701	35.0925	-2.81505	0.006514	-2.61003	-30	28.64648	0.023476	1.560101
600	71.16024	2.896189	35.51588	-3.0047	0.006101	-3.20303	30	32.91548	0.026971	1.671721
621.2341	67.69707	2.893839	36.53057	-3.45407	0.004313	-3.43781	-30	47.58674	0.038972	2.006787
659.0533	60.37116	2.882155	38.33581	-4.22391	-0.00221	-3.62665	30	103.301	0.084471	2.932897
691.1412	53.1138	2.852708	39.85884	-4.80399	-0.0133	-2.91941	-30	219.8542	0.179385	4.191716
700	50.97037	2.838667	40.27631	-4.94255	-0.01753	-3.51241	30	273.7573	0.22319	4.631497
721.2341	45.66828	2.786781	41.26696	-5.2065	-0.03667	-3.74719	-30	465.0628	0.378288	5.817965
759.0533	36.29418	2.579394	42.96022	-5.23341	-0.12092	-3.93603	30	1085.349	0.877755	7.614299
791.1412	29.51095	2.246387	44.25639	-4.61772	-0.25573	-3.22879	-30	1699.965	1.367984	7.227679
800	28.00545	2.128448	44.57937	-4.33422	-0.30083	-3.82179	30	1792.649	1.441352	6.663211
821.2341	25.07436	1.836873	45.28219	-3.67121	-0.4522	-3.94407	-30	1826.477	1.467975	5.009277
859.0533	21.55431	1.362499	46.28951	-3.20101	-0.82671	-5.383	-30	1464.063	1.175601	2.467527

891.1412	19.19773	1.058037	46.93409	-4.12917	-1.2597	-6.22685	-30	1135.8	0.901909	1.310576
900	18.49937	0.986915	47.08621	-4.62011	-1.39178	-6.56693	-30	1064.838	0.844261	1.104105
921.2341	16.69372	0.836721	47.40897	-6.25269	-1.73666	-6.33214	30	928.3663	0.740725	0.741021
959.0533	12.77534	0.616199	47.86245	-10.8894	-2.40119	-6.14331	-30	765.4669	0.630161	0.364935
991.1412	8.718114	0.464385	48.14425	-16.9625	-3.1093	-6.85055	30	670.8293	0.568601	0.194031
1000	7.5	0.428032	48.20729	-19.062	-3.35199	-6.25755	63.61491	649.1781	0.55452	0.16216

Table A-4 Profile of Problem A-4

A.5 Full comparison results of Problem A

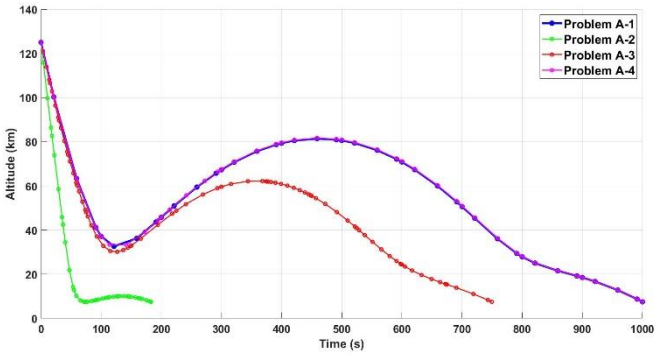

(a)Altitude

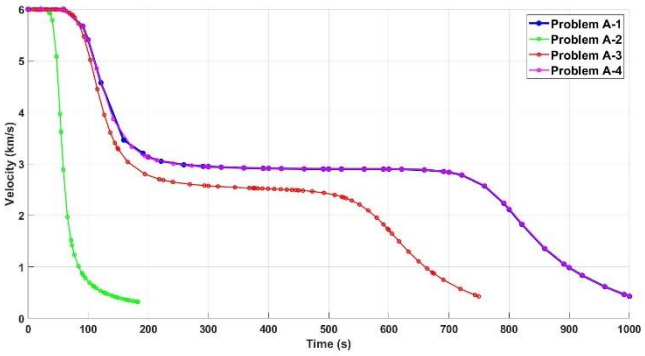

(b) Velocity

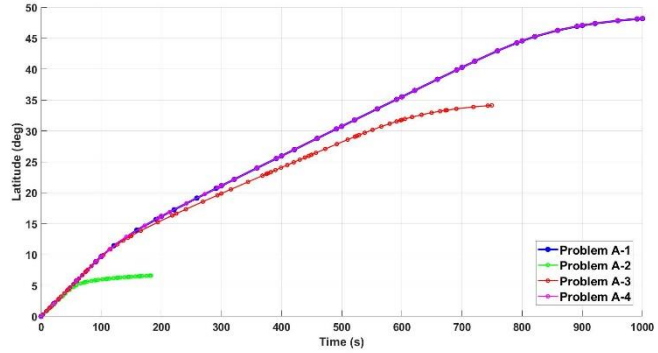

(c) Latitude

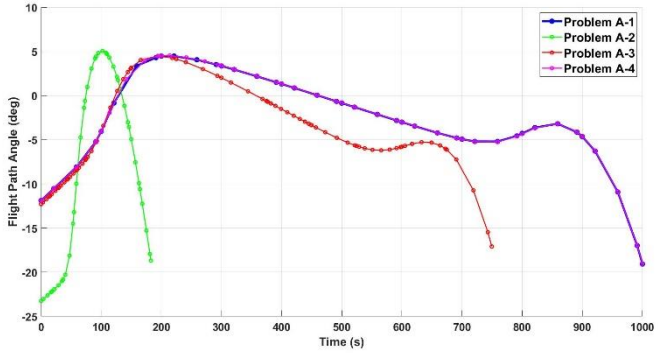

(d) Flight path angle

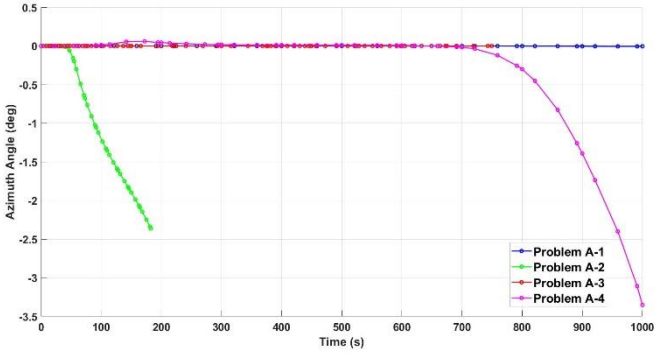

(e)Azimuth angle

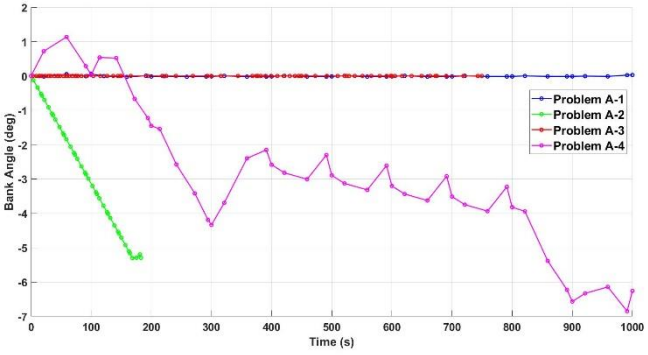

(f) Bank angle

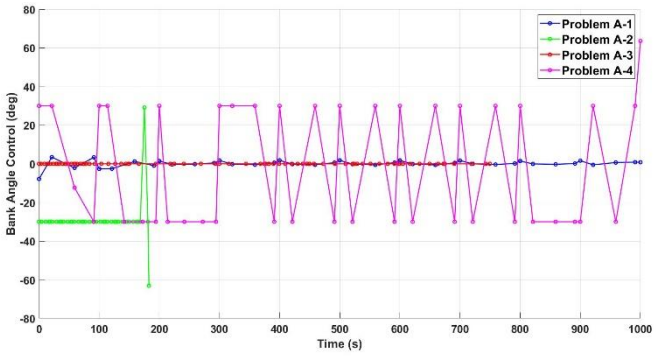

(g) Bank angle control

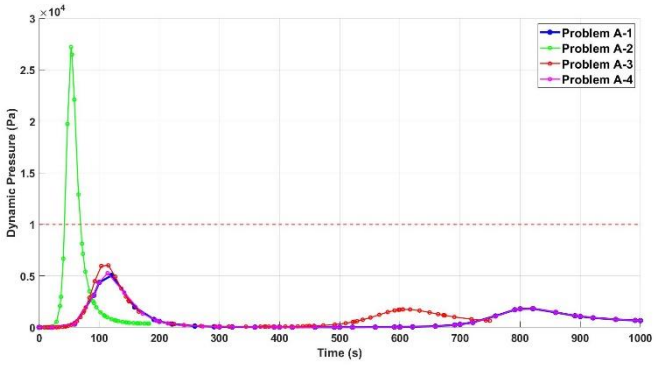

(h) Dynamic Pressure

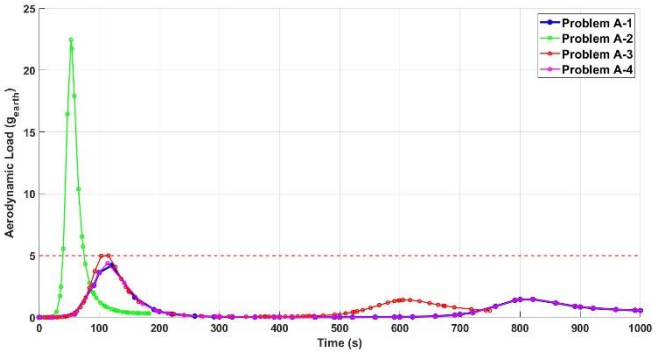

(i) Aerodynamic Load

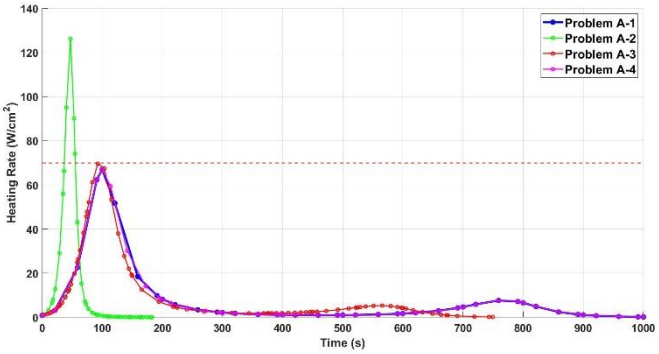

(j) Heating rate

Figure A-5 Full comparison results of Problem A

Appendix B Full results of Problem B

B.1 Full results of Problem B-1

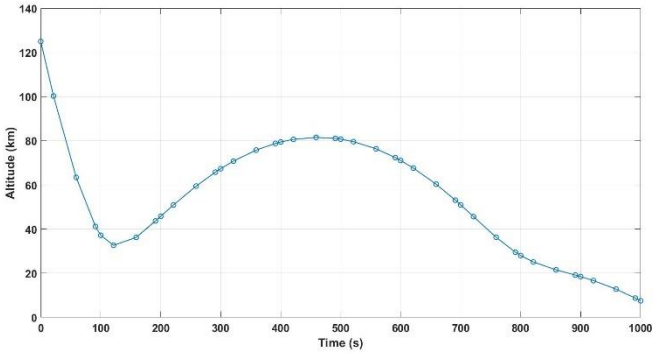

(a)Altitude

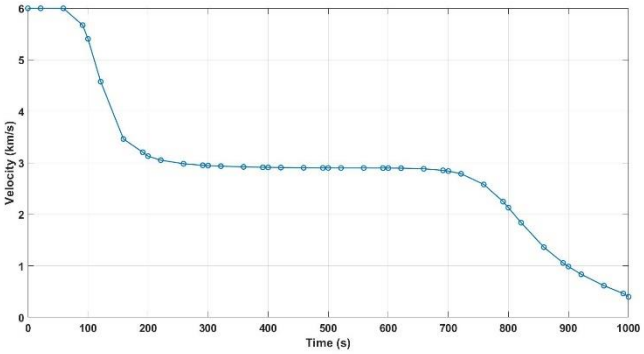

(b) Velocity

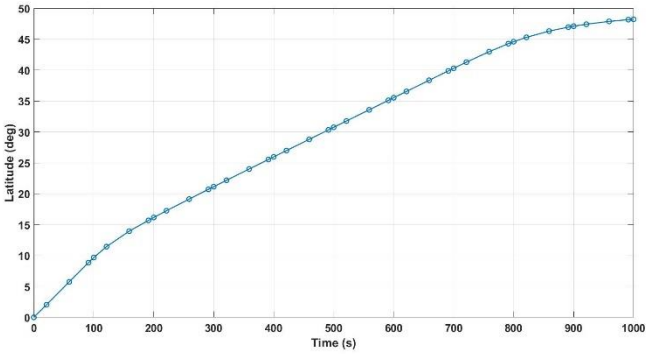

(c) Latitude

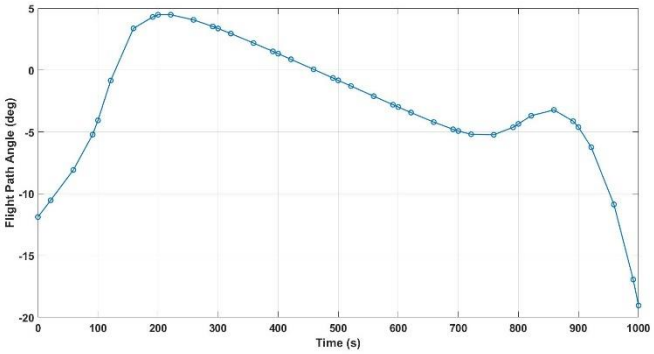

(d) Flight path angle

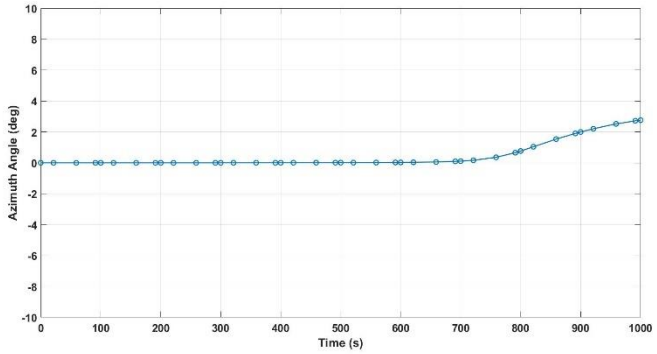

(e)Azimuth angle

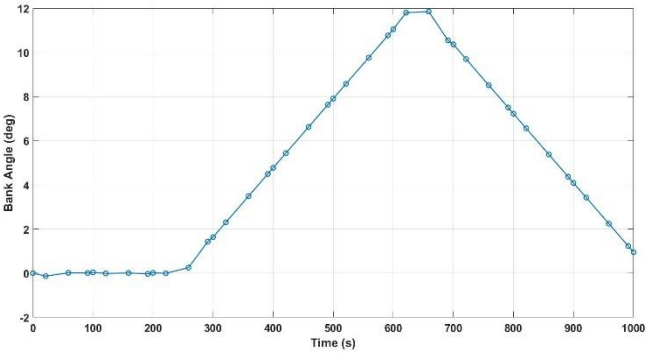

(f) Bank angle

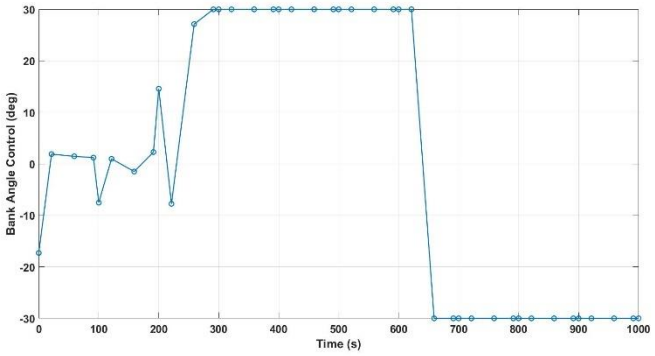

(g) Bank angle control

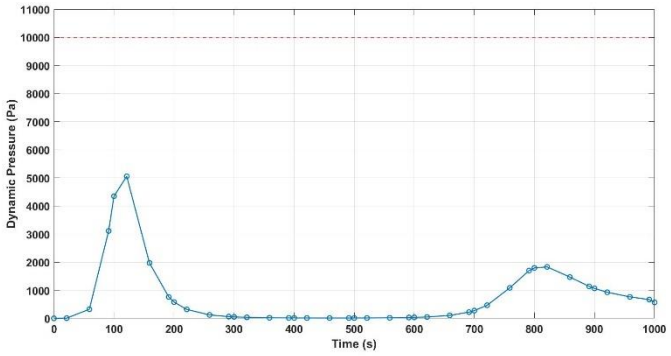

(h) Dynamic Pressure

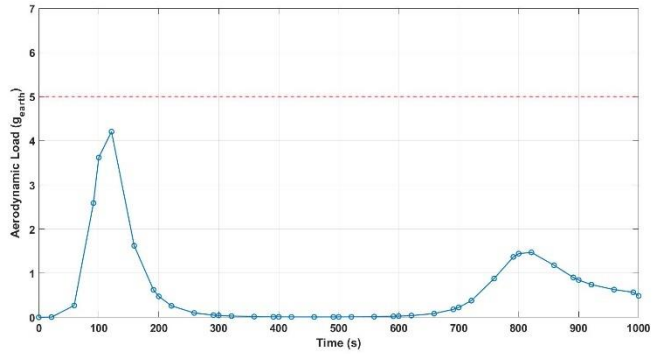

(i) Aerodynamic Load

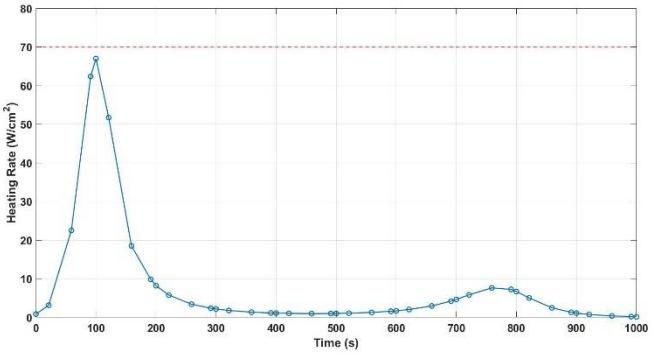

(j) Heating rate

Figure B-1 Full results of Problem B-1

t (sec)	h (km)	v (km/s)	λ (deg)	γ (deg)	ψ (deg)	σ (deg)	σ_c (deg)	q (Pa)	a (g_{earth})	$\dot{Q}$ (W/cm^2)
0	125	6	0	-11.8868	0	0	-17.2992	0.44703	0.000372	0.836143
21.23405	100.2772	6	2.038789	-10.5272	-3.7E-06	-0.1315	1.885029	6.283268	0.00521	3.134765
59.05331	63.40531	6	5.737787	-8.07289	9.17E-06	0.016038	1.454572	323.6686	0.268293	22.49896
91.1412	41.18927	5.673174	8.84885	-5.21084	0.000149	0.007538	1.210583	3111.096	2.588123	62.36179
100	37.15908	5.407025	9.671206	-4.06438	0.000231	0.038717	-7.53567	4348.05	3.620977	66.96898
121.2341	32.62564	4.575327	11.43683	-0.83918	0.000383	-0.01161	0.976581	5054.798	4.206912	51.70183
159.0533	36.21577	3.462836	13.94105	3.374914	-0.00022	0.008909	-1.49538	1972.597	1.622425	18.5009
191.1412	43.67252	3.206182	15.68439	4.300566	0.000199	-0.02877	2.280627	761.9792	0.624859	9.857288
200	45.77429	3.129599	16.16164	4.47983	-0.00011	0.014921	14.58121	579.9112	0.475078	8.193467

221.2341	50.91568	3.051218	17.24871	4.480706	-9.5E-05	-0.00547	-7.76693	318.1428	0.260542	5.768557
259.0533	59.46714	2.982344	19.13388	4.062829	0.000151	0.250473	27.12909	121.831	0.099821	3.41039
291.1412	65.77539	2.952007	20.70744	3.530068	0.001364	1.431998	29.99799	60.81254	0.049852	2.360701
300	67.35049	2.946644	21.13865	3.364188	0.001926	1.636067	29.99289	51.20162	0.041979	2.158276
321.2341	70.7944	2.935406	22.16955	2.955464	0.0031	2.30217	29.99945	35.16157	0.028834	1.774925
359.0533	75.77101	2.921481	23.99626	2.18925	0.005062	3.488685	29.9997	20.45881	0.01678	1.341084
391.1412	78.80011	2.913434	25.5395	1.517217	0.006584	4.49535	29.99956	14.71795	0.012071	1.131211
400	79.44117	2.911686	25.96473	1.329188	0.006997	4.773279	29.99838	13.72657	0.011258	1.091138
421.2341	80.63039	2.90811	26.98292	0.875768	0.007985	5.439437	29.99974	12.05816	0.009889	1.020169
459.0533	81.52988	2.903674	28.79348	0.06072	0.009845	6.625938	29.99981	10.91925	0.008954	0.967836
491.1412	81.0634	2.901465	30.3279	-0.63517	0.011695	7.63262	29.99967	11.46013	0.009397	0.990009
500	80.73534	2.901061	30.75138	-0.82765	0.012279	7.910545	29.9988	11.8659	0.00973	1.007103
521.2341	79.59769	2.900366	31.76634	-1.2891	0.013885	8.576707	29.99979	13.39405	0.010982	1.069477
559.0533	76.34478	2.899695	33.57423	-2.1094	0.017842	9.763208	29.99982	18.95569	0.01554	1.271699
591.1412	72.35949	2.898709	35.10865	-2.79989	0.023372	10.76989	29.99961	29.0052	0.023771	1.572015
600	71.06284	2.898163	35.53233	-2.98891	0.025484	11.04781	29.99768	33.30538	0.027291	1.683885
621.2341	67.61503	2.895719	36.54774	-3.43694	0.032365	11.80274	29.99928	48.06833	0.039368	2.019538
659.0533	60.31885	2.883819	38.35417	-4.20537	0.05496	11.85022	-29.9999	104.0004	0.085045	2.946207
691.1412	53.08716	2.854139	39.87808	-4.78591	0.093913	10.54418	-29.9999	220.7026	0.180082	4.20401
700	50.95051	2.840029	40.29577	-4.92498	0.109775	10.36601	-29.9999	274.6024	0.223885	4.643092
721.2341	45.66332	2.787986	41.28689	-5.19126	0.16427	9.699835	-30	465.7124	0.378825	5.827065
759.0533	36.30442	2.580523	42.98088	-5.22832	0.357082	8.513331	-30	1085.11	0.877579	7.620124
791.1412	29.51583	2.247504	44.2776	-4.62757	0.656908	7.506638	-30	1700.768	1.368643	7.236578
800	28.00534	2.129488	44.60073	-4.34883	0.76441	7.228711	-30	1794.422	1.442785	6.67302
821.2341	25.05942	1.837442	45.30375	-3.6929	1.040737	6.562535	-30	1830.531	1.471231	5.017938
859.0533	21.51636	1.361799	46.31083	-3.21978	1.533814	5.376031	-30	1468.507	1.179151	2.468731
891.1412	19.15423	1.056545	46.95461	-4.13172	1.90138	4.369338	-30	1137.878	0.903509	1.308076
900	18.45693	0.985324	47.10645	-4.61781	1.995074	4.091411	-30	1066.236	0.845363	1.101273

921.2341	16.65736	0.835019	47.42854	-6.23907	2.203558	3.425235	-30	928.1952	0.740706	0.737942
959.0533	12.7564	0.614755	47.88093	-10.8685	2.520073	2.23873	-30	763.4276	0.62864	0.362742
991.1412	8.714308	0.463444	48.16215	-16.9411	2.719554	1.232046	-29.9993	668.3868	0.566639	0.192894
1000	7.5	0.4	48.22511	-19.0385	2.76018	0.954128	-29.999	566.9327	0.487203	0.132341

Table B-1 Profile of Problem B-1

B.2 Full results of Problem B-2

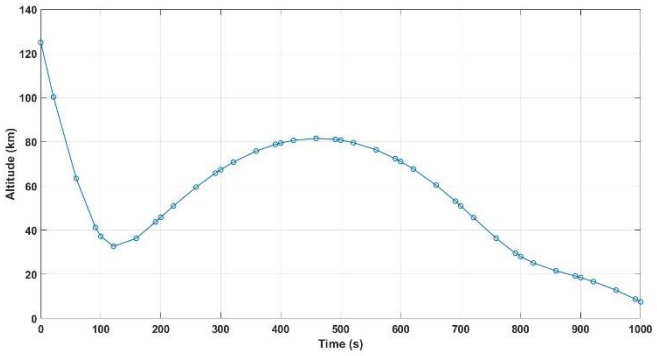

(a)Altitude

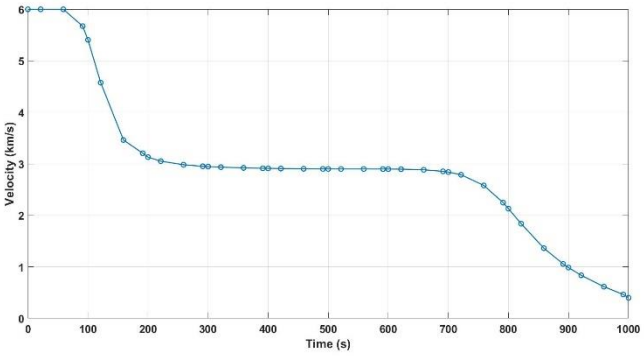

(b) Velocity

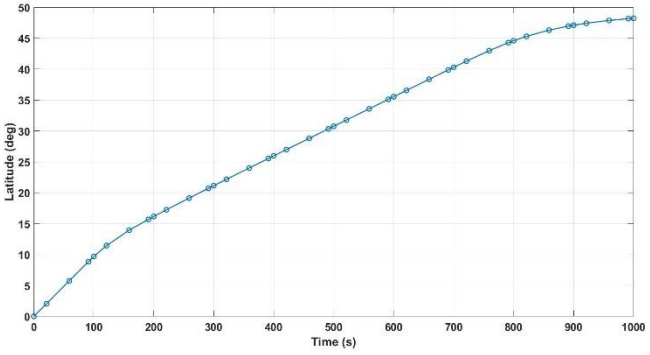

(c) Latitude

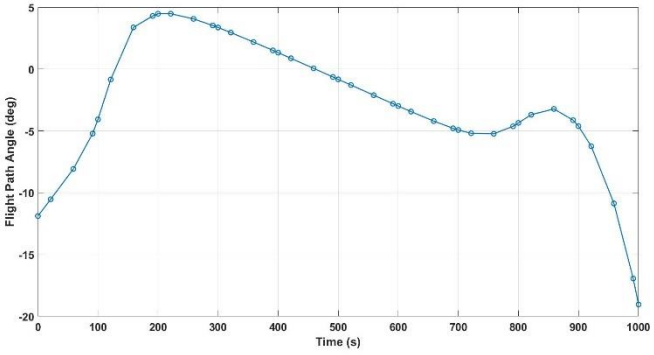

(d) Flight path angle

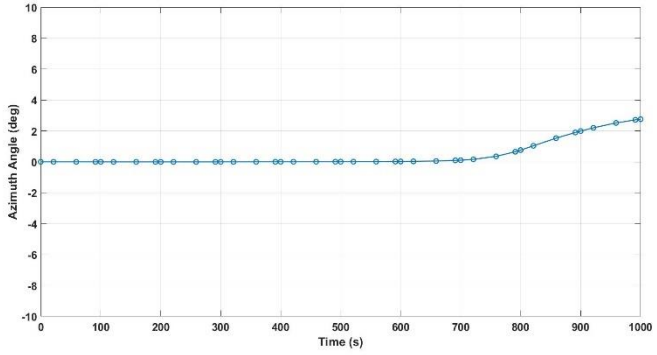

(e)Azimuth angle

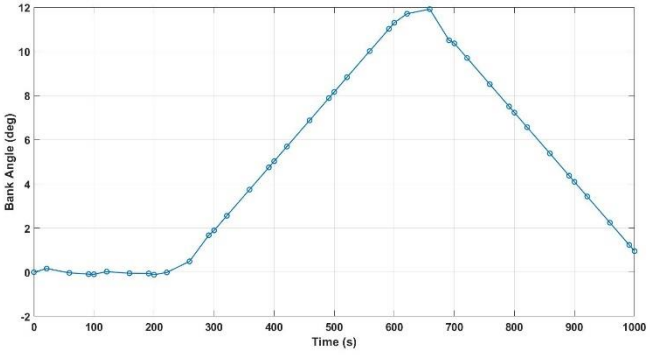

(f) Bank angle

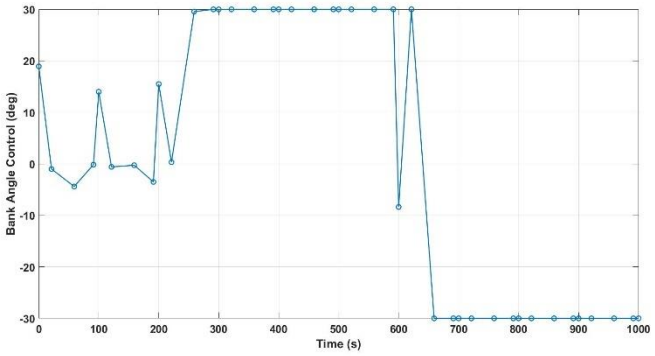

(g) Bank angle control

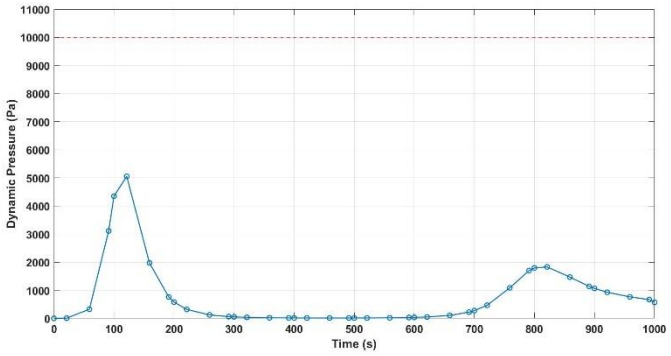

(h) Dynamic Pressure

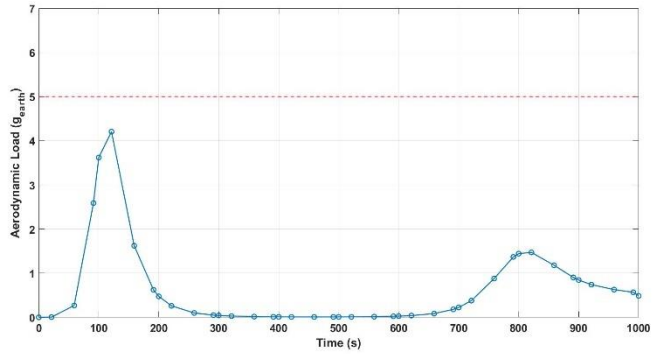

(i) Aerodynamic Load

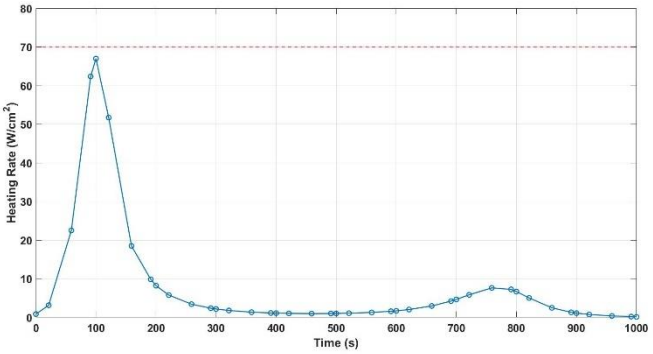

(j) Heating rate

Figure B-2 Full results of Problem B-2

t (sec)	h (km)	v (km/s)	λ (deg)	γ (deg)	ψ (deg)	σ (deg)	σ_c (deg)	q (Pa)	a (g_{earth})	$\dot{Q}$ (W/cm^2)
0	125	6	0	-11.8868	0	0	18.91885	0.44703	0.000372	0.836143
21.23405	100.2772	6	2.038789	-10.5272	-2.4E-05	0.165033	-1.00218	6.283258	0.00521	3.134762
59.05331	63.40536	6	5.737787	-8.07288	8.3E-05	-0.03079	-4.40169	323.667	0.268292	22.49891
91.1412	41.18933	5.673176	8.848851	-5.21083	-0.00112	-0.08762	-0.1662	3111.078	2.588108	62.36166
100	37.15913	5.407028	9.671207	-4.06439	-0.00215	-0.09333	13.98679	4348.029	3.620959	66.96891
121.2341	32.62568	4.575333	11.43683	-0.83919	-0.00261	0.023931	-0.59145	5054.789	4.206904	51.70192
159.0533	36.21578	3.462843	13.94106	3.374904	-0.00188	-0.04874	-0.27277	1972.601	1.622429	18.50099
191.1412	43.67254	3.206187	15.68439	4.300564	-0.0043	-0.0579	-3.51511	761.9801	0.62486	9.857329
200	45.77431	3.129604	16.16165	4.479829	-0.00412	-0.11437	15.49357	579.9119	0.475079	8.193501

221.2341	50.91572	3.051223	17.24873	4.480709	-0.00458	-0.01283	0.318131	318.1428	0.260542	5.768578
259.0533	59.4672	2.98235	19.13389	4.062838	-0.00387	0.490162	29.5577	121.8306	0.099821	3.410398
291.1412	65.77548	2.952012	20.70746	3.530078	-0.00222	1.674692	30	60.81218	0.049852	2.360703
300	67.35059	2.94665	21.13867	3.364197	-0.00159	1.889418	29.98343	51.20128	0.041979	2.158277
321.2341	70.79451	2.935411	22.16957	2.955472	-0.00029	2.555444	30	35.16128	0.028834	1.774925
359.0533	75.77115	2.921486	23.99628	2.189258	0.001793	3.742017	30	20.45858	0.01678	1.341082
391.1412	78.80026	2.91344	25.53953	1.517226	0.003369	4.748666	30	14.71776	0.012071	1.131209
400	79.44134	2.911692	25.96476	1.329197	0.003791	5.02661	30	13.72639	0.011258	1.091135
421.2341	80.63056	2.908116	26.98295	0.875777	0.004796	5.692786	30	12.05798	0.009889	1.020165
459.0533	81.53008	2.90368	28.79351	0.06073	0.006675	6.87929	30	10.91906	0.008954	0.967832
491.1412	81.06362	2.901471	30.32794	-0.63515	0.008536	7.885983	30	11.45992	0.009397	0.990004
500	80.73555	2.901067	30.75142	-0.82764	0.009124	8.16391	30	11.86567	0.00973	1.007097
521.2341	79.59791	2.900372	31.76638	-1.2891	0.010741	8.830086	30	13.39379	0.010982	1.069471
559.0533	76.34501	2.899701	33.57428	-2.1094	0.014733	10.01659	30	18.9553	0.01554	1.271691
591.1412	72.3597	2.898715	35.10869	-2.7999	0.020332	11.02328	30	29.00466	0.023771	1.572007
600	71.06304	2.898169	35.53238	-2.98893	0.022474	11.30121	-8.37468	33.3048	0.027291	1.683878
621.2341	67.6152	2.895725	36.54779	-3.43695	0.029312	11.7083	30	48.06763	0.039367	2.019532
659.0533	60.31899	2.883826	38.35422	-4.20538	0.05184	11.91723	-30	103.9993	0.085044	2.946205
691.1412	53.08726	2.854146	39.87814	-4.78593	0.090809	10.50705	-30	220.7012	0.180081	4.204017
700	50.9506	2.840036	40.29583	-4.92498	0.106558	10.36862	-30	274.6012	0.223884	4.643104
721.2341	45.66339	2.787993	41.28695	-5.19126	0.161018	9.702445	-30	465.711	0.378824	5.827086
759.0533	36.30448	2.58053	42.98095	-5.22832	0.353795	8.515941	-30	1085.11	0.877579	7.620168
791.1412	29.51587	2.247511	44.27767	-4.62757	0.653643	7.509248	-30	1700.772	1.368646	7.236633
800	28.00537	2.129495	44.6008	-4.34883	0.761164	7.231321	-30	1794.427	1.44279	6.673072
821.2341	25.05943	1.837447	45.30382	-3.6929	1.037553	6.565145	-30	1830.538	1.471237	5.01798
859.0533	21.51636	1.361803	46.31091	-3.21978	1.530779	5.378641	-30	1468.513	1.179157	2.46875
891.1412	19.15423	1.056547	46.95469	-4.13171	1.898496	4.371947	-30	1137.882	0.903513	1.308084
900	18.45693	0.985326	47.10653	-4.61781	1.992236	4.09402	-30	1066.24	0.845366	1.101279

921.2341	16.65736	0.83502	47.42862	-6.23906	2.20084	3.427844	-30	928.1981	0.740709	0.737945
959.0533	12.7564	0.614756	47.88102	-10.8685	2.517607	2.241341	-30	763.4292	0.628641	0.362743
991.1412	8.714307	0.463445	48.16224	-16.9411	2.717356	1.234647	-30	668.3875	0.56664	0.192894
1000	7.5	0.4	48.2252	-19.0384	2.758068	0.95672	-30	566.9327	0.487203	0.132341

Table B-2 Profile of Problem B-2

B.3 Full results of Problem B-3

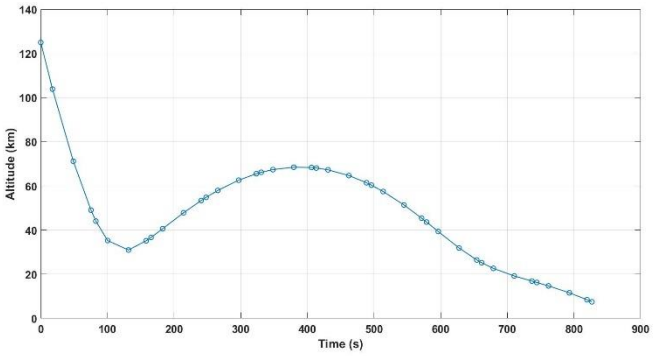

(a)Altitude

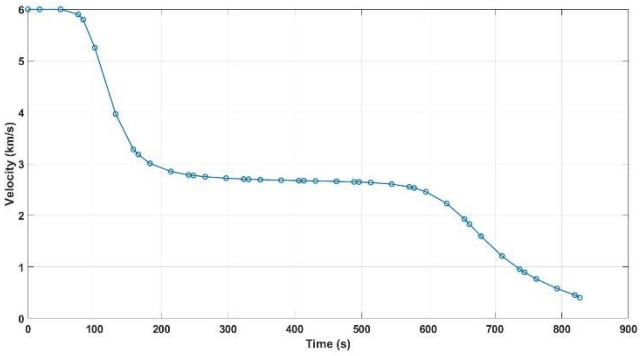

(b) Velocity

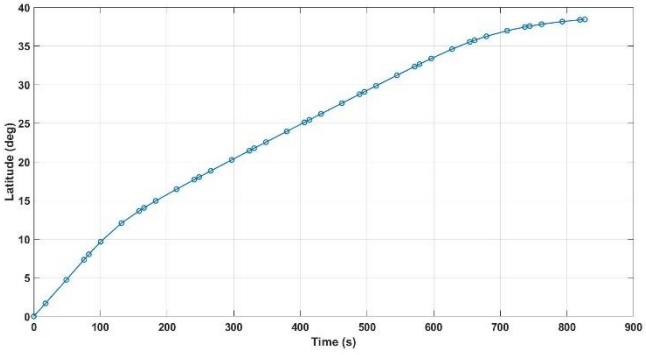

(c) Latitude

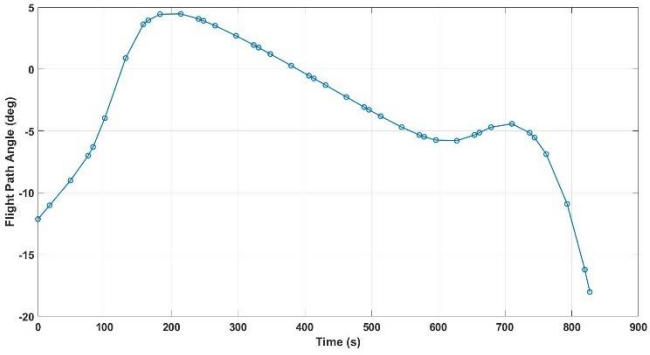

(d) Flight path angle

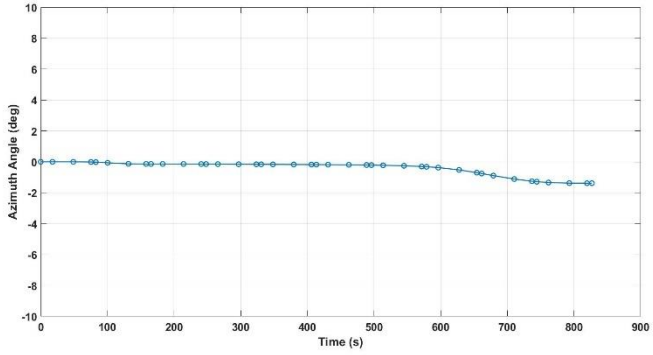

(e)Azimuth angle

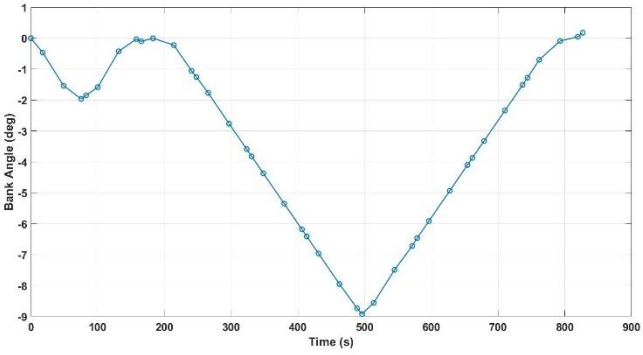

(f) Bank angle

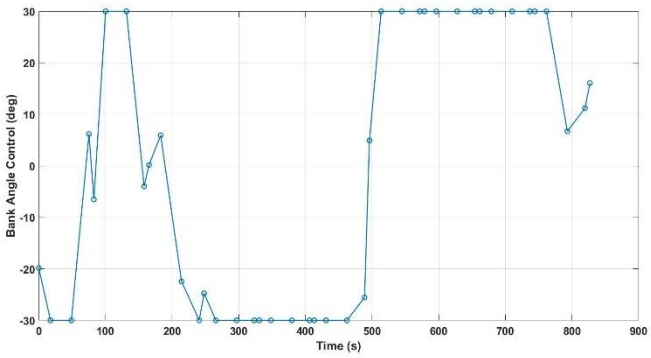

(g) Bank angle control

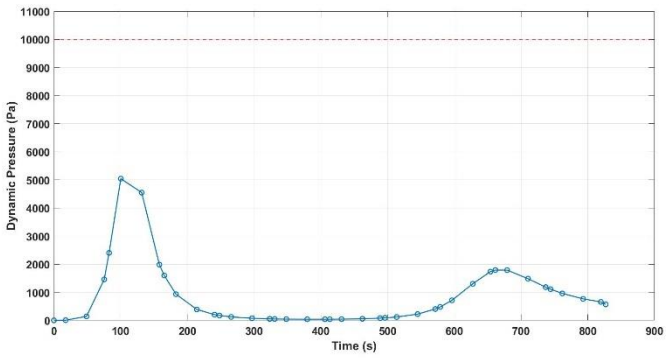

(h) Dynamic Pressure

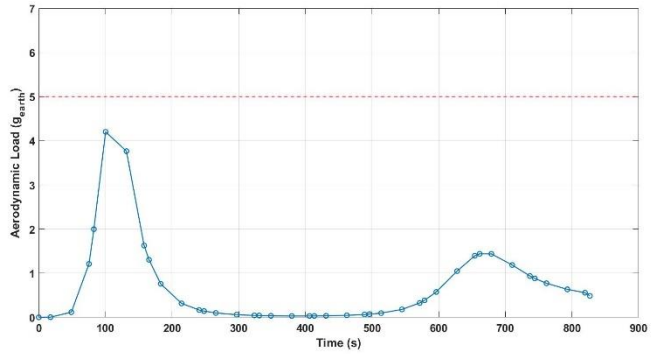

(i) Aerodynamic Load

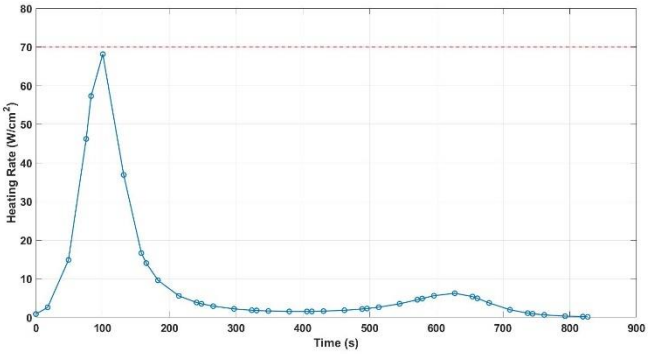

(j) Heating rate

Figure B-3 Full results of Problem B-3

t (sec)	h (km)	v (km/s)	λ (deh)	γ (deg)	ψ (deg)	σ (deg)	σ_c (deg)	q (Pa)	a (g_{earth})	$\dot{Q}$ (W/cm^2)
0	125	6	0	-12.1375	0	0	-19.8538	0.44703	0.000372	0.836143
17.55796	103.8684	6	1.683922	-11.0192	-0.0002	-0.46292	-29.9957	4.280067	0.003551	2.587244
48.82985	71.17208	6	4.725449	-9.01071	6.78E-06	-1.53457	-29.9981	141.091	0.116885	14.85463
75.36261	49.02607	5.901891	7.322464	-6.99645	-0.01079	-1.9644	6.183954	1456.768	1.209852	46.18355
82.68775	44.02748	5.800801	8.033867	-6.29803	-0.01929	-1.84934	-6.50266	2401.389	1.996234	57.28182
100.2457	35.2387	5.255113	9.652841	-3.96544	-0.06213	-1.58321	29.99959	5043.16	4.201307	68.12793
131.5176	30.94808	3.967758	12.06077	0.889625	-0.13012	-0.42315	29.99942	4548.171	3.765254	36.88234
158.0504	35.13716	3.277919	13.63767	3.628074	-0.13588	-0.02922	-3.96869	1983.578	1.625408	16.62382
165.3755	36.61574	3.181263	14.03511	3.945293	-0.1383	-0.10006	0.167585	1595.156	1.305129	14.04141

182.9335	40.61083	3.007913	14.93705	4.443102	-0.13954	-0.00222	5.918485	930.3525	0.759294	9.586585
214.2053	47.81709	2.851617	16.45177	4.467048	-0.14103	-0.22275	-22.4693	387.01	0.315379	5.557162
240.7381	53.38869	2.784654	17.69075	4.065026	-0.14489	-1.05522	-29.9957	203.4228	0.165746	3.841952
248.0632	54.81075	2.772835	18.02746	3.912398	-0.14629	-1.25694	-24.7476	173.2531	0.141172	3.515592
265.6212	57.95184	2.748912	18.83005	3.510927	-0.14967	-1.7684	-29.9991	121.7075	0.099185	2.895944
296.8931	62.59435	2.720127	20.24478	2.69768	-0.15564	-2.76774	-29.9995	72.54848	0.059138	2.189285
323.4258	65.51566	2.703551	21.43503	1.950777	-0.16058	-3.58836	-29.9993	52.44286	0.042754	1.838748
330.751	66.15307	2.699869	21.76235	1.738152	-0.16193	-3.82266	-29.9964	48.85494	0.039829	1.769902
348.3089	67.37614	2.692048	22.54522	1.221293	-0.16519	-4.37347	-29.9996	42.61899	0.034746	1.643528
379.5808	68.48024	2.680996	23.93445	0.280698	-0.17127	-5.35457	-29.9997	37.56363	0.030621	1.530332
406.1136	68.32672	2.673489	25.10909	-0.53009	-0.17705	-6.18696	-29.9994	37.97168	0.030948	1.530017
413.4387	68.10718	2.671606	25.43284	-0.75524	-0.17881	-6.41677	-29.997	38.81869	0.031636	1.54481
430.9967	67.26842	2.667225	26.20795	-1.29607	-0.18344	-6.96614	-29.9996	42.3212	0.034483	1.60771
462.2686	64.68446	2.659074	27.58552	-2.25952	-0.19389	-7.95402	-29.9995	55.44591	0.045151	1.828964
488.8013	61.40917	2.649988	28.75089	-3.06955	-0.20674	-8.73982	-25.5605	78.15636	0.063597	2.156649
496.1265	60.33283	2.646769	29.07192	-3.29059	-0.21129	-8.92625	4.920454	87.47447	0.071161	2.276053
513.6844	57.45915	2.636827	29.83968	-3.81204	-0.22444	-8.5634	29.9996	118.0414	0.095955	2.624158
544.9563	51.36692	2.605972	31.1981	-4.69056	-0.25784	-7.49507	29.99991	221.1388	0.179435	3.508179
571.4891	45.3737	2.552456	32.3332	-5.32827	-0.30403	-6.71894	29.99993	402.6242	0.325987	4.541258
578.8142	43.6197	2.530281	32.64191	-5.47466	-0.32142	-6.46765	29.9998	477.262	0.386143	4.858762
596.3722	39.32352	2.457555	33.36911	-5.74378	-0.37406	-5.9168	29.99998	712.6752	0.575525	5.600952
627.6441	31.86665	2.229493	34.59203	-5.78834	-0.52077	-4.93571	29.99999	1301.7	1.04752	6.22985
654.1768	26.45349	1.927816	35.51394	-5.32888	-0.70067	-4.1033	29.99999	1736.024	1.395137	5.379213
661.502	25.203	1.8309	35.74323	-5.13686	-0.75697	-3.87349	29.99996	1789.833	1.438537	4.926575
679.0599	22.62933	1.594481	36.24492	-4.69987	-0.89327	-3.32264	29.99999	1787.37	1.437376	3.733839
710.3318	19.20318	1.209558	36.97484	-4.42579	-1.11416	-2.34155	29.99999	1483.547	1.185582	1.957556
736.8646	16.87996	0.953511	37.4516	-5.15117	-1.25577	-1.50914	29.99997	1181.853	0.937219	1.085783
744.1897	16.24667	0.893111	37.56491	-5.54189	-1.28624	-1.27933	29.99986	1109.494	0.881746	0.92296

761.7477	14.69191	0.764223	37.80731	-6.8841	-1.33955	-0.69851	29.99993	959.2678	0.771789	0.628376
793.0196	11.57056	0.577416	38.15355	-10.9018	-1.37949	-0.08989	6.710675	764.5357	0.63387	0.320248
819.5523	8.442162	0.452643	38.37617	-16.2198	-1.38312	0.047486	11.21226	656.418	0.557746	0.182353
826.8775	7.5	0.4	38.42769	-18.0283	-1.38293	0.174895	16.0647	566.9327	0.487203	0.132341

Table B-3 Profile of Problem B-3

B.4 Full results of Problem B-4

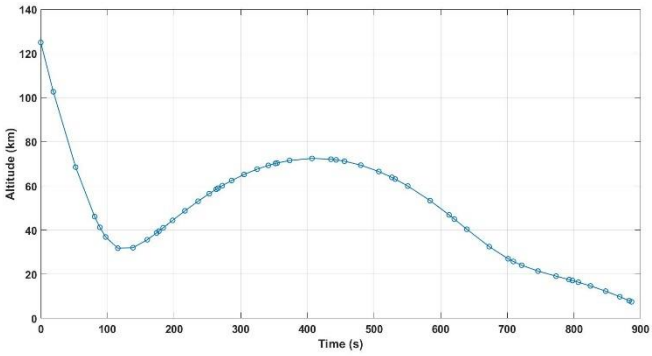

(a)Altitude

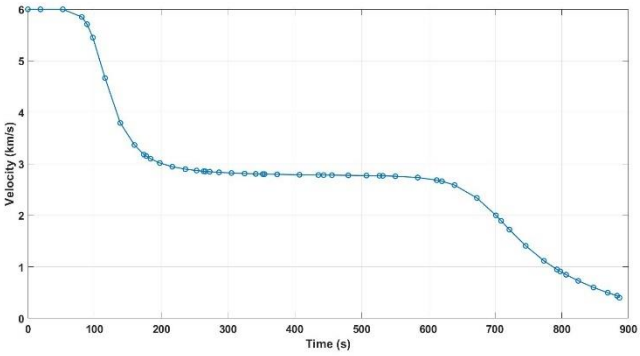

(b) Velocity

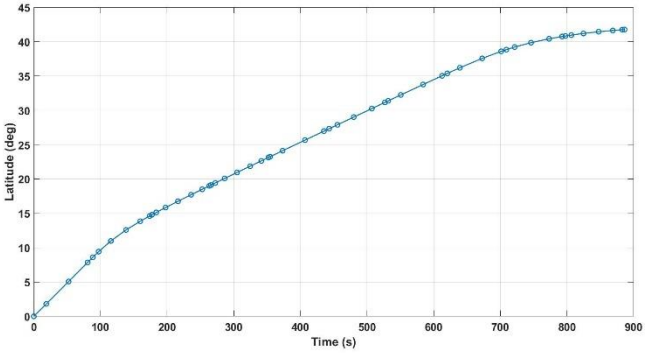

(c) Latitude

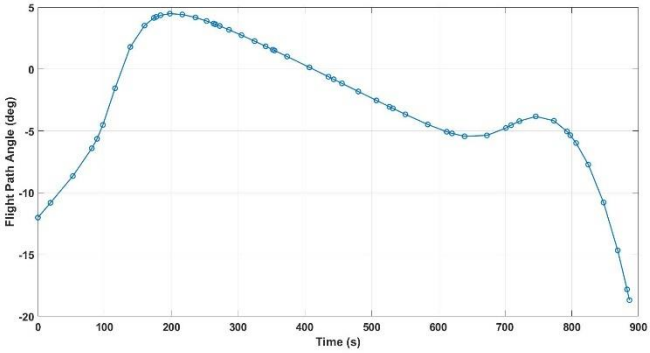

(d) Flight path angle

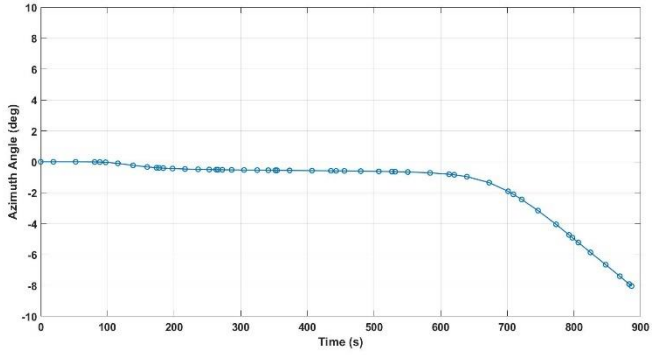

(e)Azimuth angle

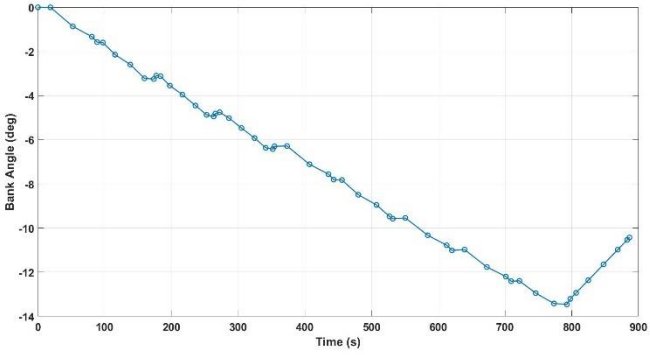

(f) Bank angle

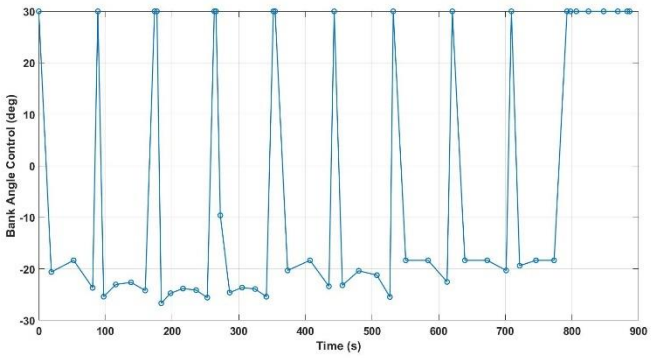

(g) Bank angle control

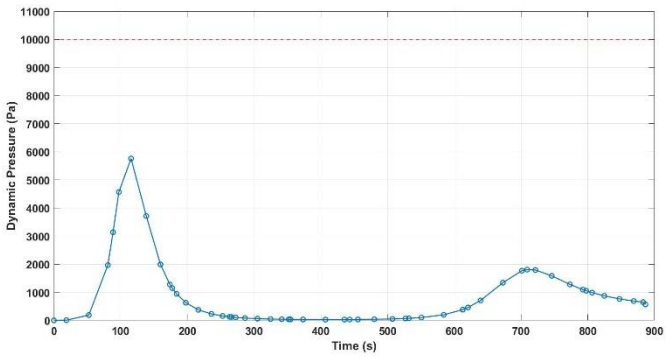

(h) Dynamic Pressure

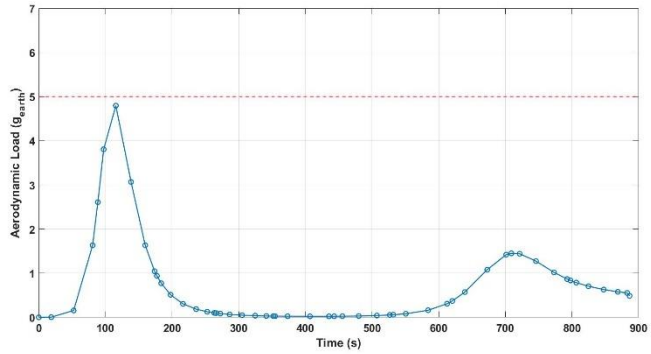

(i) Aerodynamic Load

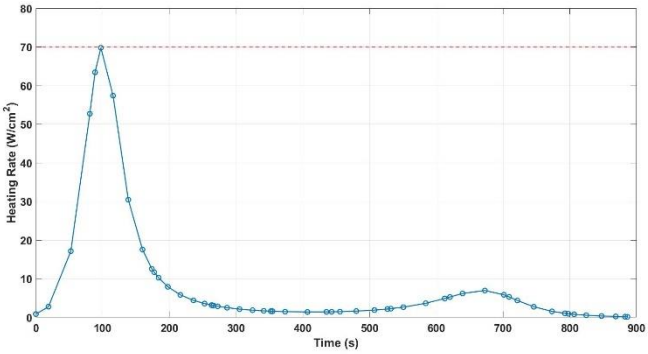

(j) Heating rate

Figure B-4 Full results of Problem B-4

t (sec)	h (km)	v (km/s)	λ (deg)	γ (deg)	ψ (deg)	σ (deg)	σ_c (deg)	q (Pa)	a (g_{earth})	$\dot{Q}$ (W/cm^2)
0	125	6	0	-12.0133	0	0	30	0.44703	0.000372	0.836143
18.82111	102.6589	6	1.806131	-10.8124	-0.00016	-0.0029	-20.6161	4.870864	0.004041	2.760039
52.34276	68.4985	6	5.071966	-8.65592	0.000165	-0.86573	-18.3471	187.7718	0.155584	17.1367
80.78432	46.06705	5.851047	7.852883	-6.40595	-0.00808	-1.32899	-23.6902	1964.531	1.632412	52.71161
88.63644	41.23616	5.710434	8.609589	-5.64031	-0.01475	-1.57692	30	3136.333	2.608754	63.43939
97.37024	36.84208	5.450678	9.42295	-4.51191	-0.02929	-1.59704	-25.4032	4570.847	3.806188	69.77648
115.6294	31.77105	4.665664	10.97452	-1.55233	-0.09869	-2.1444	-23.0376	5759.222	4.794687	57.38767
138.4524	32.00285	3.792696	12.58432	1.793476	-0.2286	-2.59437	-22.6314	3712.538	3.066896	30.44677
159.7217	35.60076	3.365227	13.84503	3.520979	-0.33169	-3.21575	-24.202	1989.559	1.633211	17.54756

173.7443	38.69337	3.179255	14.60851	4.144428	-0.38327	-3.24878	30	1275.831	1.044365	12.54172
177.2729	39.51164	3.15172	14.793	4.226377	-0.39251	-3.09553	30	1148.806	0.940062	11.69575
183.7482	41.03677	3.099653	15.12872	4.357559	-0.40793	-3.12179	-26.6866	943.9903	0.771949	10.25462
197.7272	44.36357	3.015628	15.83649	4.483858	-0.43563	-3.5475	-24.7332	626.091	0.511531	7.904672
216.3907	48.72622	2.943459	16.75609	4.420834	-0.46398	-3.95536	-23.8292	374.1501	0.305556	5.821682
236.0402	53.06845	2.896129	17.7042	4.180375	-0.48532	-4.45132	-24.1323	227.699	0.185957	4.396693
252.7842	56.4906	2.869123	18.50153	3.891184	-0.49959	-4.87018	-25.591	155.0021	0.12661	3.56022
263.3108	58.49295	2.856153	18.99919	3.683402	-0.50694	-4.94521	30	124.0039	0.101304	3.15566
265.9093	58.96855	2.853314	19.12168	3.629721	-0.50864	-4.81289	30	117.6225	0.096094	3.067284
272.3846	60.12071	2.846771	19.42638	3.49247	-0.51248	-4.75356	-9.61643	103.5149	0.084576	2.864284
286.3636	62.44346	2.834799	20.08185	3.181872	-0.51998	-5.01951	-24.6071	80.0756	0.065437	2.498068
305.0271	65.18283	2.822257	20.95288	2.74422	-0.52896	-5.4677	-23.6378	59.21931	0.048403	2.129289
324.6766	67.60667	2.812039	21.86595	2.263607	-0.53742	-5.92434	-23.9188	45.37087	0.03709	1.850295
341.4206	69.29171	2.805062	22.64147	1.842777	-0.54421	-6.36626	-25.4149	37.7038	0.030825	1.678368
351.9473	70.16962	2.801309	23.12804	1.574202	-0.54833	-6.42139	30	34.23434	0.027989	1.595007
354.5458	70.36464	2.800447	23.24804	1.507506	-0.54933	-6.29653	30	33.50736	0.027395	1.577011
373.3669	71.51943	2.79487	24.11614	1.020473	-0.55635	-6.28595	-20.3174	29.49803	0.024117	1.473769
406.8885	72.44681	2.787257	25.65835	0.140028	-0.56896	-7.11084	-18.3471	26.56849	0.02172	1.391064
435.3301	72.09167	2.78242	26.96393	-0.61506	-0.58055	-7.56003	-23.3953	27.50087	0.022479	1.410355
443.1822	71.80842	2.781265	27.32401	-0.82431	-0.58392	-7.80386	30	28.32285	0.02315	1.430089
455.57	71.19846	2.779534	27.89181	-1.15474	-0.58953	-7.82499	-23.1931	30.19366	0.024676	1.474727
480.0913	69.40318	2.7762	29.01485	-1.80893	-0.60191	-8.49079	-20.3827	36.49441	0.029817	1.617426
507.2803	66.50368	2.771878	30.25865	-2.53139	-0.61873	-8.95234	-21.2303	49.60128	0.040505	1.879768
526.7571	63.84606	2.767488	31.14846	-3.04381	-0.63397	-9.4694	-25.4619	65.69105	0.053616	2.156425
531.8187	63.07728	2.766037	31.37947	-3.17582	-0.63859	-9.57776	30	71.24331	0.058138	2.243353
550.6398	59.94288	2.758807	32.23729	-3.65998	-0.65871	-9.54232	-18.3471	99.08246	0.080796	2.631786
584.1614	53.33352	2.733488	33.75761	-4.47783	-0.71439	-10.3269	-18.3471	197.1755	0.160479	3.644772
612.603	46.85888	2.683672	35.03064	-5.06881	-0.80406	-10.7809	-22.5347	379.7404	0.308322	4.875418

620.4551	44.96859	2.66186	35.37724	-5.20225	-0.84032	-11.0125	30	457.2589	0.370955	5.263338
639.2762	40.3535	2.587081	36.19401	-5.43502	-0.95834	-10.9764	-18.3471	707.4317	0.572603	6.184036
672.7978	32.47669	2.336804	37.56448	-5.36426	-1.34545	-11.7675	-18.3471	1339.737	1.079295	6.943271
701.2394	26.97716	1.99979	38.58923	-4.76553	-1.90936	-12.1982	-20.3174	1766.364	1.419599	5.838735
709.0915	25.75429	1.892952	38.84197	-4.53828	-2.10352	-12.4053	30	1803.712	1.44956	5.286553
721.4794	24.06089	1.723501	39.21318	-4.20615	-2.43351	-12.394	-19.3985	1791.982	1.440665	4.368173
746.0006	21.42157	1.407319	39.84868	-3.82927	-3.15586	-12.9502	-18.3471	1584.295	1.272983	2.738502
773.1896	19.11229	1.117017	40.41583	-4.17698	-4.0491	-13.4158	-18.3471	1277.578	1.016859	1.549255
792.6665	17.53587	0.950059	40.74931	-5.03645	-4.73225	-13.4581	30	1093.855	0.86746	1.037028
797.728	17.1158	0.9111	40.82746	-5.34846	-4.91408	-13.2096	30	1052.19	0.835394	0.935382
806.4618	16.36854	0.847713	40.95483	-5.98181	-5.22286	-12.9356	30	986.6297	0.786527	0.784124
824.7209	14.69029	0.728316	41.19275	-7.72087	-5.86335	-12.3628	30	871.3955	0.704467	0.543948
847.5439	12.31441	0.59991	41.44205	-10.787	-6.65837	-11.6467	30	762.1782	0.629295	0.345151
868.8132	9.792938	0.49774	41.63225	-14.6662	-7.40603	-10.9795	30	687.0035	0.578349	0.225577
882.8358	7.975045	0.438572	41.73788	-17.8179	-7.91169	-10.5395	30	647.7947	0.552069	0.170063
886.3644	7.5	0.4	41.76217	-18.6887	-8.04146	-10.4288	30	566.9327	0.487203	0.132341

Table B-4 Profile of Problem B-4

B.5 Full comparison results of Problem B

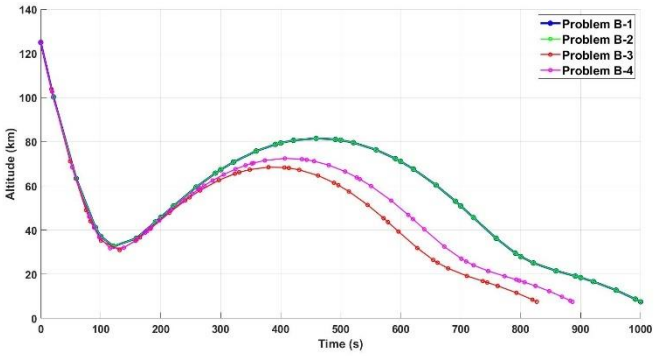

(a)Altitude

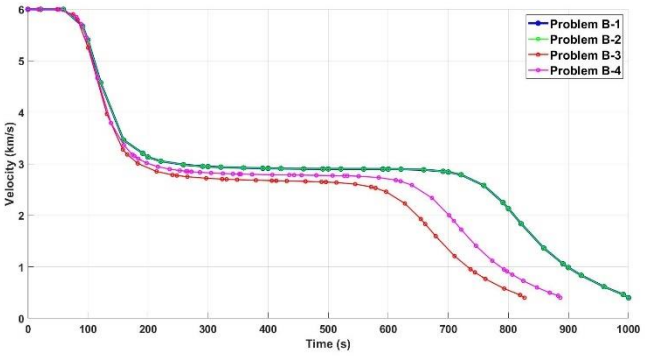

(b) Velocity

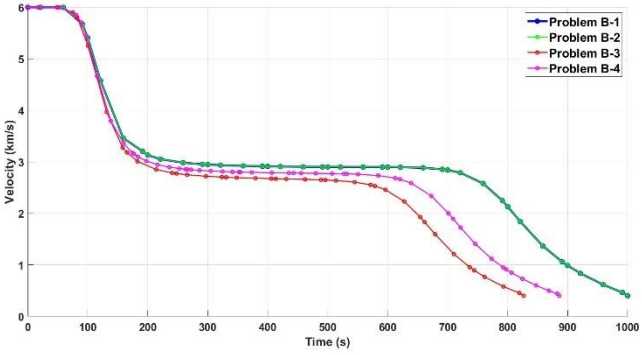

(c) Latitude

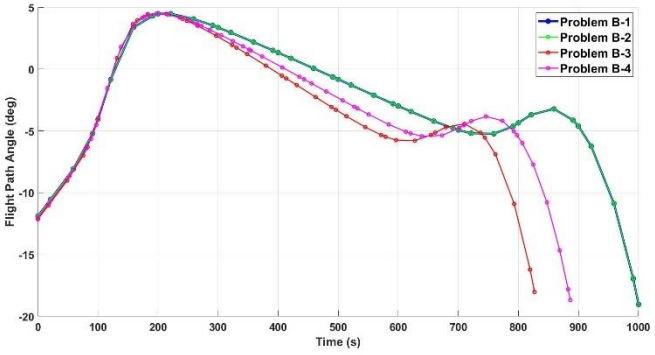

(d) Flight path angle

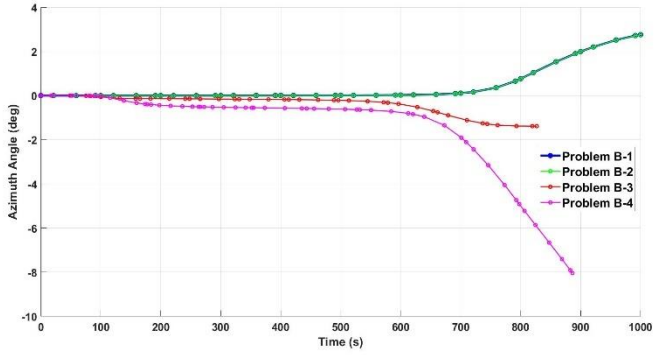

(e)Azimuth angle

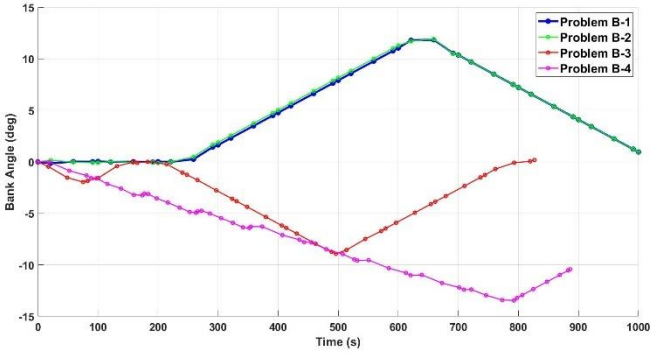

(f) Bank angle

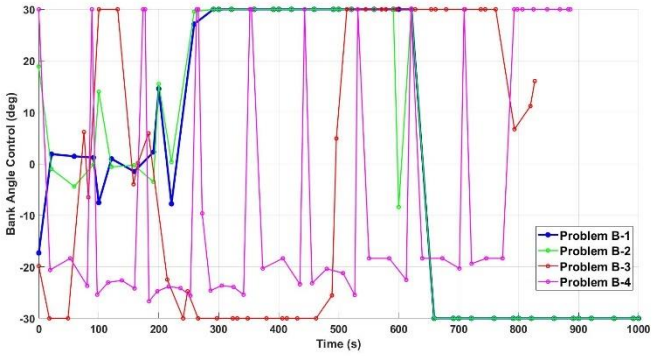

(g) Bank angle control

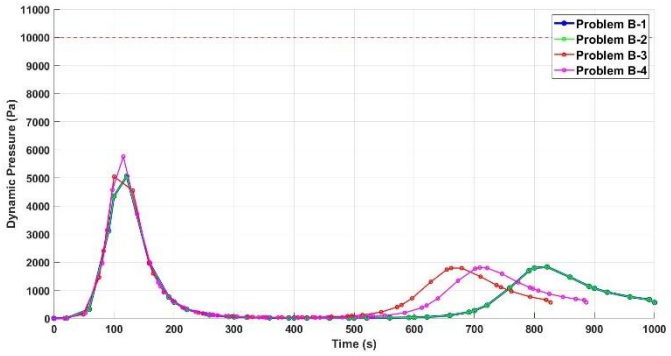

(h) Dynamic Pressure

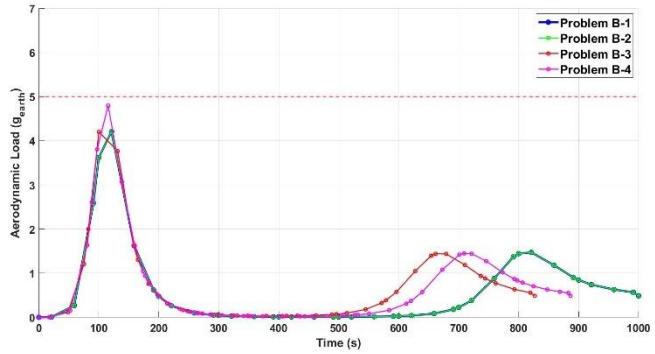

(i) Aerodynamic Load

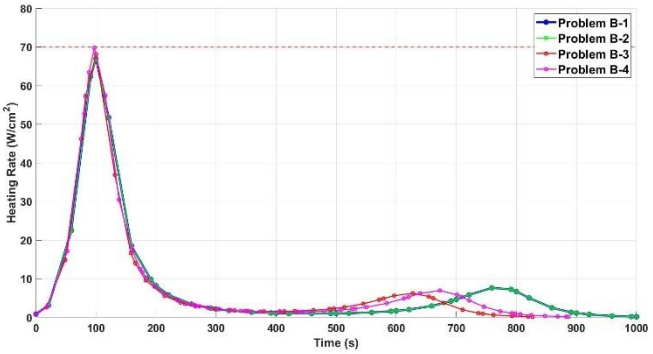

(j) Heating rate

Figure B-5 Full comparison results of Problem B

Appendix C MATLAB codes for trajectory optimisation

These functions are modified from **rlventry** package in GPOPS-II.

C.1 MarsEntryMain

```
% ---------- Reusable Launch Vehicle Entry Example ------------%
% This example is taken verbatim from the following reference:  %
% Betts, J. T., Practical Methods for Optimal Control Using     %
% Nonlinear Programming, SIAM Press, Philadelphia, 2009.        %
% -------------------------------------------------------------%
%close all
clear all
clc

m2ft=3.28083989501; %meters to feet
re=3396200; %Mars Radius, m
muM = 4.284e13;
g0 = muM/(re^2);
%-------------------------------------%
%             Problem Setup           %
%-------------------------------------%
auxdata.re      = 3396200;                          % m
auxdata.g0      = muM/(re^2);                           % 3.711
auxdata.d2r     = 0.01745329251994;                 % pi/180
auxdata.Sref    = 15.9;
auxdata.mass    = 2920;                             % kg
auxdata.muM     = 4.284e13;
ts          = sqrt(re/g0);
rs          = re;
vs          = sqrt(re*g0);
%-------------------------------------------------------------------------%
%---------------------- Boundary Conditions ----------------------%
%-------------------------------------------------------------------------%

t0          = 0/ts;
alt_0       = 125000/rs;                    alt_f       = 7500/rs;
r_0         = alt_0+auxdata.re/rs;          r_f         = alt_f+auxdata.re/rs;
theta_0     = deg2rad(0);               theta_f     = deg2rad(0);
phi_0       = deg2rad(0);               phi_f       = deg2rad(0);
v_0         = 6000/vs;                      v_f         = 400/vs;
gamma_0     = deg2rad(-50);             gamma_f     = deg2rad(0);
psi_0       = deg2rad(0);
bank0       = deg2rad(0);

%-------------------------------------------------------------------------%
%---------------------- Limits on Variables ----------------------%
%-------------------------------------------------------------------------%

tfMin       = 0/ts;                         tfMax       = 1000/ts;
r_min       = r_f;                      r_max       = r_0;
theta_min   = -pi;                      theta_max   = pi;
phi_min     = -90*pi/180;               phi_max     = 90*pi/180;
v_min       = 1/vs;                         v_max       = v_0;
v_f_min     = 1/vs;                      v_f_max     = 500/vs;
gamma_min   = -180*pi/180;              gamma_max   = 180*pi/180;
psi_min     = -180*pi/180;              psi_max     = 180*pi/180;
bank_min    = -30*pi/180;               bank_max    = 30*pi/180;

%-------------------------------------------------------------------------%
%--------------- Set Up Problem Using Data Provided Above ----------%
%-------------------------------------------------------------------------%

bounds.phase.initialtime.lower = t0;
bounds.phase.initialtime.upper = t0;

bounds.phase.finaltime.lower = tfMin;
bounds.phase.finaltime.upper = tfMax;

bounds.phase.initialstate.lower = [r_0, theta_0, phi_0, v_0, gamma_min, psi_0, bank0];
bounds.phase.initialstate.upper = [r_0, theta_0, phi_0, v_0, gamma_max, psi_0, bank0];
```

```
bounds.phase.state.lower = [r_f, theta_min, phi_min, v_min, gamma_min, psi_min,
bank_min];
bounds.phase.state.upper = [r_max, theta_max, phi_max, v_max, gamma_max, psi_max,
bank_max];

bounds.phase.finalstate.lower = [r_f, theta_min, phi_min, v_f_min, gamma_min, psi_min,
bank_min];
bounds.phase.finalstate.upper = [r_f, theta_max, phi_max, v_f_max, gamma_max, psi_max,
bank_max];


bounds.phase.control.lower = [bank_min];
bounds.phase.control.upper = [bank_max];

%---------------------------------------------------------------------%
%------------------------ Path Constraints ---------------------------%
%---------------------------------------------------------------------%
bounds.phase.path.lower = [0 0 0];              % [q   a  Qdot ]
bounds.phase.path.upper = [10000 5*9.81./g0 70];         % [pa 9.81  70(W/cm2)]


%---------------------------------------------------------------------------%
%------------------------ Set up Initial Guess -----------------------------%
%---------------------------------------------------------------------------%

tGuess                  = [0/ts; 1000/ts];
rGuess                  = [r_0; r_f];
thetaGuess              = [theta_0; theta_f];
phiGuess                = [phi_0; phi_f];
vGuess                  = [v_0; v_f_min];
gammaGuess              = [gamma_0; gamma_0];
psiGuess                = [psi_0; psi_max/2];
bankGuess               = [bank0; bank0];
bankcGuess              = [bank_min; bank_max];

guess.phase.state   = [rGuess, thetaGuess, phiGuess, vGuess, gammaGuess, psiGuess,
bankGuess];
guess.phase.control = [bankGuess];
guess.phase.time    = tGuess;

%----------------------%
% Set up Initial Mesh %
%----------------------%
meshphase.colpoints = 4*ones(1,10);
meshphase.fraction = 0.1*ones(1,10);

setup.name = 'MARSEntry';
setup.functions.continuous = @MARSEntryContinuous;
setup.functions.endpoint   = @MARSEntryEndpoint;
setup.auxdata = auxdata;
setup.mesh.phase = meshphase;
setup.bounds = bounds;
setup.guess = guess;
setup.nlp.solver = 'snopt';
setup.derivatives.supplier = 'sparseCD';
setup.derivatives.derivativelevel = 'second';
setup.scales.method = 'automatic-bounds';
setup.method = 'RPM-Integration';
setup.mesh.method = 'hp-PattersonRao';

setup.mesh.tolerance = 1e-3; % default 1e-3
setup.mesh.colpointsmin = 4;
setup.mesh.colpointsmax = 16;

%----------------------------------%
% Solve Problem Using OptimalPrime %
%----------------------------------%
output = gpops2(setup);
```

C.2 MarsEntryContinuous

```
function phaseout = MARSEntryContinuous(input)

%----------- dimensionless -----------------------------------------%
r = input.phase.state(:,1);                 % Mars' radius +alt dimensionless  in m
theta = input.phase.state(:,2);
lambda = input.phase.state(:,3);
v = input.phase.state(:,4);                 % m/s
gamma = input.phase.state(:,5);
psi = input.phase.state(:,6);
bank = input.phase.state(:,7);
bank_c = input.phase.control(:,1);

re = input.auxdata.re;                      %m
g0 = input.auxdata.g0;
d2r = input.auxdata.d2r;
Sref = input.auxdata.Sref;
mass = input.auxdata.mass;
mu = 4.284e13;

% ------------- scale ----------------------------------------------------
ts          = sqrt(re/g0);
rs          = re;
vs          = sqrt(re*g0);

alt_nd = (r.*rs-re)./1000;

%------------------- Compute density (rho in kg/m^3) ---------------------%
rho = density(alt_nd);          % kg/m^3
%------------------- Compute the lift and drag coefficients --------------%

[Cl, Cd] = aerodynamics_MSL(alt_nd.*1000, v, vs);

if isnan(rho)
    aD = v;
    aL = v;
else

        aD=rho.*((vs.*v).^2).*Sref.*Cd./(mass.*2.*g0);    % ad
        aL=rho.*((vs.*v).^2).*Sref.*Cl./(mass.*2.*g0);    % al
end

%------------ path constraints -------------------------------------%
q       = 0.5.*rho.*((vs.*v).^2);

a       = sqrt((aD).^2+(aL).^2);

k       = 1.9027e-4;    % heating rate modeel parameter
N       = 0.5;          % heating rate modeel parameter
M       = 3;            % heating rate modeel parameter
rn      = 0.6;          % nose radius in m
Qdot    = k.*sqrt((rho)./(rn)).*(((vs.*v)).^M)./10000;      %input: m ; output: m, so
/10000

size(q);
%-------------------------------------------------------------------%

sigma=bank;

rdot=v.*sin(gamma);
thetadot=(v.*cos(gamma).*sin(psi))./(r.*cos(lambda));
phidot=v.*cos(gamma).*cos(psi)./(r);

Vdot= -aD-(sin(gamma)./(r.^2));
gammadot=(aL.*cos(sigma))./v + (v.^2-1./r).*(cos(gamma)./(v.*r));
psidot = ((aL.*sin(sigma))./(v.*cos(gamma)))+(v.*sin(psi).*cos(gamma).*tan(lambda))./r;

bankdot = bank_c;


phaseout.dynamics  = [rdot thetadot phidot Vdot gammadot psidot bankdot];
phaseout.path = [q a Qdot];
```

C.3 MarsEntryEndpoint

```
function output = MARSEntryEndpoint(input)

tf = input.phase.finaltime;
vf = input.phase.finalstate(4);
% cost
output.objective = vf;
```

C.4 MarsEntryPlot

```
%-------------------------------------------%
% Extract Solution from Output (Dimensionless)%
%-------------------------------------------%
solution = output.result.solution;
time = solution.phase(1).time.*ts;                              % NON Dimensionless
altitude  = (solution.phase(1).state(:,1).*rs-re)/1000;         % km NON dimensionless
longitude = solution.phase(1).state(:,2)*180/pi;
latitude  = solution.phase(1).state(:,3)*180/pi;

speed     = solution.phase(1).state(:,4);                       % km/s dimensionless
speed_nd     = speed.*vs./1000;                                 % km/s NON dimensionless

fpa       = solution.phase(1).state(:,5)*180/pi;
azimuth   = solution.phase(1).state(:,6)*180/pi;
bank      = solution.phase(1).state(:,7)*180/pi;
bankc     = solution.phase(1).control(:,1)*180/pi;

%-------------------------------------------------------------------------%
Sref = auxdata.Sref;
mass = auxdata.mass;
% --------------- q calculation ---------------------------------------- %
rho = density(altitude);
q = 0.5.*rho.*((vs.*speed).^2);
% --------------- a calculation ---------------------------------------- %
[Cl, Cd] = aerodynamics_MSL(altitude.*1000, speed, vs);

if isnan(rho)
    aD = v;
    aL = v;
else
        aD=rho.*((vs.*speed).^2).*Sref.*Cd./(mass.*2.*g0);     % ad
        aL=rho.*((vs.*speed).^2).*Sref.*Cl./(mass.*2.*g0);     % al
end

a = sqrt((aD).^2+(aL).^2).*g0./9.81;   % in g_earth

% ----------------- Q dot calculation ----------------------------------%
k       = 1.9027e-4;     % heating rate modeel parameter
N       = 0.5;           % heating rate modeel parameter
M       = 3;             % heating rate modeel parameter
rn      = 0.6;           % nose radius in m
Qdot    = k.*sqrt((rho)./(rn)).*((vs.*(speed)).^M)./10000;    %input: m ; output: m, so
/10000



% ------------- Excel writing -------------------------------------------%
xlswrite('timeB4', time);
xlswrite('altitudeB4',altitude);
xlswrite('latitudeB4',latitude);
xlswrite('velocityB4',speed_non);
xlswrite('fpaB4',fpa);
xlswrite('azimuthB4',azimuth);
xlswrite('bankB4',bank);
xlswrite('bankcB4',bankc);
xlswrite('qB4',q);
xlswrite('aB4',a);
xlswrite('QdotB4',Qdot);



%---------------%
% Plot Solution %
%---------------%
figure(1)
pp = plot(time,altitude,'-o', 'markersize', 7, 'linewidth', 1.5);
xl = xlabel('Time (s)');
yl = ylabel('Altitude (km)');
set(xl,'FontSize',18,'FontWeight','bold');
set(yl,'FontSize',18,'FontWeight','bold');
set(gca,'FontSize',16,'FontWeight','bold');
set(pp,'LineWidth',1.25);
```

```
grid on
saveas (gcf,'Altitude vs Time','fig')

figure(2)
plot(time,latitude,'-o', 'markersize', 7, 'linewidth', 1.5);
xl = xlabel('Time (s)');
yl = ylabel('Latitude (deg)');
set(xl,'FontSize',18,'FontWeight','bold');
set(yl,'FontSize',18,'FontWeight','bold');
set(gca,'FontSize',16,'FontWeight','bold');
set(pp,'LineWidth',1.25);
grid on
saveas (gcf,'Latitude vs Time','fig')

figure(3)
plot(time,speed_nd,'-o', 'markersize', 7, 'linewidth', 1.5);
xl = xlabel('Time (s)');
yl = ylabel('Velocity (km/s)');
set(xl,'FontSize',18,'FontWeight','bold');
set(yl,'FontSize',18,'FontWeight','bold');
set(gca,'FontSize',16,'FontWeight','bold');
set(pp,'LineWidth',1.25);
grid on
saveas (gcf,'Velocity vs Time','fig')

figure(4)
plot(time,fpa,'-o', 'markersize', 7, 'linewidth', 1.5);
yl = xlabel('Time (s)');
xl = ylabel('Flight Path Angle (deg)');
set(xl,'FontSize',18,'FontWeight','bold');
set(yl,'FontSize',18,'FontWeight','bold');
set(gca,'FontSize',16,'FontWeight','bold');
set(pp,'LineWidth',1.25);
grid on
saveas (gcf,'Fpa vs Time','fig')

figure(5)
plot(time,azimuth,'-o', 'markersize', 7, 'linewidth', 1.5);
yl = xlabel('Time (s)');
xl = ylabel('Azimuth Angle (deg)');
ylim([-10 10])
set(xl,'FontSize',18,'FontWeight','bold');
set(yl,'FontSize',18,'FontWeight','bold');
set(gca,'FontSize',16,'FontWeight','bold');
set(pp,'LineWidth',1.25);
grid on
saveas (gcf,'Azimuth vs Time','fig')


figure(6)
plot(time,bank,'-o', 'markersize', 7, 'linewidth', 1.5);
yl = xlabel('Time (s)');
xl = ylabel('Bank Angle (deg)');
set(xl,'FontSize',18,'FontWeight','bold');
set(yl,'FontSize',18,'FontWeight','bold');
set(gca,'FontSize',16,'FontWeight','bold');
set(pp,'LineWidth',1.25);
grid on
saveas (gcf,'Bank angle vs Time','fig')

figure(7)
plot(time,bankc,'-o', 'markersize', 7, 'linewidth', 1.5);
yl = xlabel('Time (s)');
xl = ylabel('Bank Angle Control (deg)');
set(xl,'FontSize',18,'FontWeight','bold');
set(yl,'FontSize',18,'FontWeight','bold');
set(gca,'FontSize',16,'FontWeight','bold');
set(pp,'LineWidth',1.25);
grid on
saveas (gcf,'Bank control vs Time','fig')

figure(8)
plot(time,q,'-o', 'markersize', 7, 'linewidth', 1.5);
yline(10000,'--','linewidth',1.5,'color','r');
```

```
yl = xlabel('Time (s)');
xl = ylabel('Dynamic Pressure (Pa)');
set(xl,'FontSize',18,'FontWeight','bold');
set(yl,'FontSize',18,'FontWeight','bold');
set(gca,'FontSize',16,'FontWeight','bold');
set(pp,'LineWidth',1.25);
grid on
saveas (gcf,'q vs Time','fig')

figure(9)
plot(time,a,'-o', 'markersize', 7, 'linewidth', 1.5);
yline(5 ,'--','linewidth',1.5,'color','r');
yl = xlabel('Time (s)');
xl = ylabel('Aerodynamic Load (g_e_a_r_t_h)');
set(xl,'FontSize',18,'FontWeight','bold');
set(yl,'FontSize',18,'FontWeight','bold');
set(gca,'FontSize',16,'FontWeight','bold');
set(pp,'LineWidth',1.25);
grid on
saveas (gcf,'a vs Time','fig')

figure(10)
plot(time,Qdot,'-o', 'markersize', 7, 'linewidth', 1.5);
yline(70,'--','linewidth',1.5,'color','r');
yl = xlabel('Time (s)');
xl = ylabel('Heating Rate (W/cm^2)');
set(xl,'FontSize',18,'FontWeight','bold');
set(yl,'FontSize',18,'FontWeight','bold');
set(gca,'FontSize',16,'FontWeight','bold');
set(pp,'LineWidth',1.25);
grid on
saveas (gcf,'Qdot vs Time','fig')
```